ROLE OF REACTİVE OXYGEN AND NITROGEN SPECIES IN THE PATHOGENESIS AND SEVERITY OF COVID-19, AND THE INTERACTION BETWEEN SARS-CoV-2 AND $PM_{2.5}$ IN HUMAN BRONCHIAL EPITHELIAL ORGANOIDS

Nur Konyalılar

A Dissertation Submitted to the
Graduate School of Health Sciences in Partial
Fulfillment of the Requirements for the Degree
of

Doctor of Philosophy

in

Cellular and Molecular Medicine

KOÇ ÜNİVERSİTESİ

June 24, 2024

ROLE OF REACTIVE OXYGEN AND NITROGEN SPECIES IN THE PATHOGENESIS AND SEVERITY OF COVID-19, AND THE INTERACTION BETWEEN SARS-CoV-2 AND $PM_{2.5}$ IN HUMAN BRONCHIAL EPITHELIAL ORGANOIDS

Koc University

Graduate School of Health Sciences

This is to certify that I have examined this copy of a doctoral dissertation by

Nur Konyalılar

and have found that it is complete and satisfactory in all respects,
and that any and all revisions required by the final
examining committee have been made.

Committee Members:

Prof. Dr. Hasan Bayram (Advisor)

Prof. Dr. Füsun Can

Prof. Dr. Şerife Esra Erdal Bağrıyanık

Prof. Dr. Gülfidan Aras

Prof. Dr. Bilun Gemicioğlu

Date: June 24, 2024

ABSTRACT

Role of reactive oxygen and nitrogen species in the pathogenesis and severity of COVID-19, and the interaction between SARS-CoV-2 and $PM_{2.5}$ in human bronchial epithelial organoids

Nur Konyalılar

Doctor of Philosophy in Cellular and Molecular Mechanism, June 24, 2024

The coronavirus disease 2019 (COVID-19) has caused significant mortality and morbidity worldwide. The disease is associated with increased inflammatory status that can lead to pneumonia, cytokine storm, and acute respiratory distress syndrome (ARDS). Studies suggest that respiratory viral infections may cause redox imbalance and oxidative stress; however, the role of these phenomena in the pathogenesis of COVID-19 is not known. Although studies have reported an association between increased levels of air pollutants including particulate matter (PM) and COVID-19 morbidity and mortality, the underlying mechanisms are not clear. The aims of my study were; (i) to investigate the effects of severe acute respiratory syndrome coronavirus 2 (SARS-CoV-2) and PM ≤ 2.5μm ($PM_{2.5}$) on the production of reactive oxygen species (ROS) and reactive nitrogen species (RNS), activation of pathways involved in cell death mechanisms, and release of inflammatory cytokines in human bronchial epithelial organoids (HBEOs), and (ii) to validate markers of ROS/RNS and inflammation in plasma of COVID-19 patients. My findings demonstrated that $PM_{2.5}$ increased SARS-CoV-2 viral load in HBEOs, which was reversed by inhibitors of ROS (N-acetyl cysteine, NAC) and RNS (NG-Monomethyl-L-arginine acetate salt, L-NMMMA. Furthermore, $PM_{2.5}$ induced oxidative/nitrosative stress in HBEOs that led to activation of the Nuclear Factor E2-Related Factor 2/ Kelch-like ECH-associated protein 1 (NFE2L2/KEAP1) pathway stimulating antioxidant genes NAD(P)H dehydrogenase (NQO1), and heme oxygenase 1 (HMOX1) together with pro-oxidant nitric oxide synthase 3 (NOS3). ROS/RNS inhibitors were effective in the suppression of oxidative/nitrosative stress. Finally, $PM_{2.5}$ and SARS-CoV-2 activated the cell death mechanisms including ferroptosis and apoptosis. The analysis of plasma obtained from COVID-19 patients showed increased production of ROS/RNS and inflammatory cytokines (IL-6, IL-8), especially in severe ones. My study findings suggest that SARS-CoV-2 can lead to cellular inflammation and death by mechanisms involving

oxidative/nitrosative stress and that this can be induced by $PM_{2.5}$. Moreover, 8-isoprostane (ROS indicator) and nitrite (RNS indicator) can be used as novel plasma biomarkers in COVID-19 diagnosis.

OZETCE

COVID-19'un patogenezinde ve şiddetinde reaktif oksijen ve nitrojen türlerinin rolü ve insan bronşiyal epitel organoidlerinde SARS-CoV-2 ile $PM_{2.5}$ arasındaki etkileşim

Nur Konyalılar

Hücresel ve Moleküler Tıp Doktora, 24 Haziran, 2024

Koronavirüs hastalığı 2019 (COVID-19) dünya çapında önemli mortalite ve morbiditeye neden olmuştur. Hastalık, pnömoniye, sitokin fırtınasına ve akut solunum sıkıntısı sendromuna (ARDS) yol açabilecek artan inflamatuar durumla ilişkilidir. Çalışmalar, solunum yolu viral enfeksiyonlarının redoks dengesizliğine ve oksidatif strese neden olabileceğini önermektedir; ancak bu fenomenlerin COVID-19'un patogenezindeki rolü bilinmemektedir. Çalışmalar, partiküler madde (PM) de dahil olmak üzere artan hava kirletici seviyeleri ile COVID-19 morbidite ve mortalitesi arasında bir ilişki olduğunu bildirmiş olsa da altta yatan mekanizmalar net değildir. Çalışmamın amaçları şunlardır; (i) İnsan bronş epitel organoidlerinde (hBEO'lar), şiddetli akut solunum sendromu koronavirüs 2 (SARS-CoV-2) ve PM $\leq$ 2,5 μm'nin ($PM_{2,5}$) reaktif oksijen türlerinin (ROS) ve reaktif nitrojen türlerinin (RNS) üretimi ve aktivasyonu üzerindeki etkilerini araştırılması, hücre ölümü mekanizmalarında yer alan yolakların aktivasyonunun ve inflamatuar sitokinlerin salınımının incelenmesi ve (ii) ROS/RNS belirteçlerinin ve inflamasyonun COVID-19 hastalarının plazmasında doğrulanması. Bulgularım, $PM_{2.5}$'in hBEO'larda SARS-CoV-2 viral yükünü arttırdığını göstermiştir; bu durum, ROS (N-asetil sistein, NAC) ve RNS (NG-Monometil-L-arginin asetat tuzu, L-NMMMA) inhibitörleri tarafından tersine çevrilmiştir. Ayrıca $PM_{2.5}$, hBEO'larda oksidatif/nitrosatif stresi indükleyerek Nükleer Faktör E2 ile İlgili Faktör 2/ Kelch benzeri ECH ile ilişkili protein 1 (NFE2L2/KEAP1) yolunun aktivasyonuna yol açarak antioksidan genler NAD(P)H dehidrojenaz 1'i (NQO1) ve heme oksijenaz 1'i (HMOX1), bununla birlikte, pro-oksidan nitrik oksit sentaz 3 'ü (NOS3) uyarmıştır. ROS/RNS inhibitörleri oksidatif/nitrosatif stresin baskılanmasında etkili olmuştur. Son olarak $PM_{2.5}$ ve SARS-CoV-2 ferroptoz ve apoptoz olmak üzere, hücre ölüm mekanizmalarını aktive etmiştir. COVID-19 hastalarından elde edilen plazmanın analizi, özellikle şiddetli olanlarda ROS/RNS ve inflamatuar sitokinlerin (IL-6, IL-8) üretiminin arttığını göstermiştir. Çalışma bulgularım SARS-CoV-2'nin oksidatif/nitrosatif stres içeren mekanizmalar yoluyla hücresel

inflamasyona ve ölüme yol açabileceğini ve bunun $PM_{2.5}$ tarafından indüklenebileceğini göstermektedir. Ayrıca 8-izoprostan (ROS göstergesi) ve nitrit (RNS göstergesi), COVID-19 tanısında yeni plazma biyobelirteçleri olarak kullanılabilir.

ACKNOWLEDGEMENT

I extend my heartfelt gratitude to all those who have played a pivotal role in shaping this journey and offering unwavering support as I traverse the realm of academia. Foremost, my sincere appreciation goes to Prof. Dr.Hasan Bayram, whose unwavering support and belief in my capabilities have been instrumental. Your mentorship has not only improved my academic life but also encouraged me to explore new horizons. Collaborating with you has been an honor beyond measure.

My heartfelt gratitude extends to my esteemed committee members, whose insights and guidance have been invaluable assets throughout this thesis.

A special thanks go to Dr.Özgecan Kayalar, who was with me throughout my whole academic journey and did not let me lose my motivation and believed that I could succeed under any circumstances. I would also like to thank our lab team, Gizem Tuşe Aksoy, Hadi Rajabi, Seval Kübra Korkunç, Sinem Erkan, and Deniz Mortazavi for their help and support throughout the whole process.

During the thesis, I was supported by TÜBİTAK-BİDEB 2250 scholarship and I’m grateful for their generous stipend. This research was supported by the TUBITAK 2566-Bilateral Cooperation Project with the National Natural Science Foundation of China (NSFC)-120N806 grant. I thank the Graduate School of Health Sciences and Koc University Research Center for Translational Medicine (KUTTAM) for providing side benefits.

I can't forget the amazing members of the KUTTAM. They've been by my side, providing support all the way. To my dearest friends, Neslihan Çilek, Dr. Eda Kuşan, Merve Gözel, Ayşe Dilara Aydemir, Şeyma Tekgül, Dr. Duygu Yazıcı,– you've made this whole doctorate journey better. I can't imagine what it would have been like without you. Thanks for being like a family.

A big shoutout to my best friends, Başak Ebru Işıldaklı and Ecem Çetin. Life would’ve been much harder without you. I love knowing that you are with me no matter what.

Lastly, my mum Nurhan Konyalılar, and my dad Ali Konyalılar, I’m so grateful to have you, none of this would have been possible without you. A special thanks to my aunt Türkan Ortaç, who's believed in me more than I have. I am very lucky to have such a family.

TABLE OF CONTENT

LIST OF TABLES

LIST OF FIGURES

ABBREVIATIONS

2D	Two-Dimensional
3D	Three-Dimensional
ACE	Angiotensin-Converting Enzyme
ACF	Animal Component Free
ACSL4	Acyl-CoA Synthetase Long-Chain Family Member 4
Ang	Angiotensin
ANPEP	Alanyl Aminopeptidase
ARDS	Acute Respiratory Distress Syndrome
ARE	Antioxidant Response Elements
ASC	Adult Stem Cells
AT1	Alveolar Type 1 Cells
AUC	Area Under the Curve
Bcl-2	B-cell Lymphoma 2
BCL2A1	BCL2-related protein A1
BPI	Beta Propiolactone
C1R	Complement Component 1
CASP	Caspase
CAT	Catalases
CBF	Ciliary Beat Frequency
CCL	C-C motif Chemokine Ligand
CDC	Centers for Disease Control and Prevention
cDNA	Complementary DNA
CK	Cytokeratin
CO	Carbon Monoxide
COPD	Chronic Obstructive Respiratory Disease
CPE	Cytopathic Effect
CYGB	Cytoglobin
CXCL	Chemokine C-X-C motif Ligand
DAMP	Damage-Associated Molecular Pattern
DEG	Differentially Expressed Gene
DMSO	Dimethyl Sulfoxide
DPBS	Dulbecco's Phosphate-Buffered Salt
E protein	Envelope Protein
ECM	Extracellular Matrix
ELISA	Enzyme-Linked Immunosorbent Assay
FBS	Fetal Bovine Serum
FOXJ1	Forkhead Box Protein J1
GBD	Global Burden of Disease
GM-CSF	Granulocyte-Macrophage Colony-Stimulating Factor
GPX	Glutathione Peroxidase

GR	Glutathione Reductase
GSH	Glutathione
hAEC	Human Airway Epithelial Cell
hBEC	Human Bronchial Epithelial Cell
hBEO	Human Bronchial Epithelial Organoid
HO	Heme-Oxygenase
IC50	Half-Maximal Inhibitory Concentration
IF	Immunofluorescent
IL	Interleukin
iNOS	Induced Nitric Oxide Synthase
Keap1	Kelch-like ECH-Associated Protein 1
L-NMMA	NG-Monomethyl-L-Arginine Acetate Salt
LPCAT3	Lysophosphatidylcholine Acyltransferase 3
LYPD2	LY6/PLAUR Domain Containing 2
M protein	Membrane Protein
MDA	Melanoma Differentiation-Associated Protein
MKI67	Ki-67
MOI	Multiplicity of Infection
MTT	3-(4,5-dimethylthiazol-2-yl)-2,5-diphenyltetrazolium bromide
MUC	Mucin
NAC	N-acetylcysteine
NET	Neutrophil Extracellular Trap
NF-KB	Nuclear Factor-κB
NFE2L2/Nrf2	Nuclear Factor E2-Related Factor 2
NH_3	Ammonia
NO	Nitric oxide
NO^-_2	Nitrite
NO^-_3	Nitrate
NO_2	Nitrogen Dioxide,
NOS	Nitric Oxide Synthase
NOX	NADPH Oxidase
NQO	NADPH Quinine Oxidoreductase
O_2-	Superoxide
O_3	Ozone
ONOO−	Peroxynitrite
PAMP	Associated Molecular Pattern
PCR	Polymerase Chain Reaction
PFU	Plaque Forming Unit
PM	Particulate Matter
PRR	Pattern Recognition Receptor
PSC	Pluripotent Stem Cells

PTFE	Teflon
qPCR	Quantitative Polymerase Chain Reaction
RAS	Renin-Angiotensin System
RBD	Receptor-Binding Domain
RLR	Retinoic acid-inducible gene (RIG)-like receptor
RNS	Reactive Nitrogen Species
ROC	Receiver-Operating Characteristic
ROS	Reactive Oxygen
RSV	Respiratory Syncytial Virus
S protein	Spike Protein
SARS-CoV-2	Severe Acute Respiratory Syndrome Coronavirus 2
SCGB1A1	Secretoglobin Family 1A Member 1
SCGB3A2	Secretoglobin Family 3A Member 2
SO_2	Sulfur dioxide
SOD	Superoxide Dismutase
SpO_2	Oxygen Saturation
T1IFN	Type 1 Interferon
TAE	Tris Acetate EDTA
TCID50	Fifty-Percent Tissue Culture Infective Dose
TF	Transferrin
TLR	Toll-Like Receptor
TMB	3,3′,5,5′-Tetramethylbenzidine
TMPRSS2	Transmembrane Serine Protease 2
TNF	Tumor Necrosis Factor
TP	Tumor Protein
Treg	Regulatory T cells
VOC	Volatile Organic Compound
WHO	World Health Organization
ZO-1	Zonula occludens-1

CHAPTER 1

INTRODUCTION

1.1 COVID-19

1.1.1 Epidemiology

In late December 2019, the newly identified coronavirus, 'Severe Acute Respiratory Syndrome Coronavirus 2', SARS-CoV-2, was first detected in Wuhan, a city in Hubei province of China. Soon after the announcement, it spread worldwide and became a global health problem in early 2020 (Sigrist et al., 2020). As of March 6, 2020, there were thousands of cases in Europe including more than a hundred deaths (Lescure et al., 2020). The first case was identified in Turkey on March 11, 2020 (Güner et al., 2021). World Health Organization (WHO) declared it officially as a global pandemic on the same day. Systemic infection caused by the virus is called COVID-19 (Coronavirus disease 19) (Sigrist et al., 2020). Viral genome sequencing analysis showed 96.2% overall genome sequence identity of SARS-CoV-2 with Bat CoV RaTG13 genome suggesting that bat CoV and human SARS-CoV-2 share the same ancestor (Guo et al., 2020). The disease is characterized by acute respiratory symptoms, similar to those seen in the severe acute respiratory syndrome coronavirus (SARS–CoV) in 2002, and Middle East respiratory syndrome coronavirus (MERS–CoV) in 2012 outbreaks and features human-to-human transmission (Chowdhury & Oommen, 2020). The number of cases globally reached 775,522,404, and the number of deaths reached 7,050,201 as of May 26, 2024 (*WHO COVID-19 dashboard*)

1.1.2 Risk factors

Although the disease can affect any age group, it has been reported that especially individuals over the age of 60 are more susceptible to infection. In addition to having a higher mortality rate, elderly patients commonly have more severe symptoms, and need hospitalization, intensive care, and mechanical ventilation more frequently, Age-related alterations in the human body can affect COVID-19 pathogenesis in multiple ways such as greater cellular senescence and oxidative stress, mitochondrial dysfunction, and epigenetic dysregulations. Even though the infection ratios are similar between men and women, sex-disaggregated estimates of the fatality ratio mostly reveal higher death rates

among males in every age group (Zsichla & Müller, 2023). Comorbidities such as diabetes, cardiovascular diseases, chronic lung diseases like chronic obstructive pulmonary disease (COPD), hypertension, and cancer are associated with an augmented risk of poor clinical outcomes in SARS-CoV-2-infection (Guo et al., 2020). Coinfection which means infection of a host by two or more pathogens simultaneously or superinfection which is having a second infection after the first one can exacerbate the SARS-CoV-2 infection too. Moreover, lifestyle factors associated with increased risk of disease severity are listed as smoking, obesity, and a longer waiting time for hospital admission (Wolff et al., 2021).

1.2.3 Clinical features

The SARS-CoV-2 incubation duration is around 4-5 days before symptom onset (Grant et al., 2020). Due to the long latency period, greater infectivity, and asymptomatic carriers, this virus affected more individuals than other coronavirus epidemics. Human-to-human transmission of the virus is chiefly through direct contact or droplets spread by sneezing or coughing from an infected individual (Rahman et al., 2020). Real-time PCR method using SARS-CoV-2 RNA obtained from a nasopharyngeal swab of the patients is used as standard diagnostic test (Cascella et al., 2023).

COVID-19 which can affect all systems in the body, primarily targets the respiratory system and lungs (Sigrist et al., 2020). Approximately, in 80% of infected patients, COVID-19 is primarily limited to the upper and conducting airways with mild symptoms and a good prognosis after the infection due to the recruitment of immune cells. Their most common clinical symptoms are fever, fatigue, and dry cough (He et al., 2020). Nonetheless, the illness advances to the lung gas exchange units in around 20% of patients, where it causes hypoxia and ground-glass opacification. Viral destruction of alveolar cells causes surfactant deficiency so alveolar collapse, together with immune overactivation called a cytokine storm or hyperinflammatory syndrome, subsequently leads to pneumonia and acute respiratory distress syndrome (ARDS) in severe cases with worse outcomes and increased risk of intensive care unit (ICU) admission, especially in high-risk groups. (Alipoor et al., 2020; Lin et al., 2020). ARDS, a common cause of respiratory failure, is a chief complication in patients with severe symptoms and can manifest soon after the onset of dyspnea which may lead to multiorgan failure and death (Krynytska et al., 2021).

The National Institutes of Health (NIH) categorizes COVID-19 patients into 5, asymptomatics who have a positive test for SARS-CoV-2 without any symptoms; mild ones who have symptoms such as headache, sore throat, cough, fever, diarrhea, vomiting, muscle pain, loss of taste and smell without dyspnea, shortness of breath, or abnormal chest imaging; moderate ones who have lower respiratory disease assessed during clinical valuation or imaging and have an oxygen saturation (SpO2) ≥94% on room air at sea level; severe patients have a SpO2 <94% on room air at sea level, a ratio of arterial partial pressure of oxygen to fraction of inspired oxygen (PaO2/FiO2) <300 mm Hg, a respiratory rate >30 breaths/min, or lung infiltrates >50%; critical ones who have septic shock, respiratory failure, or multiple organ dysfunction (*NIH, COVID-19 Treatment Guidelines* 2024).

1.1.4 Pathogenesis

Cellular entrance mechanisms of SARS-CoV-2

Coronaviruses (CoVs) are large enveloped single-stranded, positive-sense RNA viruses that belong to the Beta-coronaviruses that span approximately 30 kb (Reshmi & Abi, 2020). Due to mutations and recombination, they expanded their host ranges across the species barriers (Nova, 2021). The virus membrane contains structural components: the spike (S) protein facilitates the viral entry, envelope (E), and membrane (M) proteins together determine the shape of the virus, stabilize the nucleocapsid and nucleocapsid (N) protein bound to RNA to form nucleocapsid. There is also hemagglutinin esterase protein, which is involved in the different invading mechanisms and enhances binding by allowing interactions with sialic acid residues on host cell surfaces (V'kovski et al., 2021). It is known that coronavirus entry into the host cell depends on glycoproteins, which form spikes on their surface. These proteins contain a large ectodomain, a single-pass transmembrane anchor, and a short C-terminal intracellular tail. The ectodomain includes two different units: receptor-binding unit S1, which has a receptor-binding domain (RBD) to interact with specific cell surface receptors, and a membrane-fusion unit S2, which initiates the endocytosis of virion, fuses the host membrane and viral membrane so that the viral genome can get into the host cell (Chen et al., 2020).

The initial stage of viral infection is receptor recognition. Based on the previous findings, angiotensin-converting enzyme 2 (ACE2) is the receptor of SARS-CoV in humans (Qiu et al., 2020). RBD of SARS-CoV-2 also has a strong affinity to human ACE2 molecules, indicating that this protein exhibit a vital role in viral entry, making the

cells expressing this receptor more susceptible to the infection (Xu et al., 2020). ACE2 protein is an exopeptidase that catalyzes the conversion of angiotensin (Ang) I to Ang1-9 or the conversion of AngII to Ang1-7 (Chen et al., 2020).

After the recognition, the second major factor that affects pathogenicity is the priming of S glycoprotein by the host proteases at S1/S2 and S2 cleavage sites. It is known that single-strand RNA viruses like coronaviruses tend to have several receptors (Zhang et al., 2019). SARS-CoV-2 can utilize transmembrane serine protease 2 (TMPRSS2) and cysteine proteases Cathepsin B and L for the S priming like SARS-CoV (Hoffmann et al., 2020). A novel feature that distinct SARS-CoV-2 from SARS-CoV identified by Walls et al. is a Furin cleavage site at the S1/S2 boundary that cleaved during S biosynthesis. It is hypothesized that these excessive amounts of Furin-like protease expressions affect the SARS-CoV-2's cell and tissue tropism while increasing the transmissibility and pathogenicity. As seen in SARS-CoV, SARS-CoV-2 also uses conformational masking and glycan shielding to protect themselves from the host immune system (Walls et al., 2020).

Inflammatory response to SARS-CoV-2

Upon viral entry and replication, virus-derived pattern-associated molecular patterns (PAMPs) such as nucleic acids and the virion proteins are recognized by pattern recognition receptors (PRRs) on the cell surface or in the cytoplasm of the host, leading to the activation of innate responses (Yamada & Takaoka, 2023). These PRRs can be endosomal Toll-like receptors (TLR) 3-7 or transmembrane Retinoic acid-inducible gene (RIG)-like receptors (RLR) such as RIG-1 and (melanoma differentiation-associated protein 5 (MDA5). Usually, TLR activation leads to translocation of nuclear factor-κB (NF-KB) and interferon regulatory factor 3 (IRF3) to the nucleus while RLR stimulates IRF-3 and induces type 1 IFN (T1IFN) and other proinflammatory cytokines production such as Interleukin (IL)-1, IL-6, IL-8(CXCL8), granulocyte-macrophage colony-stimulating factor (GM-CSF), tumor necrosis factor (TNF)-α through the NF-KB pathway (Harrison et al., 2020). After getting into the cell, the virus replicates itself, disrupting lysosomes, damaging mitochondria, and unbalancing ion concentration so that the host cell undergoes pyroptosis with inflammasome response production and releases damage-associated molecular patterns (DAMPS), including ATP and nucleic acids, which are recognized by neighboring cells such as epithelial and endothelial cells, and alveolar macrophages (Wieczfinska et al., 2022). This may induce the release of pro-

inflammatory cytokines and chemokines such as IL-6, interferon γ-induced protein, macrophage inflammatory protein (MIP) 1α, MIP1β, and monocyte chemoattractant protein 1, which attract inflammatory cells monocytes, macrophages, neutrophils, T cells to the site of infection leading to further inflammation and may cause severe lung damage in defective immune system due to over secretion of cytokines from accumulated immune cells (Gonzalez-Garcia et al., 2023). These cytokines may travel to other organs and cause multi-organ problems. Moreover, non-neutralizing antibodies produced by B cells may exacerbate the inflammation by antibody-dependent enhancement (ADE).

Overall, innate and adaptive immunity is activated. Approximately after a week, T cells have an important role in viral clearance due to $CD4^+$T cell-derived cytokines and $CD8^+$ T cell-mediated cytotoxicity together with B cell activation so that antibody production (Silva et al., 2022). However, lymphocytes become depleted, called lymphopenia, because of the high secretion of pro-inflammatory cytokines by immune cells recruited to the infected area from blood, causing hyperinflammation that leads to cytokine storm (Hu et al., 2021). The virus uses the host's RNA-dependent RNA polymerase to produce more single-stranded RNA molecules and the host ribosome to translate viral proteins. These substances use host Golgi to get packed, leave the host by exocytosis, and spread to the other cells (Harrison et al., 2020). Cell death due to inflammation may exacerbate the systemic cytokine storm and excessive infiltration of immune cells. If the cytokine storm circulates to the other organs, it can cause multiple organ failure and ARDS. ARDS is characterized by breath difficulty and deficient blood oxygen levels in COVID-19 patients. Inflammatory cell infiltration is one of the reasons for the overproduction of proteases and reactive oxygen species that damage the lungs, and the virus itself causes alveolar damage and limits gas exchange efficiency. Due to these reasons, some of these patients get infected with other fungi or bacteria. Cytokine storm and sepsis, together with respiratory failure, cause death in severe cases (Tay et al., 2020).

Oxidative and nitrosative stress in COVID-19

Oxidative/Nitrosative stress is characterized by an imbalance between the production and accumulation of reactive oxygen/nitrogen species (ROS/RNS) in cells and tissues, as well as a biological system's ability to reduce these reactive species (Mozos & Luca, 2017). ROS (O_2•−, H_2O_2, •OH, RO_2•, RO•, and O_3) and RNS (•NO, •NO_2, N_2O_3 and •ONOO−) are formed from many sources in several compartments (mitochondria,

peroxisome, endoplasmic reticulum etc.) within the cell, either normally or as a consequence of exposure to toxic or pathologic insults (Finkel, 2012; Ma, 2010). In normal physiological conditions, approximately 1-3% of inhaled oxygen is converted to ROS, which has multiple essential roles in the body, such as ATP production and cell signaling (Ebrahimi et al., 2021). Mitochondria are the major site of ROS production due to aerobic respiration under physiological and pathophysiological conditions. In COVID-19, PRRs and interferon type 1 response increase ROS production due to xanthine oxidase, nitric oxide synthase, or mitochondrial respiratory reactions. RNS formation initiates with nitric oxide (•NO) synthesis by NO synthase in cells. NO reacts with superoxide (O_2•−) to form a stronger oxidant peroxynitrite anion (ONOO−). ONOO− reacts with other molecules to generate different RNS such as •NO_2, NO_3, and N_2O_3 (Lewandowski & Gwozdzinski, 2017). Viral nucleic acids and proteins elevate the inducible nitric oxide synthase (iNOS) expression and activity. Pulmonary ROS and RNS derive from exogenous and endogenous sources. Exogenous ones include air pollutants such as nitrogen dioxide (NO_2), ozone (O_3), carbon monoxide (CO) and sulfur dioxide (SO_2), volatile organic compounds (VOCs), diesel exhaust emissions, industrial chimney fumes, etc. (Białas et al., 2016; Chen et al., 2007). Endogenous ROS/RNS can be produced via mitochondrial dysfunction, endoplasmic reticulum stress, infections, and inflammatory processes in local pulmonary cells, as well as inflammatory cells (Bitko & Barik, 2001; Di Meo et al., 2016; Fubini & Hubbard, 2003; Khomich et al., 2018).

It is known that viral replication and increased viral protein deposits stimulate the overproduction of ROS and RNS, which over-consume the antioxidants of host organisms while increasing the activation of redox-sensitive transcription factors such as NF-κB, activator protein-1and hypoxia-induced factor that play an essential role in lung inflammation (Delgado-Roche & Mesta, 2020; Madamanchi & Runge, 2013; Van Eeden & Sin, 2013). However, the role of ROS / RNS action in COVID-19 pathogenesis and the underlying mechanism are not fully clear.

The generation of ROS/RNS by cytokines in COVID-19 causes increased mitochondrial membrane permeabilization. The release of mitochondrial DNA into the cytosol may act as DAMP, which also activates hallmark cytokines of COVID-19 like IL-6 and IL-1β and ultimately causes cell death mechanisms activation such as apoptosis. Apoptosis is based on activating a caspase cascade characterized by nuclear fragmentation, cell shrinkage, and chromatin condensation (Elmore, 2007). It is divided into two intrinsic and extrinsic pathways. Intrinsic one starts with the permeabilization of

mitochondria, cytochrome c release to the cytosol, which is induced by pro-apoptotic proteins such as BAK1, BAX, BIM, BBC3, BID leading to apoptosome formation and caspase-3 activation. On the other hand, anti-apoptotic proteins such as BCL-2, BCL-2-A1, BCL-W, BCL-XL, and MCL1 inhibit cytochrome c release to the cytoplasm. Apoptosome formed by ATP-dependent cytochrome c binding to APAF1, pro-caspase 9 binds to it, cleaved, and activated. Further, it activates caspase 3/6/7, leading to cell death (Carneiro & El-Deiry, 2020). The extrinsic pathway is triggered by ligand binding and conformational changes in cell surface death receptors such as Fas and TNF, followed by adaptor protein and initiator caspase binding such as caspase 8/10 inducing effector caspase activation (3/6/7) and cell death(Jan, 2019). The extrinsic pathway is significant for an immune response, while the intrinsic pathway can be induced by ER stress and DNA damage when the cell cannot repair anymore repair (Elmore, 2007). Excessive ROS/RNS accumulation in cytosol and mitochondria due to COVID-19 infection induces proapoptotic proteins and predominantly activates intrinsic pathways. Moreover, SARS-CoV-2 infection downregulates the NFE2L2 pathway, which has an antiapoptotic effect on cells (Gain & Kelesidis, 2023). Furthermore, caspase 1 is an inflammatory mediator that has a role in the maturation of pro-IL-1β , which is activated by inflammasome assembly and is seen in COVID-19. Inflammasome-activated cells secrete inflammatory cytokines and undergo an inflammatory form of cell death called pyroptosis (Rodrigues et al., 2023). Caspase 1 (CASP1) activation is mainly observed in macrophages, dendritic cells, and epithelial cells. Studies demonstrated that activated caspase-1 can induce effector caspases and intrinsic apoptosis, acting as a pro-apoptotic mediator (Molla et al., 2020). Furthermore, dysfunctional mitochondria can cause iron accumulation, which also leads to ROS generation through Fenton and Haber-Weiss reactions so that lipid peroxidation, induces ferroptosis, which is a newly identified programmed cell death (Cao & Dixon, 2016; Saleh et al., 2020). ROS accumulation during iron-mediated Fenton reactions causes phospholipid peroxidation of the plasma membrane. In the Fenton reactions, Fe^{+2} is oxidized by hydrogen peroxide to $Fe^{+3,}$ causing the formation of a hydroxyl radical and a hydroxide ion. Then, oxidized iron is reduced again by another hydrogen peroxide molecule, forming a hydroperoxyl radical and a proton. Created oxygen radicals are leading lipid peroxidation. It is induced by the inactivation of cellular glutathione (GSH)-dependent antioxidants such as GPX4, causing accumulation of toxic lipids, ROS, further causing cell death (J. Li et al., 2020). Two lipid metabolism-associated genes (lysophosphatidylcholine acyltransferase 3 (LPCAT3) and acyl-CoA

synthetase long-chain family member 4 (ACSL4)) have been identified to stimulate ferroptosis (Xie et al., 2016).

Moreover, it is known that ACE2 regulates the mitochondrial function. ACE2 knockout mice showed defective mitochondrial respiration and reduced ATP production. On the other hand, overexpression of ACE2 is also related to mitochondrial dysfunction by regulating NOX4, a ROS-producing enzyme in mitochondria (Singh et al.). Moreover, ACE2 converts AngII, a stimulant for NADPH oxidase, to Ang1-7, a strong antioxidant. So, the virus binding to ACE2 occupies the receptor and downregulates its expression, enhancing ROS so that oxidative stress (Wieczfinska et al., 2022).

Intricate pulmonary antioxidant systems counterbalance ROS and RNS to maintain the redox homeostasis inside of the cell. (Kutuk et al., 2017; Oztay et al., 2019; Redza-Dutordoir & Averill-Bates, 2016). Antioxidant enzymes include superoxide dismutases (SODs), catalases (CAT), peroxiredoxins, glutathione peroxidases (GPXs), and glutathione reductase. Non-catalytic antioxidant proteins (metallothioneins, glutaredoxin, peroxiredoxin, and thioredoxin) or non-enzymatic antioxidants (mucin, urate, GSH, ascorbate, ceruloplasmin, bilirubin, vitamin E and beta-carotene) that can be present in pulmonary cells and epithelial lining fluids are also crucial in antioxidant defense. (Engedal et al., 2018; Wang et al., 2019).

The major transcription factor regulating the antioxidant defense system is nuclear factor E2-related factor 2 (NFE2L2/Nrf2). It controls the Kelch-like ECH- ECH-associated protein 1 (Keap1)-Nrf2-antioxidant response elements (ARE) pathway. In the lack of oxidative stress, NFE2L2 is bound to Keap1 in the cytosol; on the other hand, increased ROS causes a conformational change in Keap1, leading to the translocation of NFE2L2 to the nucleus. Activated NFE2L2 binds to ARE sites and upregulates antioxidant genes such as heme-oxygenase (HO)-1, NADPH quinine oxidoreductase (NQO) 1, SODs, CATs, and GPXs. Some studies have demonstrated that respiratory viruses inhibit NFE2L2, disrupting the antioxidant balance (Gain & Kelesidis, 2023). Nrf2 plays a significant role in SARS-CoV-2 replication inhibition. SARS-CoV-2 decreases antioxidants such as HO-1 and NQO-1 in lung cell (Olagnier et al., 2020). Moreover, cytoglobin (CYGB) is a member of the protein globin family that aids the diffusion of oxygen across tissues and acts as a scavenger for NO or other ROS, especially in hypoxic conditions, which is observed during severe COVID-19 infection (Mathai et al., 2023). Neutralizing the oxidative/nitrosative stress is one of the crucial strategies in treatment protocols that should have been considered (Alam et al., 2023).

1.2 Impact of air pollution on COVID-19

1.2.1 Air pollutants and health impacts

Air pollution is one of the world's most important health and environmental problems, consisting of particulate matter (PM) released into the atmosphere and harmful gases such as O_3, nitrogen oxides, sulfur oxides, carbon monoxide (CO), ammonia (NH_3) (Comunian et al., 2020). Deteriorating air quality directly affects human health, not only increasing disease risks but also changing the ecosystem and causing long-term damage to humans (Orru et al., 2017). According to Global Burden of Disease (GBD) data, 9% of deaths worldwide are caused by air pollution, which corresponds to the death of approximately 5 million people yearly (Stanaway et al., 2018). Factors such as O_3, indoor and outdoor PM, which are the underlying cause of these deaths, are increasing risk factors for diseases such as heart diseases, lower respiratory tract infections, COPD, asthma, lung cancer and diabetes (Ritchie, 2024).

PM is a heterogeneous mixture of liquid and solid elements with different diameters and chemical compositions suspended in the air. This mixture includes elemental and organic carbon, organic and biological compounds, nitrates, sulfates, and metals (Rai, 2016).Unlike larger particles, $PM_{2.5}$ (diameter $\leq$2.5 μm) can reach the alveoli and enter the bloodstream due to the small size (Pu et al., 2022). It has been shown that PM may cause pulmonary inflammation due to an escalation in oxidative stress and damage the defense system against infections (Donaldson et al., 2001). Outdoor air pollution caused by meteorological factors, industrialization level, and regional topography may play a role in viral carriage and the severity of infection. Chronic exposure to pollutants can make people more susceptible to COVID-19 (Copat et al., 2020).

1.2.2 Epidemiologic studies related to air pollution and COVID-19

Determining the transmission routes of SARS-CoV-2 is very important in preventing the disease. The common ways of transmission are (i) Person-to-person, by coughing, sneezing, and inhaling droplets (>5-10 um in diameter) from approximately 1.8 meters; (ii) by direct contact with the mucous membranes of the mouth, nose, and eyes. Airborne transmission is defined as the shedding of a viral agent that is still infectious while remaining suspended in the air by aerosols (droplets < 5 μm in diameter) over longer distances and durations (Lauxmann et al., 2020). Setti et al. isolated SARS-

CoV-2 RNA from PMs in Bergamo, an industrial region of northern Italy. They demonstrated for the first time that PM could act as a vector in SARS-CoV-2 transmission (Setti et al., 2020). In a more comprehensive study, Kayalar and colleagues detected the presence of SARS-CoV-2 in PM samples collected from 10 different provinces and 13 different locations in Turkey. RNA of the virus was found in 9.8% of the collected PMs. In particular, the genetic material of SARS-CoV-2 was encountered in samples taken from hospital gardens and crowded places in cities where the infection is common (Kayalar et al., 2021). Surface retention of the virus on airborne dust and PM contributes to the long-range transport of the virus (Qu et al., 2020).

Most reports relating air pollution to COVID-19 cases are published in countries severely affected by the pandemic, such as Italy, China, and the USA. For example, Zhu et al. (2020), in a study using data from 120 cities in China, stated a 1.76% and 6.94% increase in daily confirmed cases with 10 $\mu g/m^3$ escalation in $PM_{2.5}$, PM_{10}, respectively (Zhu et al., 2020). Additionally, the same rise in $PM_{2.5}$ and PM_{10} augmented the case fatality rate by 0.24% and 0.26%, respectively (Yao et al., 2020). In the study conducted in Wuhan and XiaoGan, a correlation was shown between the incidence of COVID-19 and $PM_{2.5}$ concentration (H. Li et al., 2020). At the beginning of the pandemic, it was reported that the number of cases was concentrated in northern Italy, especially in the Po Valley cities of Lodi, Bergamo, and Cremona, among Italy's five most polluted cities due to industrialization. Furthermore, the highest death ratio was detected in Lombardy and Emilia Romagna, Italian provinces where air pollution is intense (Conticini et al., 2020). Research conducted in the USA presented that an increase of just 1 $\mu g/m^3$ in $PM_{2.5}$ was associated with an 8% augmentation in deaths due to COVID-19 (Wu et al., 2020). Pansini and Fornaca established a direct correlation between high SARS-CoV-2 infection rates and high $PM_{2.5}$ values in eight severely affected countries (China, USA, Germany, Italy, France, Iran, Spain, and the UK) (Pansini & Fornacca, 2021). Similar results were obtained in England, and the highest incidence and fatality ratios were recorded around London and the Midlands, the regions with the highest air pollution (Travaglio et al., 2021). Finally, a study combining data from 355 municipalities in the Netherlands revealed that $PM_{2.5}$ was an essential indicator of cases and hospitalization (Andrée, 2020). In a recent study conducted in Turkey by Aykaç and Etiler, they found a moderate correlation between the COVID-19 death rate per 100,000 individual in Istanbul and PM_{10} (Aykaç & Etiler, 2022).

1.2.3 Mechanisms involved the interaction between air pollution and COVID-19

$PM_{2.5}$ may facilitate the establishment of viral infections by affecting the airways and activating the renin-angiotensin system (RAS). This system proceeds on two opposing paths; the first one consists of ACE/ Ang II/AT1 receptor (R), which causes the release of pro-inflammatory cytokines interleukin (IL)-6 and TNF-α. The second pathway is ACE-2/Ang1-7/Mas, which has an anti-inflammatory effect. ACE2 splits Ang II into Ang1-7. The spike protein of SARS-CoV-2 enters the target cell by binding through the ACE-2 receptor on the host (Frontera et al., 2020). In rodent models, exposure to $PM_{2.5}$ increased ACE-2 expression in the lungs on days two and five (Lin et al., 2018). Another mouse model study showed that PM exposure increased ACE2 and TMPRSS2 protein expression, especially in alveolar macrophages and type 2 alveolar cells, by immunohistochemistry analysis (Sagawa et al., 2021). In mouse studies in which the ACE2 gene was blocked, it was shown that lung damage was more significant in these mice exposed to $PM_{2.5}$, suggesting that ACE2 has a protective effect in preventing inflammation. It has been determined that chronic exposure to $PM_{2.5}$ in places such as Northern Italy and China's Hubei province causes an increase in ACE2 expression, which facilitates the entry of the virus into the cell. It is thought that the virus binds to ACE2 and reduces its level by using ACE2 while entering the cell, thus eliminating the protective effect of ACE2 on the cell from inflammation, causing more severe lung damage. It is also suggested that high levels in the same environment can lead to more severe disease by further increasing inflammation in the cell (Frontera et al., 2020).

Studies on different continents have shown the association between COVID-19 cases and poor air quality. It is thought that short-term exposure to pollutants triggers a pro-inflammatory response, while long-term exposure may cause immune dysregulation, leading to distinctive diseases. It has been shown that the phagocytic activity of alveolar macrophages decreases due to PM exposure. In addition, PM has been found to have a negative effect on the promoter activity and subsequent transcription of interferon (IFN)-β, a crucial antiviral cytokine (B. Wang et al., 2020). Mouse experiments have shown that PM can cause alveolar collapse by changing the structure of the surfactant on the alveolar epithelial surface (F. Wang et al., 2020). Surfactant deficiency causes ARDS. Therefore, people residing in locations with advanced PM concentrations have an augmented risk of severe COVID-19 with ARDS (B. Wang et al., 2020). However, the relationship and underlying mechanisms between air pollution and COVID-19 are not fully understood.

The airway epithelium is the first line of defense against inhaled irritants, including pathogenic agents. Pollutants have been demonstrated to impair the epithelial barrier integrity by reducing occludin in plasma membranes and dissociating ZO-1, which might allow larger quantities of SARS-CoV-2 to enter the host cell. A dysfunctional barrier raises the probability of COVID-19 morbidity. Studies on air pollution found that O_3 and NO_2 enhanced the permeability of human primary bronchial epithelial cell cultures and that cells from asthmatic patients were more vulnerable to this process. One of the major causes of an ineffective immune system is disrupted mucociliary clearance (Fiorito et al., 2022). Bayram et al. previously established that DEP could reduce ciliary beat frequency (CBF) and stimulate the release of inflammatory mediators, as well as modulate cell cycle progression and apoptosis in human airway epithelial cells in various investigations (Bayram et al., 1998; Bayram et al., 2013; Bayram et al., 2006). Recent animal models and in vitro investigations have shown that SARS-CoV-2 infection shortens and deteriorates ciliary structure, resulting in alterations in ciliary function and reduced muco-ciliary clearance in airways (Robinot et al., 2021).

Another focus is on microbiome diversity and how it is affected in SARS-CoV-2-infected people. The respiratory tract microbiota is an vital aspect of immune development from birth, and environmental influences such as pollution have been shown to change the diversity of these organisms (Fiorito et al., 2022). RNA sequencing studies conducted in the United States with COVID-19 patients and a control group revealed differences in the diversity and abundance of some bacterial species in the upper respiratory tract microbiome, indicating that bacterial and viral interactions can impact viral load, host immunity, and acute severity (Rosas-Salazar et al., 2021).

1.3 Bronchial epithelium

1.3.1 Bronchial epithelial cell types

The respiratory system is divided into two as respiratory and conducting zones. The respiratory zone, which contains the alveolar duct to alveoli where the gas exchange occurs, is connected to the conducting zone through the nasal cavity, trachea, bronchi, and bronchioles (Kia'i & Bajaj, 2019). The bronchial tree is a complicated structure made up of 23 divided generations. No gas exchange exists between the trachea and the terminal bronchioles (generations 15–16). Terminal bronchioles are divided into respiratory bronchioles (generation 17-19), further into the alveolar duct and sacs. The conducting

component is crucial for heating, humidifying, and purifying the air that is inhaled (Patwa & Shah, 2015). The airway epithelium is a continuous layer that starts from nasal passage through the trachea and reaches alveolar sacs (Simukoko, 2021). From the nasal cavity to the bronchi, the respiratory epithelium covering the upper respiratory tract is categorized as ciliated pseudostratified columnar epithelium. To maintain appropriate airway function, bronchial epithelial cells, which line the airway lumen, are among the initial sites of contact for environmental stimuli (allergens, pathogens and gasses). Based on biochemical, functional, and ultrastructural standards, bronchial epithelial cells can be divided into four distinct categories: basal, club, ciliated and goblet cells (Denney & Ho, 2018).

Basal cells

Basal cells are multipotent stem cells, cuboidal in shape, residing near basal lamina anchored by integrins in the pseudostratified epithelium. They are significant for lung homeostasis since they provide self-renewal and regenerate all the luminal cell types. The proliferation and differentiation of specific epithelial stem/progenitor cells along the bronchial tree renew lung epithelium. The integrity of the epithelium is very significant for proper lung function. However, environmental inhaled pathogens continuously injure it, so basal cells are crucial for a steady state's repair and regular turnover. They are a subset of undifferentiated cells that undergo asymmetric cell division for lung morphogenesis or regeneration (Alysandratos et al., 2021). It is a continuous layer in larger airways while becoming clusters or individual cells in distal bronchioles. At steady-state, they are identified by cytokeratin (CK) 5 (it dimerizes with CK14 to form intermediate filaments) and TP (Tumor protein) 63 (member of the p53 family of transcription factors) markers (Davis & Wypych, 2021). Besides their structural and progenitor roles, basal epithelial cells also generate different bioactive substances such as cytokines, and neutral endopeptidases (W. Gao et al., 2015).

Club cells

Club cells are dome-shaped cells that dominate the airway epithelium in the respiratory bronchioles (Davis & Wypych, 2021). They secrete bronchiolar surfactants and particular anti-proteases that control bronchiolar epithelial integrity and immunity. Moreover, these cells act as progenitors for both ciliated and goblet cells. SCGB1A1 (Secretoglobin family 1A member 1; club cell secretory protein), SCGB3A1, and

SCGB3A2 (earliest marker to commitment to this cell type) are cell markers of them. Also, CK17-9 is enriched in club cells. (Wu et al., 2022).

Goblet cells

Goblet cells are large secretory cells, augmented in proximal airways, mostly lacking in terminal and respiratory bronchioles. They generate mucus, which is essential for moisturizing the epithelium and mucociliary clearance. Mucus contains mucin glycoproteins, water, and some other associated molecules having antimicrobial activity, such as peptides, IgA, lysozyme, and collectin (Cortez & Schultz-Cherry, 2021). Mucin (MUC)5B and 5AC are goblet cell markers.

Ciliated cells

Ciliated epithelial cells are the predominant cell type making up more than half of the epithelial cells, in the airways. They are columnar epithelial cells, rich in mitochondria. Each ciliated cell contains approximately 200-300 cilia (Bustamante-Marin & Ostrowski, 2017). The directional beating of these cilia is critical for clearing mucus from airways. Forkhead box protein J1 (FOXJ1) and acetylated alpha-tubulin are ciliated cell markers (Cortez & Schultz-Cherry, 2021).

1.3.2 The function of bronchial epithelium

Physical barrier function

Respiratory epithelium is always exposed to the environment and has a critical role in coordinating early responses to pathogens, toxins, and allergens. Moreover, regulation of gas exchange for normal pulmonary function is essential. The integrity of respiratory epithelium, fluid balance, and transport of substances is controlled by an epithelial barrier (Godbole et al., 2022). Adherens junctions, tight junctions, desmosomes, and hemidesmosomes are part of the epithelial barrier and crucial for linking adjacent cells and controlling paracellular diffusion. The main transmembrane tight junction proteins are occludins, claudins, and junction adhesion molecule (JAM) proteins (Heinemann & Schuetz, 2019). Occludins, which are 60 kDa, have an essential role in sealing and creating the barrier function by interacting with one another in the membranes of adjacent cells. Zonula occludens-1 (ZO-1) protein binds them to actin microfilaments. Transmembrane proteins claudins (~20 kDa) forming the backbone of the junction facilitates cell-cell adhesion independent of Ca^{+2}. The junction's selective permeability is determined by the kinds and quantity of claudins present in (Hartsock & Nelson, 2008).

Adherence junction proteins are located just below the tight junction, linking the plasma membrane of 2 neighboring cells with Cadherin proteins. They are Ca^{+2}-dependent transmembrane proteins connected to the actin filaments through anchor proteins, classified as types 1 and 2. Epithelial (E)-cadherins are members of type 1 (Loh et al., 2019). Desmosomes are cell-cell adhesion structures facilitated by E-cadherin which is important for mechanical support of the tissue. They link columnar and basal cells and are largely found along the lateral side of columnar epithelial cells, especially toward the basal surface. In the basement membrane, hemidesmosomes including integrins are required to link basal cells to the extracellular matrix (Kucukural et al., 2019; Yuksel & Turkeli, 2017)

Mucociliary clearance

Mucociliary clearance is essential for clearing the airways of inhaled toxicants, pollutants, and microorganisms. Against the numerous insults, mucus a liquid bilayer, that lines the internal surface of airways acts as a primary innate defense (Bustamante-Marin & Ostrowski, 2017). It is secreted by goblet cells and submucosal glands, containing mucin glycoproteins, antimicrobial and anti-inflammatory peptides, enzymes, electrolytes, and water. The abundance and components of the mixture vary along the response to external stimuli so the viscoelasticity of mucus is a significant part of the clearance. Due to its viscosity, it traps the particles, with the help of synchronized ciliary beating frequency of ciliated cells and cough they are removed outside of the airways. (Whitsett, 2018).

Biochemical properties

Bronchial epithelium plays a significant role in immunity as a 1st line of defense against pathogens and a key regulator of lung inflammation. It serves as a biochemical barrier secreting enzymes, protease inhibitors, antimicrobial peptides, oxidants, various cytokines, and growth factors. It is also crucial for tissue remodeling (Hiemstra et al., 2015). For instance, lysozyme, an enzyme effective against the peptidoglycan layer of gram-positive bacteria; lactoferrin, an iron chelator effective in degrading the outer membrane of gram-negative bacteria so that lysozyme can reach the peptidoglycan layer are secreted by epithelium as an antimicrobial protein. Secretory leukoprotease inhibitor, elastase inhibitor, antichymotrypsin and α1-antiprotease are examples of protease inhibitors essential for the requirement of immune cells. Human β defensins and cathelicidins are among the antimicrobial peptides against various bacteria and viruses

(Ganesan et al., 2013). Nitric oxide (NO) and hydrogen peroxide (H_2O_2) are major oxidants produced by airway epithelium. Viral infections along with the pro-inflammatory cytokine secretion induce the expression of iNOS which is required for the inhibition of viral replication in cells. Moreover, H_2O_2, produced by dual oxidase (DUOX) 1 and 2 secreted to the extracellular milieu acts as a microbicidal (Polito & Proud, 1998).

During the inflammation, the recruitment of inflammatory cells with cytokines is an essential step of the immune response. Cytokines produced by airway epithelium can be classified as colony-stimulating factors, pleiotropic cytokines, chemoattractant cytokines, and growth factors. Colony-stimulating factors are listed as Granulocyte-macrophage colony-stimulating factor (GM-CSF), granulocyte colony-stimulating factor (G-CSF), and macrophage colony-stimulating factor (M-CSF). GM-CSF is one of the major ones constitutively secreted by airway epithelial cells. It has a role in the maintenance of eosinophil survival and augmentation of the cytotoxic effect, mediator release, and phagocytic activity of immune cells such as eosinophils, neutrophils, and macrophages. IL-1β, IL-6 and IL-11 and TNF-α. are the best-studied epithelial-derived pleiotropic cytokines. They can affect a variety of targets such as the inactivation of monocytes and B cells; and induction of acute-phase protein synthesis. For instance, IL-6 can induce the cell adhesion molecules expression while IL1-β and TNF-α can stimulate eosinophilic and neutrophilic inflammation by activating different cell types that elevate the expression of cytokines, cell adhesion molecules including IL-8, RANTES, intercellular cell adhesion molecule 1 (ICAM-1), vascular cell adhesion molecule 1 (VCAM-1) and E-selectin (Mills et al., 1999). Moreover, elevated IL-6 and IL-11 levels are associated with airway hyperresponsiveness that may lead to epithelium remodeling. IL-8 is an example of chemoattractant cytokines (chemokines) which is especially chemotactic for neutrophils and some subtypes of T cells, active eosinophils. Regulated on activation, normal T cell expressed and secreted (RANTES) is another chemoattractant for eosinophils that is mostly produced due to stimuli such as TNF-α secretion or respiratory viruses. Growth factors such as transforming growth factor β (TGF-β) synthesized by bronchial epithelial cells are essential for cell proliferation, migration, differentiation, epithelial repair mechanism, and signaling (Knight & Holgate, 2003).

1.3.3 In vitro cultures of bronchial epithelium

Monolayer (2D) cell cultures

To understand the basic biophysical and biomolecular principles by which cells aggregate into tissues and organs, how these tissues function, and how that function is disturbed in disease, cell culture has been used as a vital method extensively used in biomedical area, tissue engineering, regenerative medicine, and industry. 2-dimensional (2D) cultures have been used as an in-vitro model for over a century (Duval et al., 2017). Adherent 2D cell cultures require a glass or polystyrene petri dish or culture flask to attach so that proliferate as monolayers, such as epithelial cells. Due to the equal access of monolayer cells to the nutrients and growth factors in the media, the growth and proliferation of the cells are uniform which makes them simple and effective. (Kapałczyńska et al., 2018). 2D cell cultures can be divided into 2: primary cell cultures and cell line cultures. Primary cell cultures are cultures of cells that have been directly isolated from parental tissue of interest containing rinsing, dissection, mechanical or enzymatic digestion, and separation protocols with a limited life span, while cell lines are mostly immortalized through transformation or genetic alteration of primary cells and are typically used to increase cell population and extend life span. Primary cells reflect the characteristics of the tissue better however, have a higher risk of contamination so they should be handled more carefully (Richter et al., 2021). BEAS-2B epithelial cells, extracted from the normal human bronchial epithelium of non-cancerous individuals is an example of an immortalized cell line that is extensively used in bronchial epithelium research. In recent years, primary bronchial epithelial cells and BEAS-2B cell line have been very useful for COVID-19 studies due to the expression of SARS-CoV-2 entrance-related receptors and proteases (Erickson et al., 2023; Stölting et al., 2022; Xu et al., 2024; Zhou et al., 2021; Zhu et al., 2022).

3D cell cultures and bronchial epithelial organoids

Conventional 2D cell culture models have significantly impacted both clinical and basic sciences in the lung research area. However, especially in the last few decades, it has not been adequate to answer all the research questions compared to in vivo and clinical observations and applications (Konar et al., 2016). The three-dimensional (3D) structure reflects the multilayered, complex tissue structure much better. It allows the formation and observation of cell-cell and cell-matrix interactions necessary to preserve the physiological properties of the system (Hynds & Giangreco, 2013). Organoids are

types of 3D cultures defined as multicellular systems with a proper self-organizing ability, self-renewal capacity, and differentiation into some other cell types. They can be derived from multipotent adult stem cells (ASC), which are also called organ progenitor/basal cells or pluripotent stem cells (PSC) (Peng et al., 2022). They offer greater tissue complexity and heterogeneity compared to 2D cultures (Joo et al., 2024). More specifically, an organoid must meet several criteria. Examples of these include a 3D structure including cells that form or preserve the identity of the modeled organ; the presence of more than one cell type, as in the organ itself; the created organoid is shown to exhibit some aspects of the specialized functions of the organ and to be able to self-organize according to the same principles of internal organization as the organ itself (Lancaster & Huch, 2019). During the organoid formation process, some common factors are used to regulate self-renewal and differentiation of stem cells/basal/progenitor cells or to aid self-organization. Growth factors, a variety of activator or inhibitor small molecules, are used to operate various signaling pathways critical in self-renewal, cell survival, and proliferation often in a tissue-specific manner (Yin et al., 2016). The extracellular matrix (ECM) is also essential in creating 3D models to provide biochemical cues and structural sustenance, such as porosity and stiffness, which facilitate signaling for cell migration and polarization in organoid formations. Today, numerous organoids are cultured in Matrigel, a material derived from the secretion of Engelbreth-Holm-Swarm mouse sarcoma cells and enriched in ECM proteins (Kozlowski et al., 2021). It is a common and significant element of the system that provides a scaffold and additional reinforcement of signaling cues through basement membrane ligands to assist cell attachment and survival as well as organoid establishment (Xu et al., 2001).

Latest advances in isolating lung epithelial progenitor and stromal cells and detecting stem cell niche factors vital for lung development have enabled the formation of an in vitro 3D culture system (Choi et al., 2016). Human airway organoids, a 3D miniaturized form of the lung that mimics the epithelial organization of their respective anatomical districts, have been successfully generated from nasal (Guimbellot et al., 2017; Liu et al., 2020), bronchial(Sachs et al., 2019), and alveolar (Barkauskas et al., 2017; Katsura et al., 2020) tissues using adult or pluripotent stem cells as starting substances (Choi et al., 2016; Dye et al., 2015; Karekla et al., 2017). These systems, also called airway organoids or pulmonary organoids, have been reported to represent better the in vivo epithelial structure (Fatehullah et al., 2016; Hynds & Giangreco, 2013; Nadkarni et al., 2016). Organoids formed by ASCs/basal/progenitor cells have been

established to represent different lung regions. Mostly, ASCs were dissociated from lung tissue biopsies. Sorting was done to obtain the desired cell type (Joo et al., 2024). Furthermore, complex in vitro models have been established containing cells of different compartments of the lung, such as immortalized airway basal cells and human bronchial cells together with endothelial cells or fibroblasts to obtain embryonic-like branching structures (Nadkarni et al., 2016).

Today, lung organoids are used to study chronic lung diseases such as COPD and asthma, as well as lung cancer and cystic fibrosis, and also to evaluate infections such as respiratory syncytial virus (RSV), influenza and, more recently, SARS-CoV-2 (Chan et al., 2022). In addition to disease modeling and the study of intercellular interactions, organoids are also of great importance in the fields of drug discovery, toxicology, and regenerative medicine (Demchenko et al., 2022). In 2019, the COVID-19 pandemic urged a rapid escalation in the need for in vitro respiratory models to study viral infections. Even if many animal and 2D cell culture models have been developed, there was a requirement for in vitro lung models, especially to enlighten the SARS-CoV-2 infection mechanism to conduct the large-scale evaluation for candidate therapeutics (Sano et al., 2022). In 2020, single-cell analysis demonstrated that ACE2 is predominantly expressed in the transient secretory cells, which can be differentiated into goblet or ciliated cells in bronchi, while TMPRSS2 is also highly expressed in this tissue. Therefore, the bronchial organoid model is one of the most valuable models to study SARS-CoV-2. (Lukassen et al., 2020). PSC-derived bronchial or alveolar organoids were also used for SARS-CoV-2 infection and replication research. Still, there was a requirement for adult-type 3D cultures, especially to study severe COVID-19 cases (Han et al., 2020; Sano et al., 2022).

Moreover, the first site of infection is the nasal epithelium, in which ACE2, TMPRSS2, and Furin are expressed. Robust ciliated cell damage was observed in nasal organoids after the infection. The damage was spotted even in basal cells with increased severity. Augmented inflammatory cytokines such as IL-6 and IL-8 were thought to be the reason for the damage (Chiu et al., 2022). Another study conducted with bronchial organoids demonstrated similar results and showed that most injuries were sustained in ciliated cells, concluding that ciliated cells are the key target of the infection. Subsequent harm by inflammatory factors, basal cells renew the epithelium by differentiating into ciliated cells (Sano et al., 2022). Sequencing analysis by using infected and uninfected bronchial organoids presented upregulation of genes related to leukocyte migration, cell chemotaxis together with the chemokine (C-X-C motif) ligand 1,8,10 (CXCL1,8,10) that

have a role in lung damage and chemokine (C-C motif) ligand 5 (CCL5) that have a role in the induction of white cells damaged area migration (K.-Y. Fang et al., 2021). Human alveolar organoids containing type 1 and 2 cells are also used to study SARS-CoV-2 infection due to ACE2 and TMPRSS2 expression. A study conducted with iPSC-derived alveospheres showed that AT2 cells are the center of inflammation in the alveolar region and upregulate the NF-KB pathway with IFN response (Huang et al., 2020). Another research using $PM_{2.5}$-treated PSC-derived alveolar organoids demonstrated elevated expression of ACE2 and TMPRSS2 (Kim et al., 2020).

Compared with 2D and animal models, 3D lung cultures have various advantages in SARS-CoV-2 infection studies in terms of mimicking cellular microenvironment and host-pathogen relationships. However, lung organoids have some limitations, too. They cannot mimic whole organs, only specific tissues in the body (Peng et al., 2022). Besides epithelial diversity, there are various cell types in the lungs, such as immune, mesenchymal, and endothelial cells, which need a comprehensive understanding of each type's differentiation and optimization of culture formation. Nowadays, advanced culture systems such as microfluidics, air-liquid interphase systems, and newly developed biomaterials like hydrogels are being used to improve culture conditions (Joo et al., 2024). Interactions between organs cannot be modeled yet, either. Also, currently, these cultures are very expensive and time-consuming. Elimination of these limitations will pave the way for animal experiments to be replaced entirely by 3D culture

Hypothesis

Air pollution increases SARS-CoV-2 infection, COVID-19 mortality, and morbidity by increasing ROS/RNS, using ROS/RNS inhibitors can prevent disruption of oxidant/antioxidant balance so that severe inflammation which may lead to cell death and multiorgan damage. Moreover, ROS/RNS can be used as a plasma biomarker in the severity of COVID-19 pathogenesis.

Aims

Epidemiological studies demonstrated the correlation between hospitalization and fatality rates due to COVID-19 and air pollution. There is an increased ROS/RNS production together with cytokine storm in SARS-CoV-2 infection. However, the underlying

mechanism of oxidative/nitrosative stress due to air pollutants' association with infection, and the severity of the disease is not clear yet. In our study, the major aim was to evaluate the role of ROS/RNS in the pathogenesis and severity of COVID-19, investigate the interaction between SARS-CoV-2 and $PM_{2.5}$ in terms of antioxidant mechanisms, inflammation, and cell death pathways, and determine whether it could be prevented with ROS/RNS inhibitors by using human bronchial epithelial organoids (hBEOs). The other aim was to investigate whether reactive oxygen and nitrogen species could be used as biomarkers in the severity of COVID-19 disease in patient plasma samples. This study may reveal potential preventive and therapeutic interventions.

Objectives

- Establishment of a methodology for hBEOs production and SARS-CoV-2 infection of these organoids.
- Collection of $PM_{2.5}$ and treatment of hBEOs with them.
- Determination of the effects of SARS-CoV-2 and the impact of $PM_{2.5}$ on the production of ROS/RNS in hBEOs and inhibiting this with ROS/RNS inhibitors.
- Elucidation of the molecular mechanisms of ROS/RNS induced by SARS-CoV-2, $PM_{2.5}$, and ROS/RNS inhibitors in hBEOs.
- Validation of ROS/RNS markers and inflammatory cytokines in blood plasma of COVID-19 patients.

CHAPTER 2

METHODOLOGY

2.1 Culture of human bronchial epithelial organoids (hBEO)

2.1.1 Culture of primary human bronchial epithelial cells (hBECs)

For the explant culture technique (Bayram et al., 1998; Devalia et al., 1990), bronchial explants were recruited from patients undergoing surgery for various reasons at Koç University Hospital. Tissue donor inclusion and exclusion criteria were as follows: **Inclusion criteria:** All subjects (males or females) aged 18-65 years and without any respiratory tract infections within one month of the study were included. Control (Non-smoker) subjects had normal lung function on spirometry with no smoking history (<100 cigarettes/lifetime). Smokers had a smoking history (>100 cigarettes/lifetime). **Exclusion criteria:** Pregnancy or lactation for females, patients with an FEV1 < 1L, any other active lung condition, and subjects unable to consent were excluded.

After obtaining the pathologists' approval, bronchial explants were immediately brought to the primary cell culture laboratory, in transfer solution for the culture process. Explants were examined under a dissection microscope; the epithelium was dissected and cut into 0.5 mm^3 or smaller pieces. All explants were washed using a medium containing 0.1% antibiotic solution and seeded in the complete medium within 1-2 hours. Tissues were attached to the culture plates in 1-2 days, and cell proliferation started in 5-6 days. After cells began to proliferate, the culture media was changed to Nu-Serum, which contained a complete medium to induce differentiation and proliferation. Cultures were maintained for approximately 2 -3 additional weeks. Media was changed every other day. The protocol is summarized in Figure 2.1 below. Culture media ingredients are listed in Table 2.1.

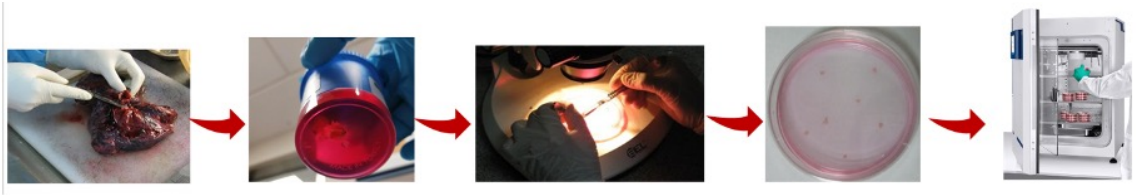

Figure 2. 1 Culture of human primary bronchial epithelium obtained from bronchial tissue.

Table 2. 1 Media ingredients are used in the bronchial explant culture technique.

Name of the Media	**Ingredients**	**Percentage (%)**
Transfer/Washing Media	Medium 199 (Sigma M4530)	99.9
	Geneticin (Gibco, 10131-027)	0.1
Complete Culture Media	Medium 199 (Sigma M4530)	93.455
	FBS (Fetal Bovine Serum) (Sigma, F7524)	2.5
	Bovine pancreatic insulin (Sigma I-6634)	1
	Hydrocortisone (Sigma H0396)	1
	Human Transferrin (Sigma-T2036)	1
	Gibco™ Antibiotic-Antimycotic (100X) (15240062)	1
	Epidermal Growth Factor (Pepro tech. AF-100-15)	0.045
Nu Serum Complete Culture Media	Medium 199 (Sigma M4530)	93.455
	Nu Serum (Becton Dickinson, 355504)	2.5
	Bovine pancreatic insulin (Sigma I-6634)	1
	Hydrocortisone (Sigma H0396)	1
	Human Transferrin (Sigma-T2036)	1
	Gibco™ Antibiotic-Antimycotic (100X) (15240062)	1

	Epidermal Growth Factor (Pepro tech. AF-100-15)	0.045

Characterization of primary hBECs by immunofluorescent (IF) staining

Primary human bronchial epithelial cells were characterized by the IF technique. Staining was performed for basal cell markers CK5, 14, p63; ciliated cell marker FOXJ1, secretory cell marker SCGB3A2, goblet cell marker MUC5AC; adherence junction marker E-cadherin; tight junction marker occludin. Briefly, cells were washed with DPBS and fixed with 1:1 acetone-methanol solution (Merck,100014. 2500; Sigma-Aldrich, 67-56-1) for 10 min, at room temperature, then washed 3 times with 0.1% BSA (Sigma, A9418) containing PBS for 5 min., and they were blocked with Superblock (ScyTek Laboratories, AAA125) at room temperature for 30 min. Primary antibody incubation, diluted with 0.1% BSA containing PBS-T, was conducted overnight at 4°C. The next day, cells were washed 3 times with 0.1% BSA containing PBS-T for 5 min. Secondary antibody incubation was performed in PBS-T containing 0.1% BSA for 1 hour at room temperature. Consequently, cells were washed 3 times with PBS-T containing 0.1% BSA for 5 min. Nuclei staining was performed using Hoechst dye (Sigma, B2261) for 3 min. Lastly, cells were again washed 3 times with PBS-T containing 0.1% BSA. 1:1 Glycerol (Sigma-Aldrich, G5516): PBS mixture was used as mounting media. Cells were kept at 4°C in the dark until imaging. Images were taken using a fluorescent microscope (Leica DMi8). Antibodies and their dilutions are listed in Tables 2.2 and 2.3.

Table 2. 2 Primary antibodies used in immunofluorescence imaging of hBECs.

Name of the antibody	**Dilution ratio**
CK5 (Abcam, ab53121)	1:500
CK14 (Abcam, ab7800)	1:250
P63 (Abcam, ab53039)	1:250
FOXJ1 (SantaCruz, sc-53139)	1:100
SCGB3A2 (Abcam, ab181853)	1:500
MUC5AC (Invitrogen, 45M1)	1:100
E-Cadherin (Invitrogen, HECD-1)	1:200
Occludin (Invitrogen, OC-3F10)	1:200

Table 2. 3 Secondary antibodies used in immunofluorescence imaging of hBECs.

Name of the antibody	Dilution ratio
Goat anti-Rabbit IgG (H+L) Highly Cross-Adsorbed Secondary Antibody, Alexa Fluor Plus 488 (Invitrogen, A32731)	1:100
Goat anti-Mouse IgG (H+L) Highly Cross-Adsorbed Secondary Antibody, Alexa Fluor Plus 488 (Invitrogen, A32723)	1:100
Goat anti-Rabbit IgG (H+L) Highly Cross-Adsorbed Secondary Antibody, Alexa Fluor Plus 594 (Invitrogen, A32740)	1:100
Goat anti-Mouse IgG (H+L) Highly Cross-Adsorbed Secondary Antibody, Alexa Fluor Plus 594 (Invitrogen, A32742)	1:100

2.1.2 Culture of healthy primary human bronchial epithelial cell line (02AB0839.02, Epithelix)

The purchased healthy non-smoker primary human primary bronchial epithelial cells (02AB0839.02, Epithelix) were transferred into the lab in dry ice and kept in the nitrogen tank until the day of culture. During culture, cells were thawed according to the manufacturer's instructions. They were kept at 37°C for 2-3 min. and centrifuged at 2000 rpm for 10 min inside pre-warmed DMEM media containing 10% FBS. Firstly, cells were resuspended in 1 ml human airway epithelial cell (hAEC) culture media (EP09AM, Epithelix) and seeded into a 75 cm^2 flask with 30 ml culture media. They were kept at 37°C, 5% CO_2, and 99% humidity in the incubator. The cell culture medium was changed every 3 days. These cells were passaged for several months, and backup cell freezing was performed at each passage.

2.1.3 hBEOs Formation

At the end of approximately 3. week of BECs cultures, they were maintained in PneumaCult™-Ex Plus Medium (Stemcell Tech., USA) for 3-5 additional days. It was a serum- and BPE-free medium which supports more expansion and proper differentiation of primary human airway epithelial cells at each passage, compared to other commercially available expansion media (Rayner et al., 2019). After the expansion, cells were washed with DPBS and detached from dishes using Animal Component Free (ACF) Enzymatic Dissociation Solution (Stemcell Tech., 05427). BECs in the pellet were counted using trypan blue. Matrigel (Corning, USA) was incubated at 4°C overnight before application and added to the plate on ice. Pipette tips were cooled at -20°C for Matrigel usage. 96 well plates (pre-heated overnight at 37°C) were coated with a solution containing 90% Matrigel and 10% seeding medium incubated at 37°C, 15 min. 2500 cell/well seeded in PneumaCult™ Airway Organoid Seeding Medium. For the organoid formation cells were kept in seeding media for 7 days. Media was changed every other day. At the end of 1st week, cultures were treated in PneumaCult™ Airway Organoid Differentiation Media (Stemcell Tech. USA) for an additional 2-3 more weeks, and the medium was changed every other day. The protocol is summarized in Figure 2.2 below. Medium ingredients used for organoid formation are listed in Table 2.4. Characteristics of patients whose bronchial tissues were used to form hBEOs are listed in Table 2.5.

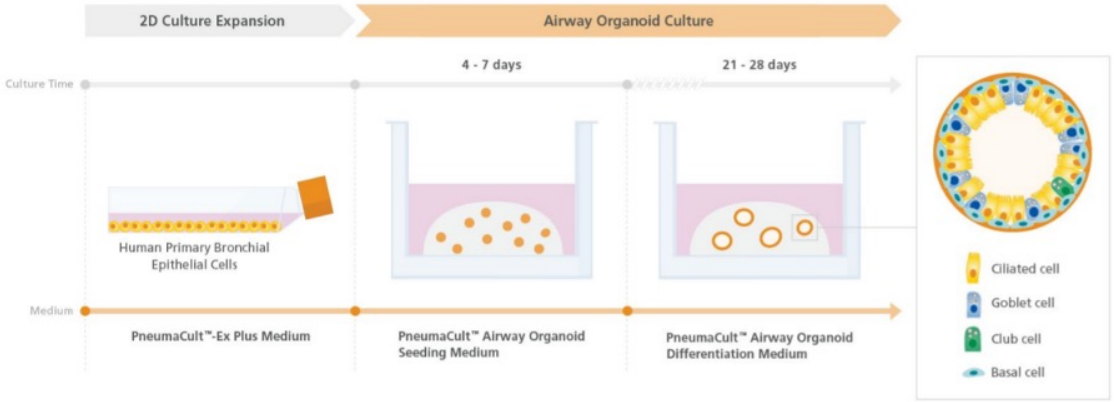

Figure 2. 2 hBEOs formation steps.

Table 2. 4 Organoid Formation media types and ingredients.

Name of the Media	**Ingredients**	**Percentage (%)**

PneumaCult™-Ex Plus Medium	PneumaCult™-Ex Plus Basal Medium (Stem Cell Tech., 05041)	96.736
	PneumaCult™-Ex Plus 50X Supplement (Stem Cell Tech. 05042)	2
	Hydrocortisone (Sigma H0396)	0.264
	Pen/Strep (Gibco, 10,000 U/mL)	1
PneumaCult™ Airway Organoid Seeding Medium	PneumaCult™ Airway Organoid Basal Medium (Stem Cell Tech., 05061)	89
	PneumaCult™ Airway Organoid Seeding Supplement (Stem Cell Tech., 05062)	10
	Pen/Strep (Gibco, 10,000 U/mL)	1
PneumaCult™ Airway Organoid Differentiation Medium (ODM)	PneumaCult™ Airway Organoid Basal Medium (Stem Cell Tech., 05061)	87.468
	PneumaCult™ Airway Organoid Differentiation Supplement (Stem Cell Tech., 05063)	10
	Pen/Strep (Gibco, 10,000 U/mL)	1
	Hydrocortisone (Sigma H0396)	1.332
	Heparin (Stem Cell Tech., 07980)	0.2

Table 2. 5 Characteristics of patients whose bronchial tissues were used to form hBEOs.

Number of Patient	Smoking Status	Smoking Pack/Year	Gender	Age
1	Nonsmoker	-	Male	64
2	Nonsmoker	-	Male	55
3	Nonsmoker	-	Female	75
4	Nonsmoker (hAEC)	-	Male	-
5	Smoker	20	Female	63
6	Smoker	22.5	Male	79
7	Smoker	49	Male	60

Characterization of hBEOs by IF staining

Human bronchial organoids were characterized by the immunofluorescence (IF) technique. Staining was performed for basal cell markers CK5, CK14, p63; ciliated cell marker acetylated alpha-tubulin, secretory cell marker SCGB3A2, goblet cell marker MUC5AC. Briefly, organoids were washed with DPBS before starting the protocol, then, 1%BSA (Sigma, A9418) containing DPBS was used for Matrigel dissociation. Organoids were incubated at 4°C for 1 hour on a shaker with gentle shaking. After the dissociation of organoids, they were collected into tubes and centrifuged for 3 min, at 100g. The supernatant was discarded, and cells were washed with DPBS containing 1% BSA, and incubated for 30 min at 4°C. Centrifuge was performed again. The IF protocol was applied after the total dissociation of organoids from Matrigel. Fixation was done with 4% paraformaldehyde. At the end of the permeabilization and blocking steps, primary antibodies were applied overnight at 4°C. The next day, after the washing steps, which were 2 hours of incubations with PBST at 4°C for 3 times, secondary antibody incubation was applied overnight at 4°C. Nuclei staining was performed using Hoechst dye (Sigma, B2261) together with secondary antibodies. Organoids were kept at 4°C in the dark until imaging. Images were taken by confocal microscope. Antibodies and their dilutions are listed in Tables 2.6 and 2.7.

Table 2. 6 Primary antibodies used in immunofluorescence imaging of hBEOs.

Name of the antibody	Dilution ratio
CK5 (Abcam, ab53121)	1:250
CK14 (Abcam, ab7800)	1:125
P63 (Abcam, ab53039)	1:125
Acetylated alpha tubulin (Abcam, ab24610)	1:50
SCGB3A2 (Abcam, ab181853)	1:250
MUC5AC (Invitrogen, 45M1)	1:50

Table 2. 7 Secondary antibodies used in immunofluorescence imaging of hBEOs.

Name of the antibody	Dilution ratio
Goat anti-Rabbit IgG (H+L) Highly Cross-Adsorbed Secondary Antibody, Alexa Fluor Plus 488 (Invitrogen, A32731)	1:100
Goat anti-Mouse IgG (H+L) Highly Cross-Adsorbed Secondary Antibody, Alexa Fluor Plus 594 (Invitrogen, A32742)	1:100

2.2 Treatment of hBEOs with $PM_{2.5}$ and ROS/RNS inhibitors

2.2.1 Collection and isolation of $PM_{2.5}$

$PM_{2.5}$ samples were collected from Alibeyköy, Istanbul Metropolitan Municipality Air Quality Centre by high volume samplers onto Teflon (PTFE) filters between 27.11.2021-16.06.2022, approximately for 7 months. Sampling was performed for 24 hours for each filter. Following the collection period, filters were kept in sterile dishes at 4°C until transferred to the laboratory. In the laboratory, firstly filters were cut into small pieces and sonicated in distilled water for 3-4 hours at 40 kHz. At the end of 3-4 hours, filters were transferred to dimethyl sulfoxide (DMSO) followed 3-4 hours more sonication. At the end of sonication, the solution containing particles was filtered with 40 µM filters to exclude filters from the $PM_{2.5}$ solution and kept overnight at -80°C. The next day, the solution was freeze-dried with a freeze dryer (ALPHA 1-2 LDplus, Christ) to exclude liquids. At the end of the sampling and extraction period, $PM_{2.5}$ samples

were aliquoted as 1 mg/ml $PM_{2.5}$ in DPBS and kept at -20°C until used in the experiments. The isolation protocol is summarized in Figure 2.3 below.

Figure 2. 3 $PM_{2.5}$ isolation protocol.

2.2.2 Dose optimization of $PM_{2.5}$ and ROS/RNS inhibitors by using BEAS-2B cell line

BEAS-2B cell culture

BEAS-2B cell line (normal human bronchial epithelial cells; CRL-9609, ATCC, 2022) was used to determine the effects of $PM_{2.5}$, and ROS/ RNS inhibitors on cell viability. BEAS-2B cells were cultured with RPM I-1640 medium (R6504, Sigma) containing 10% FBS (Sigma, F7524) and 1%Pen/Strep (Gibco, 10,000 U/mL) in T75 flasks. Confluent cultures were passaged onto 96-well plates as 10.000 cells/well, confluent cultures were used for treatment and cell viability analysis.

Treatment of BEAS-2B cells with $PM_{2.5}$ and ROS/RNS inhibitors

N-Acetyl-L-cysteine (NAC, 210-498-3, Merck) is widely used as an antioxidant and was used as an inhibitor of ROS at doses of 100, 500 µM, 1,2,4,5,8,10 and 20 mM doses. NG-Monomethyl-L-arginine acetate salt (L-NMMA, M7033, Sigma) was used at concentrations of 1,10,100,300,600 µM as an RNS inhibitor, which is a NOS inhibitor. Previously isolated $PM_{2.5}$ was used at concentrations of 25, 50, 100, 200, 400, 500, 800 µg/ml. Treatments were applied in single, double, and triple combinations for 24 hours.

MTT ((3-(4,5-dimethylthiazol-2-yl)-2,5-diphenyltetrazolium bromide) assay of BEAS-2B cells treated with $PM_{2.5}$ and ROS/RNS inhibitors

Culture media of confluent cultures of BEAS-2B cells were changed with serum-free media, cells were incubated in that media for a day, and treatments were done. At the end of 24 and 48 hours, the treatment protocol media was discarded.100 ul/well MTT (1mg/ml) dissolved in DPBS was applied to the cells for 1 hour at 37°C, 5% CO_2. After

1 hour, the solution was discarded, and 100 ul/well DMSO was added; cells were incubated for 10 more minutes. Then, cells were gently shaken for 5 min with a shaker, and measurements were done with a spectrophotometer at 540 nm.

2.2.3 Incubation of hBEOs with $PM_{2.5}$ and ROS/RNS inhibitors

Media was discarded at the end of the differentiation period of hBEOs (3-4 weeks), and hBEOs were washed with pre-warmed Dulbecco's phosphate-buffered salt solution (DPBS). Matrigel was dissolved by pipetting with ice-cold pipette tips using 1%BSA containing DPBS. hBEOs were kept at +4°C on mild shaking for approximately 1 h. for matrigel dissolvent. At the end of this procedure, they were collected and centrifuged at 320 x g for 5 min. The washing protocol was repeated until all matrigel residues were discarded and transferred into low attachment plates (83.3925.400, Sarsted). hBEOs were incubated at low attachment plates for 2 days. At the end of the second day, combined treatment of $PM_{2.5}$ (100 ug/ml) L-NMMA (100uM) and NAC (8 mM) dissolved in culture media was applied for 24 hours.

2.3 SARS-CoV-2 infection of hBEOs

2.3.1 SARS-CoV-2 isolation

Human SARS-CoV-2 was isolated from the nasopharyngeal swab samples of RT-PCR-positive COVID-19 patients. The swabs were cultured with Vero E6 cells in high glucose DMEM supplemented with %5 FBS, %1 Penicillin-Streptomycin, and Amphotericin B. Cytopathic effect (CPE) was monitored for 5-7 days. The growth of SARS-CoV-2 was confirmed by RT-PCR using primers for the N gene of SARS-CoV-2. A fifty-percent tissue culture infective dose (TCID50) assay was performed in 96 well plates, and TCID50 was calculated according to Spearman&Karber and Reed&Muench algorithms.

2.3.2 SARS-CoV-2 infection of hBEOs

After $PM_{2.5}$, ROS/RNS inhibitors treatment, at the end of 3rd day in low attachment plates, hBEOs were collected in 15 ml falcons in 1% BSA containing DPBS and transferred to the BSL-3 lab. Infection was done with a multiplicity of infection (MOI) of 0.5 for 2 hours in culture media at 37C, with 5% CO_2 in low attachment 96-well plates. At the end of 2 hours, media containing the virus was collected for further ELISA and

qPCR experiments. As a post-infection period, organoids were transferred into matrigel for 3 more days (72h). Lastly, matrigel was dissolved at the end of 3 days, and organoids were collected for gene analysis. Also, 3 days of culture media were collected for further ELISA and qPCR experiments.

2.5 Gene expression analysis of hBEOs and their supernatants treated with $PM_{2.5}$ and $PM_{2.5}$+inhibitors with or without SARS-CoV-2 infection

2.5.1 RNA isolation from hBEOs and supernatants treated with $PM_{2.5}$ and $PM_{2.5}$+inhibitors with or without SARS-CoV-2 infection

Total RNA isolation from hBEOs treated with $PM_{2.5}$ and $PM_{2.5}$+inhibitors with or without SARS-CoV-2 infection

At the end of hBEOs treatment with or without infection, they were collected with TRIzol reagent (Thermo Fischer; 15596026). RNA isolation was performed by Quick-RNA Miniprep Kit (R1054, Zymo Research). Organoids were lysed inside of TRIzol by the vortex. Chloroform was added with a 1:5 ratio, vortexed, and samples were centrifuged. The upper phase was collected for further RNA extraction. %100 ethanol was used with a 1:1 ratio to precipitate the RNAs, transferred to the RNeasy Mini Spin Column, where RNA molecules were selectively bound to the column membrane after centrifugation. Washing was done with wash buffers. Subsequently, the spin column was placed in a new microcentrifuge tube, and RNase-free water was added to elute the RNA. Centrifugation facilitated the collection of the eluted RNA, ensuring its separation from the column. RNA amount and purity were measured with Nanodrop 1000 (Thermo, USA).

Viral RNA isolation from hBEOs and supernatants treated with $PM_{2.5}$ and $PM_{2.5}$+inhibitors with SARS-CoV-2 infection

Supernatants OF hBEOs collected after 2 hours of infection and 72 hours post-infection were lysed with lysing buffer. The tube was then vigorously vortexed for 15 seconds to ensure proper mixing and subsequently incubated at room temperature for 10 minutes to facilitate complete lysis of viral particles. At this point, samples were transferred to BSL2 lab from BSL3 on ice. Following lysis, a 1:1 ratio of 96-100% ethanol was used for viral RNA precipitation. The entire lysate, including any precipitate, was then transferred to a Qiagen spin column placed in a 2 ml collection tube. Centrifugation

was carried out to facilitate the binding of viral RNA to the column membrane. Washing steps were performed to remove impurities and contaminants. The isolated viral RNA was eluted from the spin column membrane by transferring the column to a new 1.5 ml microcentrifuge tube provided by Qiagen. Next, RNase-free water was added directly to the center of the membrane, followed by incubation at room temperature for 1 minute. Centrifugation facilitated the elution of viral RNA into the microcentrifuge tube. RNA amount and purity were measured with Nanodrop 1000 (Thermo, USA).

2.5.2 Complementary DNA (cDNA) synthesis by using hBEO RNAs and SARS-CoV-2 RNAs

cDNA was obtained using an iScript kit (Bio-rad; 1708890). Tables 2.8 and 2.9 explain the mixture and protocol respectively.

Table 2. 8 cDNA synthesis mixture.

Components	**Volume per Reaction (µl)**
5x iScript Reaction Mix	4
iScript Reverse Transcriptase	1
RNA template (100 fg-1µg RNA)	Variable
Nuclease-free water	Variable
Total	20

Table 2. 9 cDNA synthesis thermal protocol.

Stage	**Temperature and Duration**
Priming	25°C- 5 min.
cDNA synthesis	46°C- 20 min.
Inactivation	95°C-1 min.
Hold	4°C-∞

2.5.3 Gradient PCR (Polymerase Chain Reaction) for primer optimization

Lyophilized primers were solubilized with distilled water. 56-58-60-62 °C were analyzed for each primer. PCR mix components and protocol are described in Tables 2.10 and 2.11 respectively.

Table 2. 10 Gradient PCR mixture.

Components	Amount
Dream Taq	10 ul- 1X
Primer mix	0.33-0.5 uM
cDNA	Variable (25 ng)
Nuclease free water	Adjust to 20 µl -

Table 2. 11 Gradient PCR Protocol

Stages	Temperature	Time duration	Cycle(s)
Stage 1	95 °C	2 min.	1
Stage 2	95 °C	30 sec.	40
	Different Temperatures	30 sec.	
	72 °C	1 min.	
Stage 3	72 °C	10 min.	1
	2 °C	∞	

2.5.4 Agarose gel electrophoresis for primer optimization

At the end of the gradient PCR protocol, samples and the DNA Ladder were mixed with nucleic acid binding dye and loaded into the 1.5% agarose gel, which was prepared with 1X TAE (Tris Acetate EDTA) buffer and run at 100V for 30 mins. Visualization was done with the ChemiDoc Imaging System (Bio-Rad).

2.5.5 Quantitative(q) PCR by using cDNA obtained from hBEOs and their supernatants treated with $PM_{2.5}$ and $PM_{2.5}$+inhibitors with or without SARS-CoV-2 infection

After RNA isolation, cDNA synthesis, and primer annealing temperature optimization, qPCR was applied to the samples. qPCR amplification mixes and thermal protocols for hBEOs can be seen in Tables 2.12 and 2.13 below. qPCR amplification mixes and thermal protocols for virus samples can be seen in Tables 2.14 and 2.15 below. The sequence of all human and SARS-CoV-2 primers used in the project is listed in Tables 2.16 and 2.17, respectively.

Table 2. 12 qPCR amplification mix content of hBEOs.

Content Name	**Volume**	**Final Concentration**
Roche Sybr Green (2x)	5 µl	1x
Primer (10 mM)	0.33 µl	0.33 mM
DNA (25 ng)	1 µl	-
Nuclease free water	Adjust to 10 µl	-

Table 2. 13 qPCR thermal protocol of HBEOs.

Pre incubation	**Amplification**	**Melting curve**
95 ºC- 5 min	95 ºC-10 sec.	95 ºC-5 sec.
1 cycle	Annealing: 60 ºC-30 sec.	65 ºC-1 min.
	Extension: 72 ºC-30 sec.	97 ºC-5 continuous
	40 cycles	

Table 2. 14 qPCR amplification mix contents of SARS-CoV-2.

Content Name	**Volume -Final Concentration**
Tagman Master Mix	10 µl- 1x
Forward Primer (5 mM)	0.5 µl -0.125 mM
Reverse Primer (5 mM)	0.5 µl -0.125 mM
Probe (2.5 mM)	0.25 µl -0,3125 mM
cDNA (125 ng)	5 µl -
Nuclease free water	Adjust to 20 µl -

Table 2. 15 qPCR thermal protocol OF SARS-CoV-2.

Stage	**Cycles-Temperature-Time**
Pre incubation	1X -95°C 7 min
Denaturation	45X-95°C-10 sec
Annealing	63°C-1min
Extension	72°C-30 sec
Cooling	4 °C- ∞

Table 2. 16 Sequences of human primers.

NCBI GENE SYMBOL (Gene Name)	GENE ID	Forward primer (5'-->3')	Reverse primer (5'-->3')	Annealing Temperature
SOD1 (Superoxide dismutase)	SOD1	TGAAGGTGTGGGGAAGCATT	TTTGGCCCACCGTGTTTTCT	58°C
NRF-2 (nuclear factor erythroid 2–related factor 2)	NFE2L2	ATGCAGCTTTTGGCGCAGAC	CAAGTGACTGAAACGTAGCCG	58°C
Caspase-1	CASP1	GAACTGGAGCTGAGGTTGACA	CCAGCTCTGTAGTCATGTCCG	58°C
HO-1 (heme oxygenase 1)	HMOX1	GGCCAGCAACAAAGTGCAAG	GTGTAAGGACCCATCGGAGAA	58°C

Bcl-2 (B-cell lymphoma 2)	BCL2	CTTTGAGTTCGGTGGGGTCA	GGGCCGTACAGTTCCACAAA	58°C
Caspase-9	CASP9	ATTTGGTGATGTCGGTGCTCT	ACTCACGGCAGAAGTTCACA	58°C
NQO1 (NAD(P)H dehydrogenase [quinone] 1)	NQO1	GGTTTGGAGTCCCTGCCATT	TTGCAGAGAGTACATGGAGCC	58°C
Keap1 (Kelch-like ECH-associated protein 1)	KEAP1	AGAGGAACGAGTGGCGAATG	GGCTACGAAAGTCCACGTCT	58°C
CYGB (Cytoglobin)	CYGB	GCCATCCTGGTGAGGTTCTT	ATGCAGGTTCTCCACGACAG	58°C
GPX4 (Glutathione peroxidase 4)	GPX4	TGAAGATCCAACCCAAGGGC	GCAGCCGTTCTTGTCGATGA	58°C
ACSL4 (acyl-CoA synthetase long-chain family	ACSL4	GGTTCTACTGGCCGACCTAA	TATGTCTCCTCCGGTCCCAG	58°C

member 4)				
ACE2 (Angiotensin converting enzyme 2)	ACE2	TCATGCCTATGTGAGGGCAAA	ACCCCACATATCACCAAGCA	60°C
TMPRSS2 (Transmembrane serine protease 2)	TMPRSS2	AAACCAGTGTGTCTGCCCA	GCCAGAACCCCAGCTTGTAT	60°C
FURIN (Furin)	FURIN	CATGGGTTCCTCAACCTGGG	GTTTAGTCCGTCGCTTTGCC	60°C

Table 2. 17 Sequences of hSARS-CoV-2 primers and probes.

Gene Name	**Sequences (5'-3')**
N1 Forward Primer	GACCCCAAAATCAGCGAAAT
N1 Reverse Primer	TCTGGTTACTGCCAGTTGAATCTG
N1 Probe	FAM-ACCCCGCATTACGTTTGGTGGACC-BHQ1
RdRP Forward Primer	AGATTTGGACCTGCGAGCG
RdRP Reverse Primer	

	GAGCGGCTGTCTCCAC AAGT
RdRP Probe	FAM – TTCTGACCTGAAGGCTC TGCGCG – BHQ-1

2.6 RNA Sequencing and data analysis of hBEOs treated with $PM_{2.5}$ and $PM_{2.5}$+inhibitors with SARS-CoV-2 infection

RNA isolation was performed as detailed in Section 2.5.1. Following isolation, the integrity and purity of RNA were assessed by NanoDropTM spectrophotometer (Thermo Scientific, Nanodrop 2000c) and RNA Nano 6000 Assay Kit of the Agilent Bioanalyzer 2100 system (Agilent Technologies, CA, USA), respectively. RNAs with integrity values >6.5 were retained for further processing. Filtering and analysis of the raw readings obtained as a result of the RNA sequencing reaction were performed in our laboratory. Raw data were first filtered to obtain high-quality reads ready for analysis. The filtering process was carried out using Trimmomatic v0.39 (Bolger et al., 2014)and fastp v0.20.0 (Chen et al., 2018) software. The filtering process included the following steps: (i) removal of adapter sequences, (ii) filtering of low-quality reads (< Q20, Phred score), (iii) removal of reads with a base length of less than 50 bp, and (iv) removal of low-quality sequences appearing in the first 5 bases of the reads. The reads before and after filtering were visualized with FASTQC v0.11.9 (https://www.bioinformatics.babraham.ac.uk/projects/fastqc/) software and quality data were collected by combining MultiQC v1.6 (Ewels et al., 2016) tool files. control file has been created. The high-quality RNA-Sequencing reads obtained as a result of filtering were transferred to the most current human genome in the GENCODE database (https://www.gencodegenes.org/human/) “human genome Release 34 (GRCh38.p13)”, genome annotation file (“Aligned using .gtf”). HISAT, StringTie, and Ballgown workflow software were used to align the genome, create the transcript sequence and model, and identify differentially expressed genes, respectively (Pertea et al., 2016). From the “.bam” file obtained as a result of genome alignment with HISAT2 software, transcript model (“.gtf”) and “transcript.fasta” sequences were obtained with StringTie software. The ".gtf" model in GENCODE with Gffcompare (https://ccb.jhu.edu/software/stringtie/gffcompare.shtml) software was compared with

the ".gtf" annotation model obtained as a result of StringTie software. Thus, the reference transcriptome data in GENCODE was compared with the transcriptome data we obtained as a result of the experiment, and the presence of new transcripts/transcript isoforms specific to our experimental groups was investigated. In addition, information regarding gene/transcript abundance estimation between groups was obtained in a normalized manner with StrigTie. Gene/transcript expression differences between groups were obtained with Ballgown software. Whether there was a statistical difference in the expression of a gene between groups was determined according to the following criterion: fold increase value log2FC > 1, adjusted p-value (< 0.05). These criteria are valid for both genes whose expression increases (up-regulated) and whose expression decreases (down-regulated). Principal component analysis was performed to determine whether there was harmony between the groups in terms of gene expression values, and the clustering status of the groups was visualized using the ClustVis (Metsalu & Vilo, 2015) internet tool. Visualization of differences in gene expression values between groups (volcano plot, MA plot, heatmap, etc.) was done with the DEBrowser (Kucukural et al., 2019)R package. Gene ontology (GO) enrichment analyses for categories such as biological process, molecular function, and cellular component of genes that differ in gene expression were performed using ShinyGO v0.61 (Ge et al., 2020). This was done via the internet tool (/bioinformatics.sdstate.edu/go/). Pathway enrichment analyses were performed using g: Profiler, GSEA, Cytoscape, and EnrichmentMap software together and by (Reimand et al., 2019) as carried out by following the methods developed.

2.4 Measurement of ROS (8-isoprostane)/RNS (nitrate+nitrite, nitrate, nitrite) and inflammatory cytokines (IL1β, TNFα, GM-CSF, IL-6 and IL-8) in COVID-19 patients and healthy individuals plasma samples and hBEOs' supernatants

2.4.1 Measurement of ROS(8-isoprostane) /RNS (nitrate+nitrite, nitrate and nitrite) and inflammatory cytokines (IL1β, TNFα, GM-CSF, IL-6 and IL-8) in COVID-19 patients and healthy individuals plasma samples

Subject Requirement

A total of 55 patients from Koc University Hospital, 40 from Yedikule Chest Diseases and Thoracic Surgery Training and Research Hospital, and 20 control subjects were recruited between 01.07.2020 and 23.03.2021. Patients who were 18 or older with a confirmed diagnosis of COVID-19 (with PCR and tomography) and healthy individuals

who were not diagnosed with COVID-19 were included in the study. The severity of the patients was determined based on WHO guidelines named “Living guidance for clinical management of COVID-19” (WHO, 2021). The study was approved by the Koc University Biomedical Research Ethical Committee (2020. 448.IRB2.122). Each participant gave informed consent before participating in the study. Demographics of patients and healthy controls are presented in Table 2.18. The number of samples used for each parameter is exhibited in Table 2.19.

Table 2. 18 Demographics of COVID-19 patients and healthy controls.

	CONTROL	**MILD**	**MODERATE**	**SEVERE**
Age (Mean-Range)	41.10 (58-24)	45.84 (24-85)	59.03 (22-81)	66 (23-83)
Female	n=11 (55%)	n=16 (50%)	n=19(54.28%)	n=12 (42.86%)
Male	n=9 (45%)	n=16 (50%)	n=16(45.72%)	n=16 (57.14%)

Table 2. 19 The number of healthy controls and patients included in each assay.

	CONTROL (n)	MILD (n)	MODERATE (n)	SEVERE (n)
Total Subjects	20	32	35	27
8-isoprostane	9	11	11	10
Nitrate+nitrite	20	20	20	20
Nitrate	20	20	20	20
Nitrite	18	20	20	19
IL-6	13	20	18	20
IL-8	18	18	19	19
IL-1β	14	17	20	19
TNF-α	16	18	20	16
GM-CSF	16	18	18	17

Plasma Sampling

A total of 9 ml of human blood samples were collected into whole blood tubes containing EDTA. Samples were transferred to the lab on ice. Plasma samples were isolated via centrifugation at 4°C, 2500 x g for 10 min, and then, stored at -80°C until they were analysed.

Nitrate/Nitrite colorimetric assay kit, 8-isoprostane kit, and ELISA (Enzyme-Linked Immunosorbent Assay) application

As a reactive nitrogen species indicator nitrate+nitrite, only nitrate and nitrite levels of isolated plasma samples were measured using a Nitrate/Nitrite colorimetric assay kit according to the manufacturer's instruction (780001, Cayman Chemical). Before the assay application, plasma samples were ultrafiltered with Amicon 30 kDa ultrafilters (UFC503096, Merck). Firstly, all reagents were equilibrated at room temperature. Lyophilized standards are prepared with sample diluent for standard curve constitution separately for nitrate and nitrate+nitrite. For nitrate+nitrite measurement, samples and standards were loaded into wells, and an enzyme cofactor mixture together with Nitrate reductase mixture was added onto them and incubated at room temperature for 3 hours. At the end of 3 hours, Griess reagent R1 was added together with R2 and incubated at room temperature for 10 mins. for color development. Absorbance was measured at 540 nm. For nitrite measurement, color was developed 10 mins after the addition of the Griess reagents. incubation at room temperature and directly absorbance was measured at 540 nm. To calculate nitrite concentration, nitrate concentration is subtracted from nitrate+nitrite concentration.

As a reactive oxygen species indicator, the 8-isoprostane level of isolated plasma samples was measured using an 8-isoprostane kit according to the manufacturer's instructor (ab175819, Abcam). Firstly, all reagents were equilibrated at room temperature. Lyophilized standards were prepared with sample diluent for standard curve constitution. Firstly, plasma samples were mixed with acetic acid and ethyl acetate, vortexed, and centrifuged, and 3 phases were obtained for each sample. The lower phase, an aqueous phase, was used to repeat the ethyl acetate step 2 times more. Each time, the upper phase, which contains lipoproteins, was pooled. At the end of the third time,

lipoproteins were dried to get extracted sediment containing dried fatty acids. The saponification step was applied to cleave fatty acids from the glycerol backbone. Later, samples were diluted with distilled water, and the pH was arranged to 5.5 with formic acid, centrifuged, and the upper phase was collected. It was repeated 2 more times too. Lastly, the upper phase containing saponified lipids was dried. Dried sediments were mixed with ethanol and sample dilution buffer. Samples and standards loaded into wells. HRP conjugate was added to each well and incubated for 2h at room temperature. Washing was done, and TMB (3,3′,5,5′-Tetramethylbenzidine) substrate was used for colorimetric measurement. Incubated 15-20 min. at room temperature, and sulfuric acid was used for color formation. Absorbance was measured at 450 nm.

Cytokine measurements were performed for IL-6 (Human IL-6 DuoSet ELISA, DY206-05), IL-8 (Human IL-8/CXCL8 DuoSet ELISA, DY208-05), IL-1β (Human IL-1 beta/IL-1F2 DuoSet ELISA, DY201-05), TNF-α (Human TNF-alpha DuoSet ELISA, DY210-05) and GM-CSF (Human GM-CSF DuoSet ELISA, DY215-05) according to manufacturer's instructor (R&D Systems). Firstly, all reagents were equilibrated at room temperature. Lyophilized standards were prepared with sample diluent for standard curve constitution. Wash buffer, together with substrate and stop solutions, were prepared based on the manufacturer's instructions. 96 well plate coated with capture antibody, incubated overnight at room temperature at dark. Following-day washings were done to eliminate unbounded antibodies; blocking was performed to prevent non-specific binding. Samples and standards were loaded into the wells and incubated at room temperature for 2h. At the end of 2 hours, washing was done, and the detection antibody was loaded into the wells and incubated at room temperature for 2 hours. Later, washing was repeated. Streptavidin/ HRP incubation was done for 20 minutes. For colorimetric measurement, substrate solution was used and incubated for 20 mins. Lastly, a stop solution was used to terminate the reaction. Measurements were done with a spectrophotometer at 450 nm.

2.4.2 Measurement of inflammatory cytokines (IL-6 and IL-8) in hBEOs supernatants

Transfer of SARS-CoV-2-infected culture media from the BSL3 lab to the BSL2 lab

A deactivation protocol was applied to transfer the organoids' supernatant from the BSL3 to the BSL2 lab. So, at the end of the infection protocol, 1/1000 media volume of beta propiolactone (BPI) was added to the supernatants. Samples were incubated at 4C

for 16 hours and then 37C for 2 hours. At the end of 18 hours, samples were taken out of the BSL3 lab and kept at -80C until used.

ELISA

Cytokine measurements from supernatants of hBEOs treated with $PM_{2.5}$ and inhibitors with or without SARS-CoV-2 infection were performed for IL-6 (Human IL-6 DuoSet ELISA, DY206-05) and IL-8 (Human IL-8/CXCL8 DuoSet ELISA, DY208-05) according to the manufacturer's instructor (R&D Systems) as described in 4.1.3.

2.7 Statical Analysis

Data were tested for normality with the D'Agostino and Pearson omnibus normality test, and comparison among groups was performed using one-way analysis of variance (ANOVA)/Dunnett's multiple comparison tests or Kruskal–Wallis/Dunn's multiple comparison tests together with 2-way ANOVA test. To assess the predictive accuracy of measured data, receiver-operating characteristic (ROC) analysis was performed. The results are expressed as means ± STD or medians ± interquartile ranges (Q1 and Q3). $p \leq 0.05$ was regarded as significant. Statistical analysis was performed using PRISM version 9 (GraphPad Software Inc., San Diego, CA, United States).

CHAPTER 3

RESULTS

3.1 Culture of hBEOs

3.1.1 Culture of hBECs

Bronchial epithelial cells started to proliferate approximately 5-6 days after the dissection and culture of the bronchial epithelium. As shown in Figure 3.1B below, in 10-15 days, cells around the tissue piece can be visualized under the phase contrast microscope.

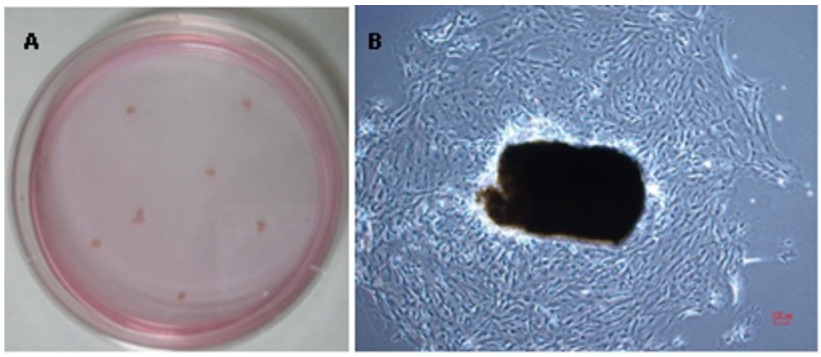

Figure 3. 1 Bronchial epithelium explants in the petri dish after dissection (A), bronchial epithelial cells outgrown from the explant, 2 weeks after dissection (B). The image was taken by phase-contrast microscopy at 4X magnification. Scale bar=100 µm

At the end of the 3rd-4th week, they become confluent cultures, epithelial cuboidal shape, and barrier in between neighboring cells can be seen in Figure 3.2 below with 10X,20X, and 40X magnification.

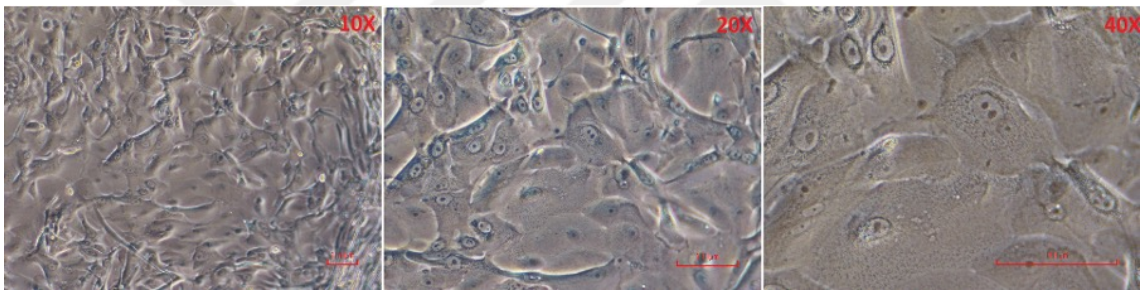

Figure 3. 2 Bronchial epithelial cell images were taken by phase-contrast microscopy at 10X, 20X, and 40X magnification, respectively. Scale bar=100 µm.

Characterization of primary hBECs by IF staining

Primary bronchial epithelial cell cultures obtained from the explants were characterized by demonstrating the presence of basal cells (CK5, CK14, and p63 positive), secretory cells (SCGB3A2 positive), goblet cells (MUC5AC positive), and ciliated cells (FOXJ1 positive) in cultures together with epithelial barrier markers E-cadherin, occludin as shown in Figures 3.3-3.8.

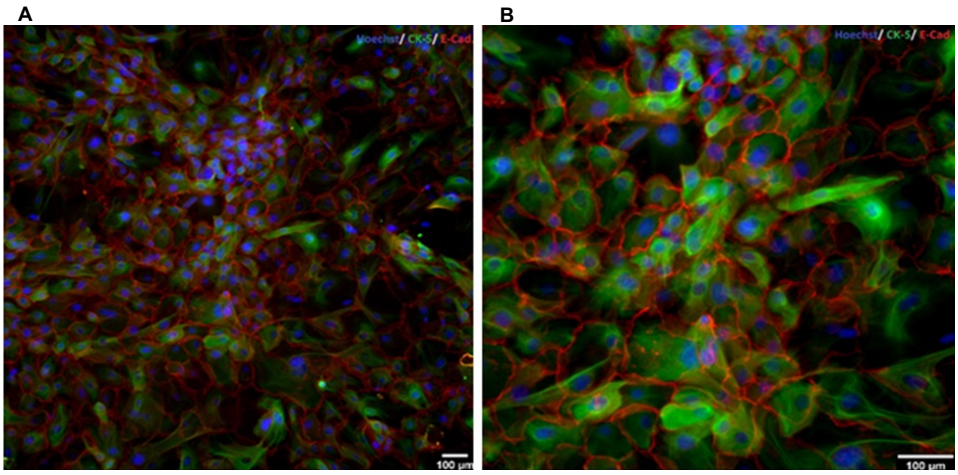

Figure 3. 3 Immunofluorescence staining of CK5 (green) and E-Cadherin (red) in primary bronchial epithelial cells at 10X (A) and 20X (B) magnification, respectively. Hoechst (blue) was used for nuclear staining, scale bar=100 µm.

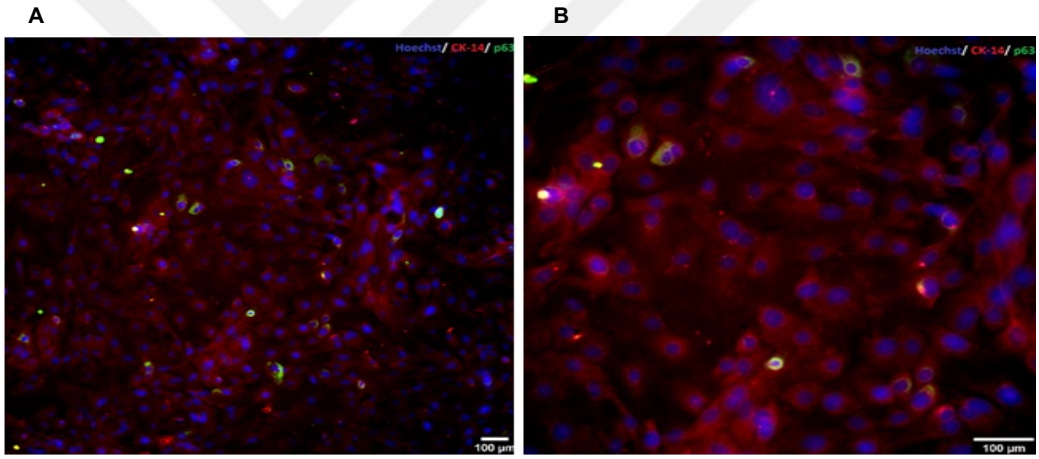

Figure 3. 4 Immunofluorescence staining of CK14 (red) and p63 (green) in primary bronchial epithelial cells at 10X (A) and 20X (B) magnification, respectively. Hoechst (blue) was used for nuclear staining, scale bar=100 µm.

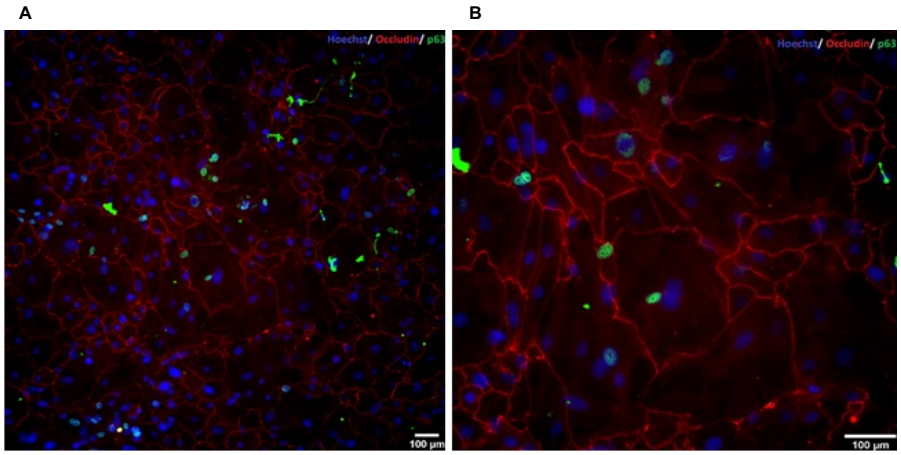

Figure 3. 5 Immunofluorescence staining of occludin (red) and p63 (green) in primary bronchial epithelial cells at 10X (A) and 20X (B) magnification, respectively. Hoechst was (blue) used for nuclear staining, scale bar=100 µm

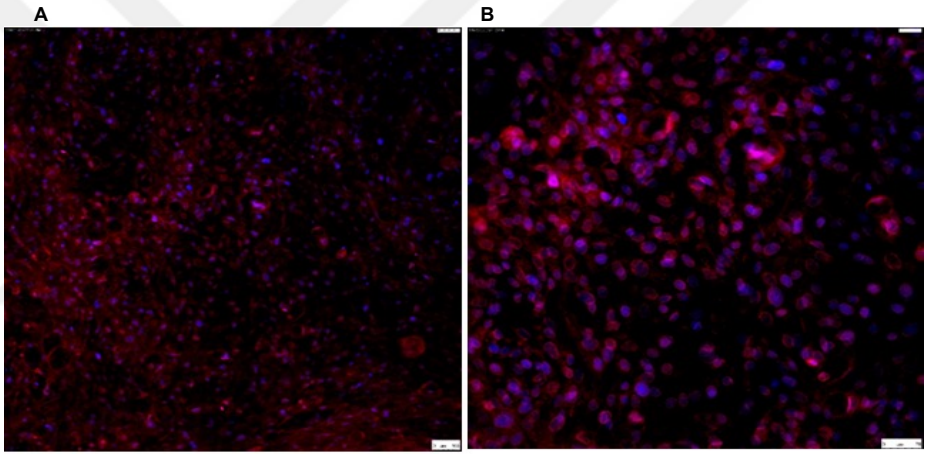

Figure 3. 6 Immunofluorescence staining of FOXJ1 (red) in primary bronchial epithelial cells at 10X and 20X magnification, respectively. Hoechst (blue) was used for nuclear staining, scale bar=100 µm and 75 µm, respectively.

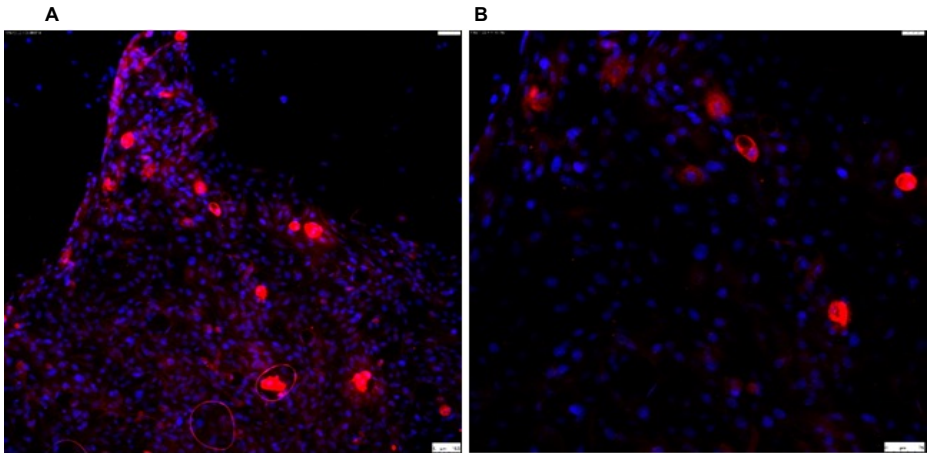

Figure 3. 7 Immunofluorescence staining of MUC5AC (red) in primary bronchial epithelial cells at 10X and 20X magnification, respectively. Hoechst (blue) was used for nuclear staining, scale bar=100 µm, 75 µm, respectively.

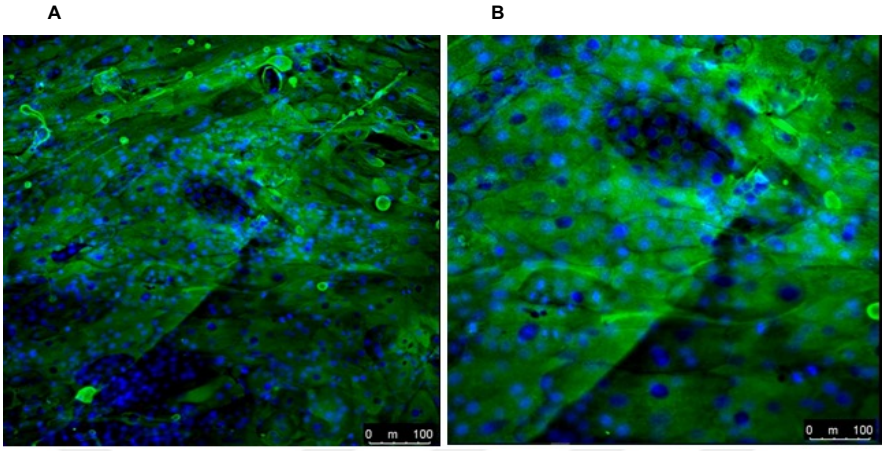

Figure 3. 8 Immunofluorescence staining of SCGB3A2 (green) in primary bronchial epithelial cells at 10X and 20X magnification, respectively. Hoechst (blue) was used for nuclear staining, scale bar=100 µm.

3.1.2 Culture of healthy primary human bronchial epithelial cell line (02AB0839.02, Epithelix)

The purchased healthy primary human bronchial epithelial cell line was proliferated and passaged as a backup plan to produce organoids from non-smokers. As seen in Figures 3.9 and 3.10 below, it took approximately 15-20 days for each flask to become confluent and ready for further experiments. Passage 3 cells were used for organoid production.

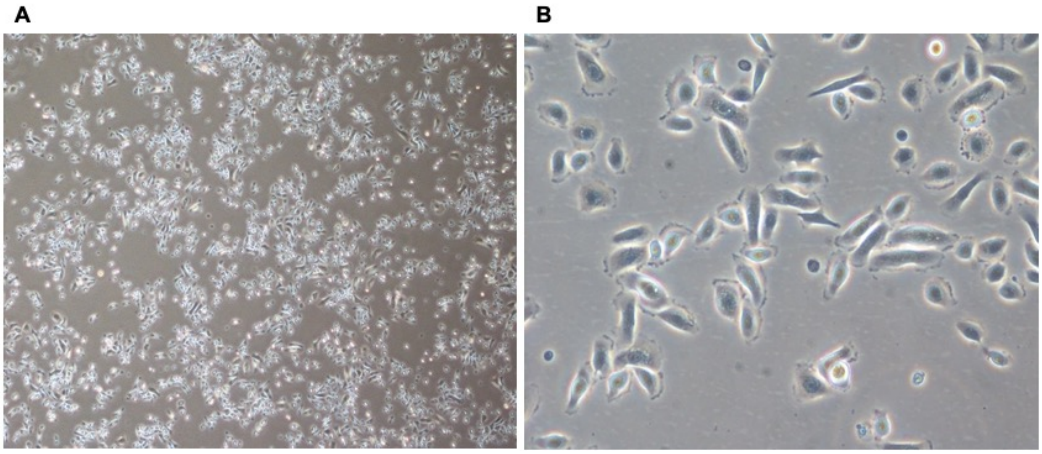

Figure 3. 9 Phase contrast images of 1-week healthy human primary bronchial epithelial cells at 4X (A) and 20X(B).

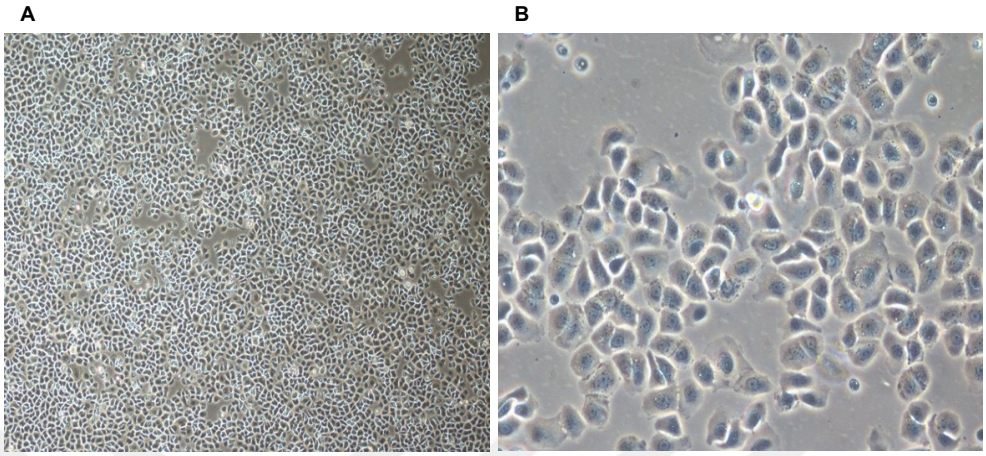

Figure 3. 10 Phase contrast images of 3-week healthy human primary bronchial epithelial cells at 4X (A) and 20X (B).

3.1.3 hBEOs Formation

~75.000-150.000 cells from one patient's bronchial explants were obtained, and organoids were established in approximately 30-50 wells. Also, 60-80 well organoids were obtained from the cell line in each setup. Organoids were maintained for 1 month.

At the end of 1st week, the organoid shape started to appear, as shown in Figure 3.11. Images of 1-month organoids are presented in Figure 3.12.

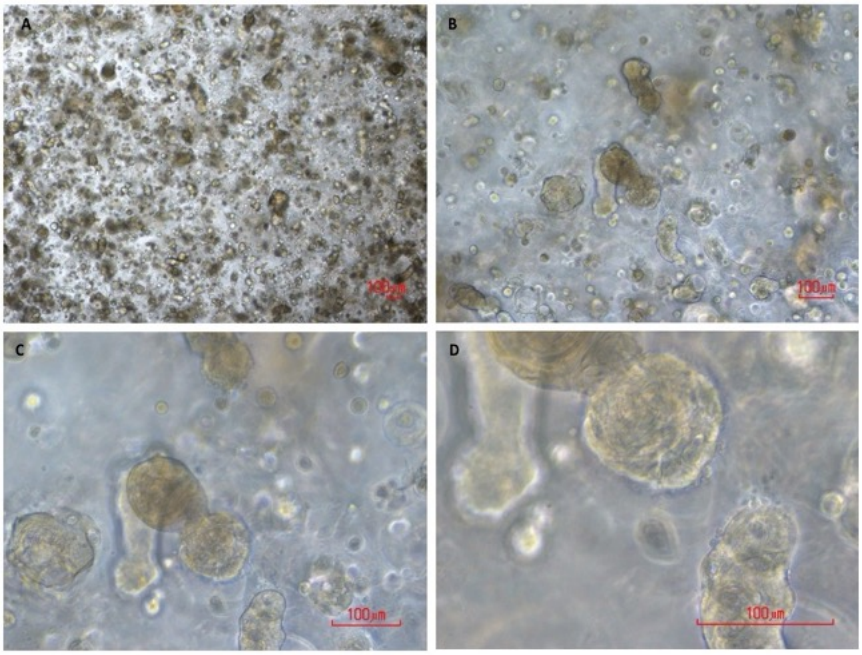

Figure 3. 11 Phase contrast microscope images of primary human bronchial epithelial organoids obtained from primary bronchial epithelial cells isolated from bronchial tissue at the end of 1st week at 4X, 10X, 20X, and 40X magnification, respectively. Scale bar=100 µm.

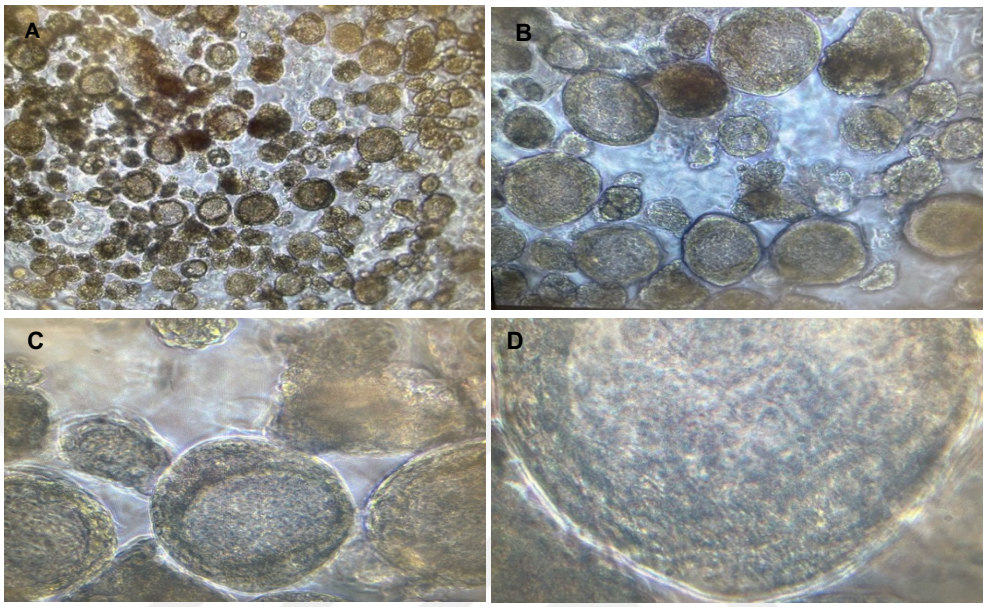

Figure 3. 12 Phase contrast microscope images of primary human bronchial epithelial organoids obtained from primary bronchial epithelial cells isolated from bronchial tissue at the end of 1st week at 4X, 10X, 20X, and 40X magnification, respectively. Scale bar=100 µm.

As seen in Figures 3.13- 15 respectively, the diameter of organoids was measured at the end of the 2nd, 3rd, and 4th week. It was approximately 150-200 µm at the end of 2nd week. It became around 200-250 µm 1 week later, and the lumen started to be seen that week. At the end of 4th week, the diameter of organoids was higher than 250 µm, and a lumen was formed. There were 30-50 organoids per well.

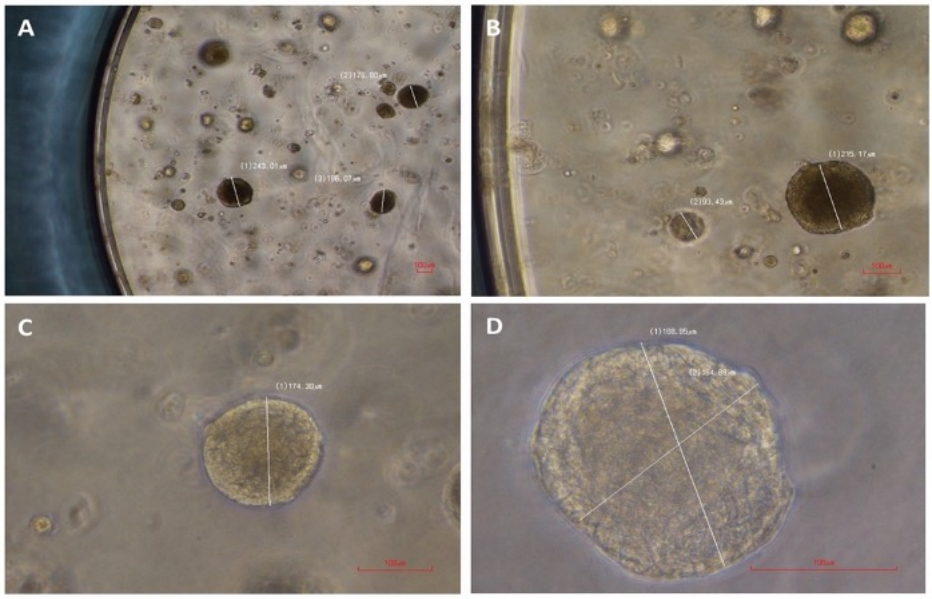

Figure 3. 13 Phase contrast microscope images of primary human bronchial epithelial organoids at the end of 2nd week at 4X, 10X, 20X, and 40X magnification, respectively. Scale bar=100 µm

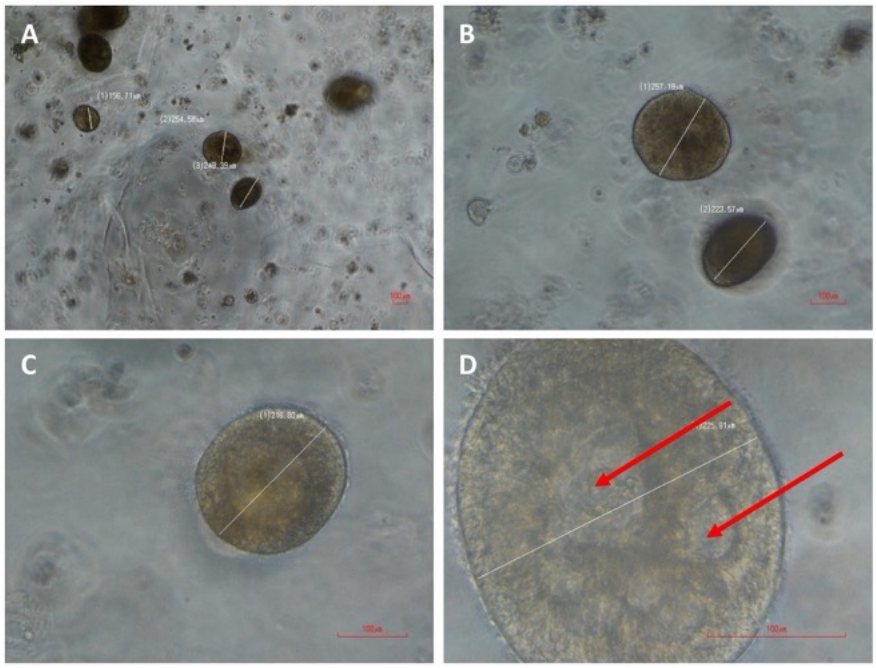

Figure 3. 14 Phase contrast microscope images of primary human bronchial epithelial organoids at the end of 3rd week at 4X, 10X, 20X, and 40X magnification, respectively. Scale bar=100 µm. Arrows show the lumen formation points.

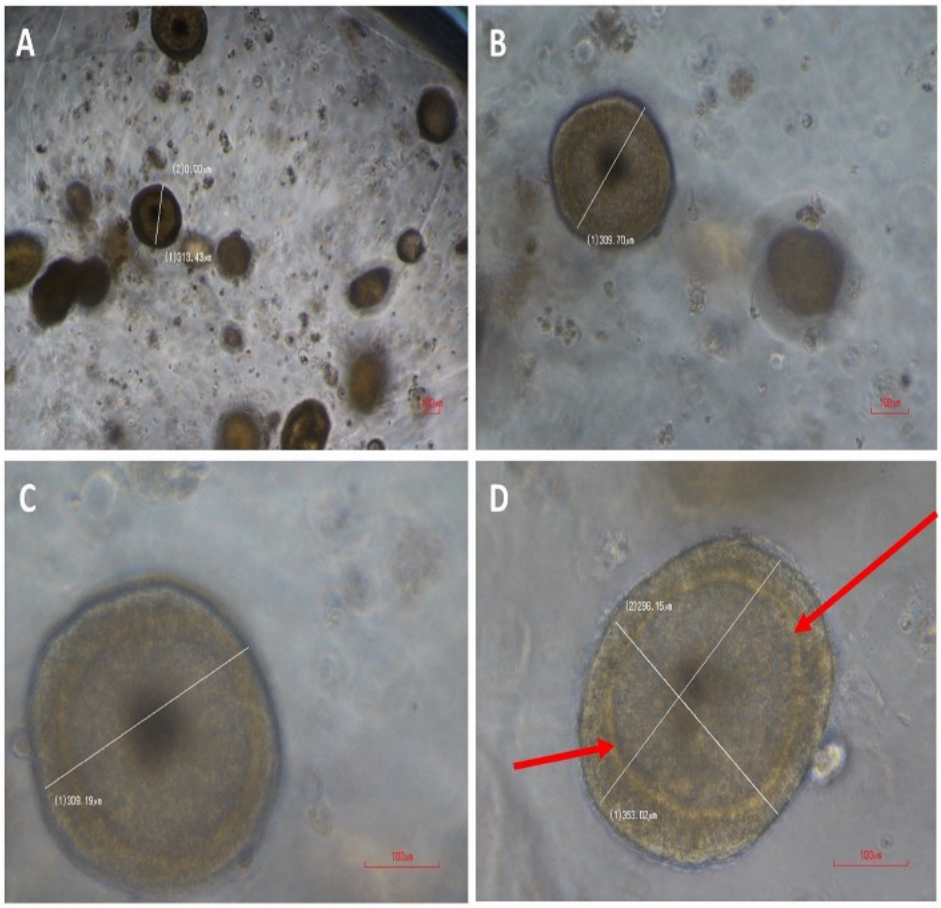

Figure 3. 15 Phase contrast microscope images of primary human bronchial epithelial organoids obtained from primary bronchial epithelial cells line at the end of 4th week at 4X, 10X, 20X, and 40X magnification, respectively. Scale bar=100 µm. Arrows show the lumen boundary point.

At the end of 4th week, also bright-field microscope images were taken at 10x and 20x with LEICA DMi8) as seen in Figures 3.16 and 3.17, respectively.

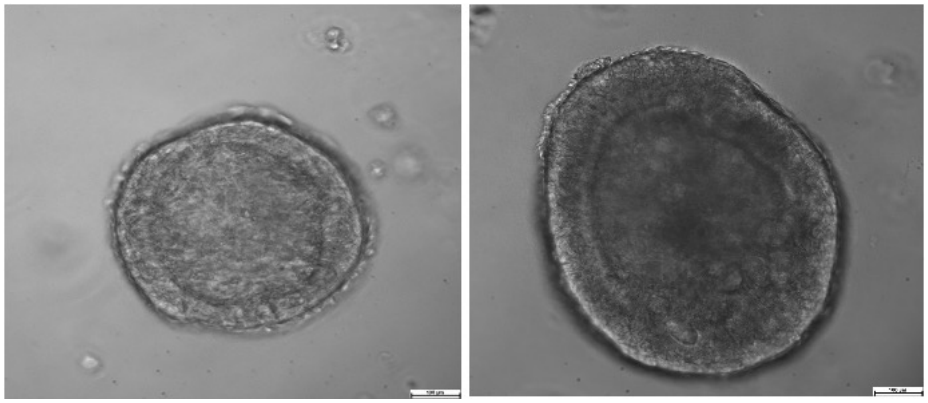

Figure 3. 16 Bright-field microscope images of primary human bronchial epithelial organoids at the end of 4th week at 10X magnification. Scale bar=100 µm.

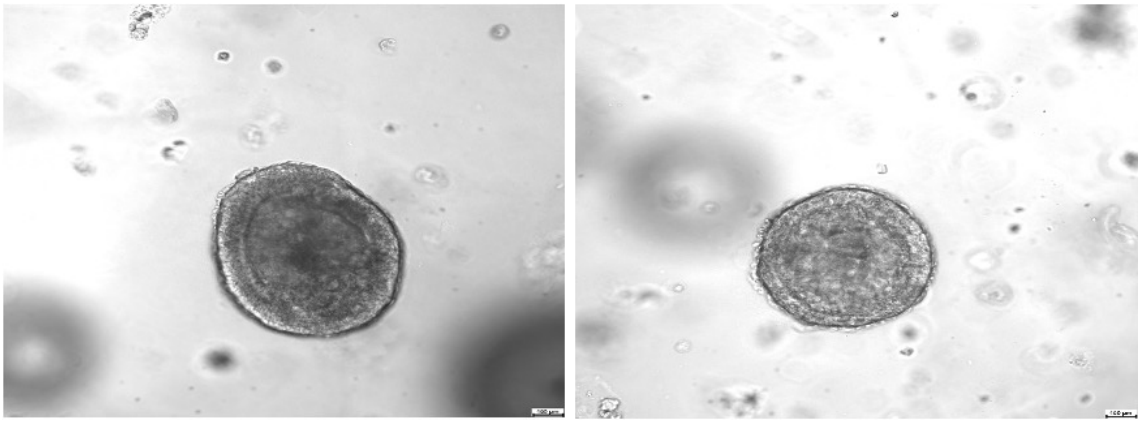

Figure 3. 17 Bright-field microscope images of primary human bronchial epithelial organoids at the end of 4th week at 20X magnification. Scale bar=100 μm.

Obtained hBEOs were treated with $PM_{2.5}$, ROS, and RNS inhibitors with or without infection as described in the methods. They were used for further analysis. As shown in Table 2.5 below, organoids were obtained from 6 different patient's tissue-derived bronchial epithelial cells and healthy primary bronchial epithelial cell lines. All of them were treated with $PM_{2.5}$ and $PM_{2.5}$ + inhibitors for further experiments. Furthermore, organoids obtained from healthy primary bronchial epithelial cell lines and one of the smoker patients' organoids were used for SARS-CoV-2 infection experiments following treatments. Passage 3 cells were used for the cell line to establish organoid structure. However, smoker organoids infected with SARS-CoV-2 were only used for qPCR analysis from supernatant to prove SARS-CoV-2 infection and incubation of organoids. Due to the low number of organoids, they were not enough to conduct gene analysis.

Characterization of hBEOs by IF staining

Human bronchial organoids were characterized by the IF technique. Staining was performed for basal cell markers CK 5, 14, and p63; ciliated cell marker acetylated alpha-tubulin; secretory cell marker SCGB3A2; and goblet cell marker MUC5AC. Images were taken with a confocal microscope, as shown in Figures 3.18, 3.19, and 3.20 below.

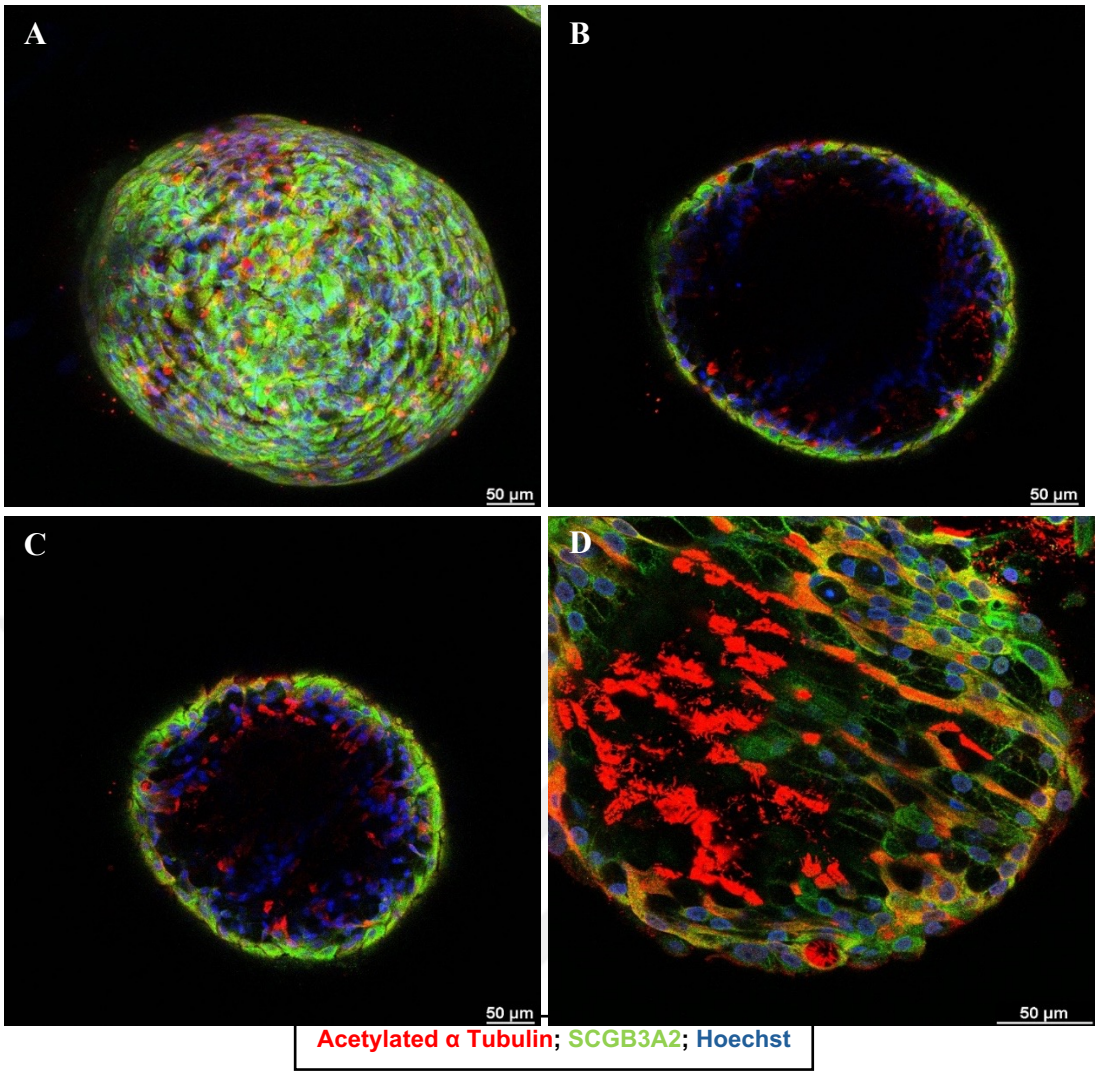

Figure 3. 18 Immunofluorescence staining of acetylated alpha-tubulin (red, cilia) and SCGB3A2 (green, cytoplasm) of primary human bronchial epithelial organoids at the end of 4th week at 20X (A-C) and 40x (D) magnifications. Hoechst (blue) used for nuclear staining, Scale bar=50 µm.

As seen in Figure 3.18C, acetylated alpha-tubulin mainly observed in the luminal part of the organoids while club cell marker SCGB3A2 is mostly located in the outer surface of the organoids.

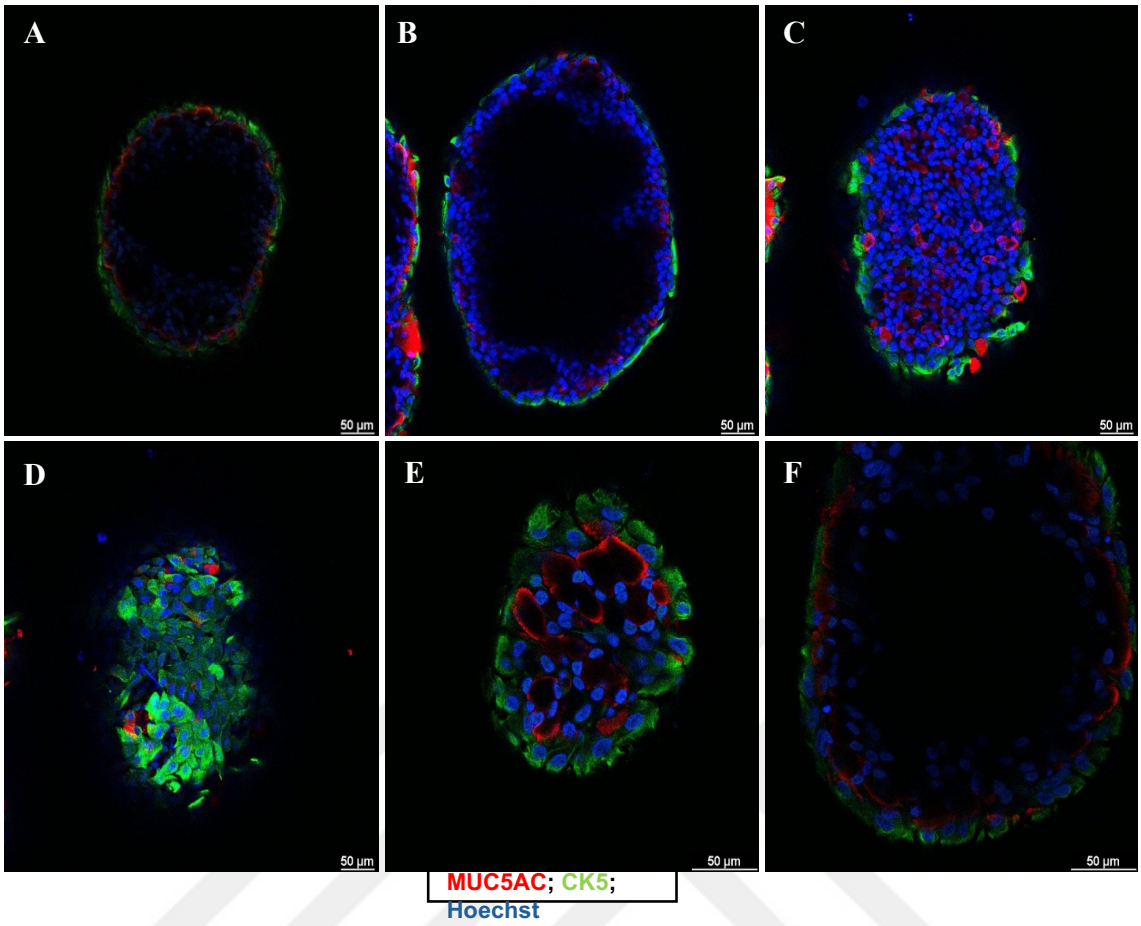

Figure 3. 19 Immunofluorescence staining of MUC5AC (red, lumen and cytoplasm) and CK5 (green, cytoplasm) of primary human bronchial epithelial organoids at the end of 4th week at 20X (A-D) and 40X (E and F) magnifications. Hoechst (blue) used for nuclear staining, Scale bar=50 µm.

As seen in Figure 3.19, MUC5AC is mainly observed on the surface of the epithelial cells that form the organoid, facing the lumen and occasionally in the cytoplasm. CK5, on the other hand, marked the cytoplasm of basal cells, which mainly covers the outer surface of the organoid and is located at the base of the further differentiated epithelial cells in vivo.

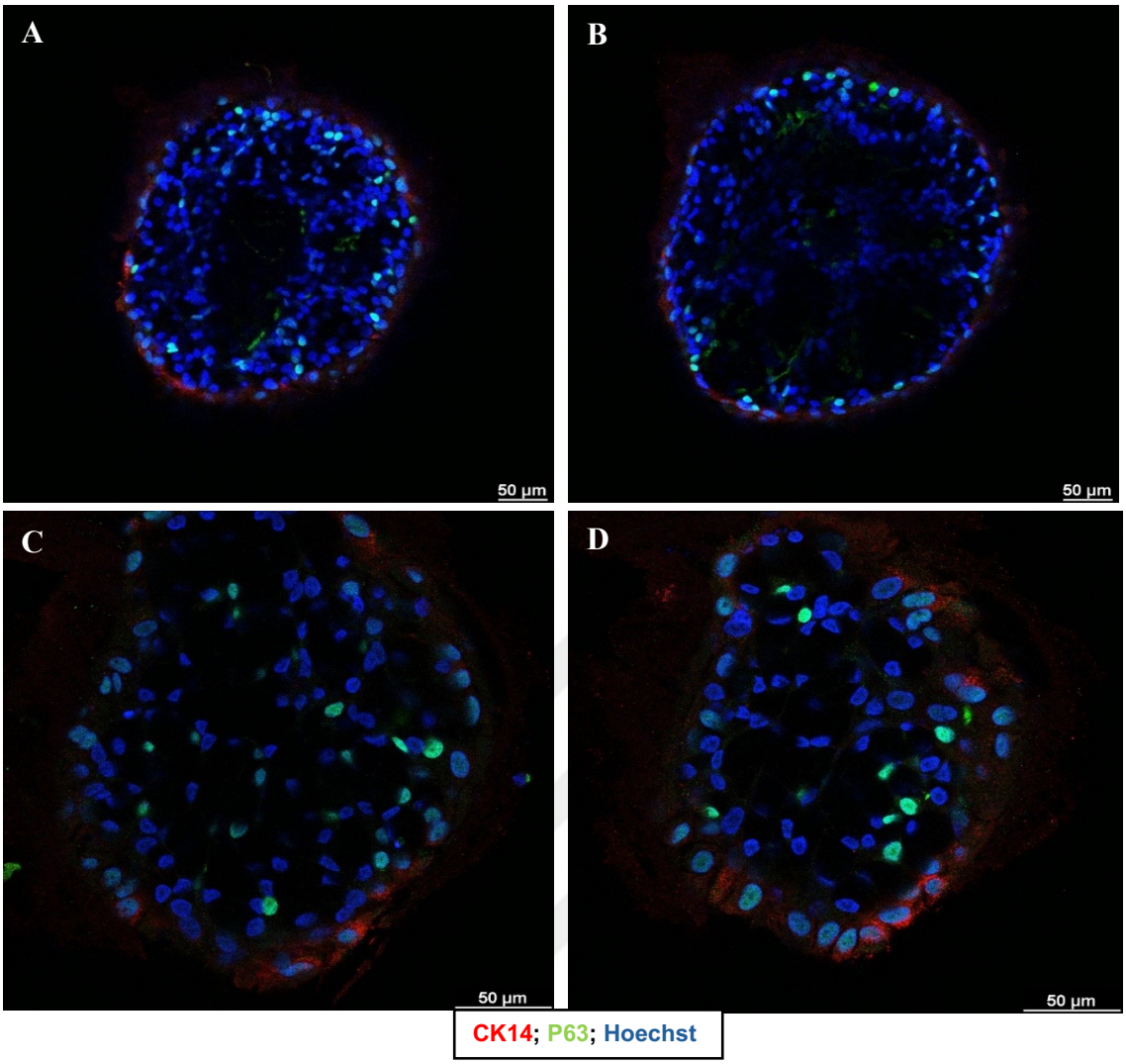

Figure 3. 20 Immunofluorescence staining of CK14 (red, cytoplasm) and p63 (green, nucleus) of primary human bronchial epithelial organoids at the end of the 4th week at 20X (A and B) and 40X (C and D) magnifications. Hoechst (blue) used for nuclear staining, Scale bar=50 µm.

CK14 marked the cytoplasm of basal cells, mainly covering the organoid's outer surface, as shown in Figure 3.20, and it is located at the base of the differentiated epithelial cells in vivo. Another basal cell marker is p63, located in the cell's nucleus, and CK14 is expressed in the cytoplasm of basal cells. Both markers are expressed in the outermost layer, forming the organoid. This indicates that basal cells form the outermost layer of luminous organoids. On the other hand, the organoids we obtained contained progenitor cells forming the airway epithelium and highly differentiated cells containing ciliated, mucous, and secretory cell markers.

Z stack images were analyzed using the FIJI program. Six different images were used for each sample. Red and green colors were normalized by using nucleus staining blue color. Counts of each cell type were calculated as shown in Figure 3.21. These results have demonstrated that the organoids we obtained are fully differentiated in one month, which may represent the features of bronchial epithelium. The percentages of cells are also presented in Table 3.1.

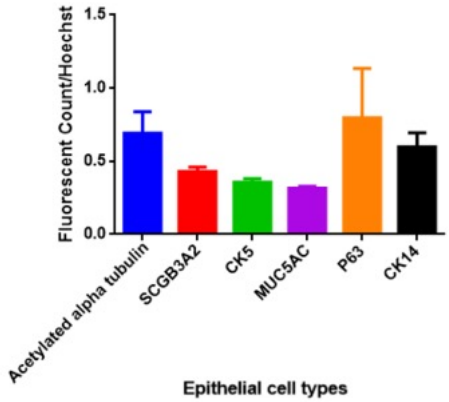

Figure 3. 21 The ratio of each epithelial cell type in organoids is normalized by nucleus staining (Hoechst).

Table 3. 1 Percentage of each epithelial cell type in organoids.

Epithelial Cell Type	**Percentage in organoid**
Acetylated alpha tubulin	21.66%
SCGB3A2	13.47%
CK5	11.19%
MUC5AC	9.87%
P63	25.01%
CK14	18.77%

3.2 Treatment of hBEOs with $PM_{2.5}$ and ROS/RNS inhibitors

3.2.1 Dose optimization of $PM_{2.5}$ and ROS/RNS inhibitors by using BEAS-2B cell line

BEAS-2B cell culture

Confluent BEAS-2B cells, seen in Figure 3.22 below, were used for cell viability analysis.

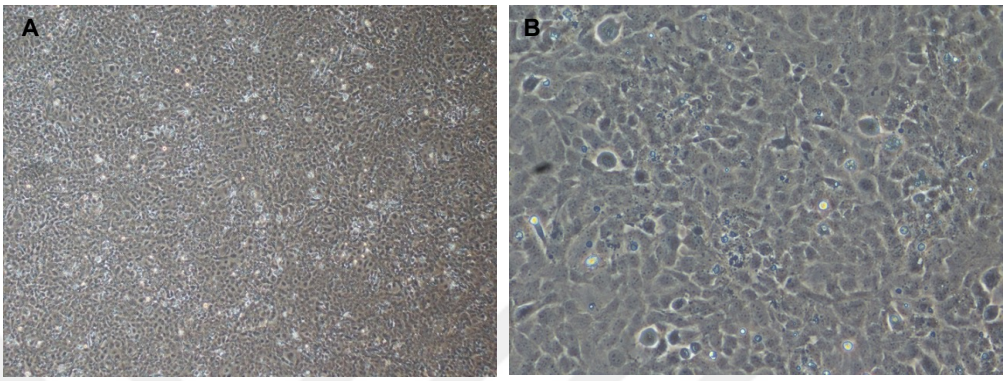

Figure 3. 22 Phase contrast images of confluent BEAS-2B cell cultures at 4X (A) and 20X (B).

MTT assay of BEAS-2B cells treated with $PM_{2.5}$ and ROS/RNS inhibitors

Firstly, $PM_{2.5}$, NAC, and L-NMMA were applied in different concentrations separately to choose the optimum dose for cell viability (MTT) experiments. As seen in figure 3. 23, for $PM_{2.5}$, there was a significant decrease in 100 µg/ml (mean=72.63; *p<0.05), 400 µg/ml (mean=64.22; **p<0.01), 500 µg/ml (median=39.449=0.122; ****p<0.0001) and 800 µg/ml (mean=17.55; ****p<0.0001) compared to control (mean=100). Since 100 µg/ml and 400 µg/ml were almost the same, 100 µg/ml was chosen as a proper concentration above the IC50 (Half-maximal inhibitory concentration) value. Also, 200 µg/ml was selected for further analysis. For L-NMMA, there was a significant increase in cell viability in 10 µM (mean=0.411; *p<0.05), 100 uM (mean=134.50; **p<0.01), 300 µM (mean=145.50; **p<0.01), compared to control (mean=100). These concentrations were chosen for further tests. For NAC, there was no significant decrease in the viability of cultures incubated with any doses of NAC; only 8 mM (mean=129.33; *p<0.05) increased the viability significantly compared to the control (mean=100).

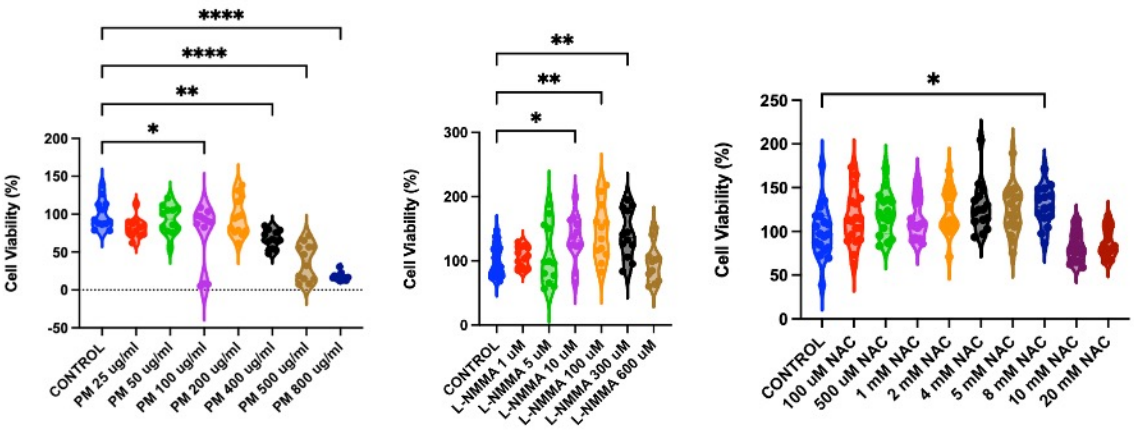

Figure 3. 23 MTT results of BEAS-2B cells only treated with $PM_{2.5}$ (25-50-100-200-400-500-800 µg/ml) (A), L-NMMA (1-5-10-100-300-600 µM) (B), NAC (100-500 uM,1-2-3-5-8-10-20 mM) (C). *p<0.05, **p<0.01, ****p<0.0001. $PM_{2.5}$, particulate matter; L-NMMA, NG Methyl-L-arginine acetate salt; NAC, N-acetyl cysteine.

Secondly, inhibitors and $PM_{2.5}$ are applied simultaneously to understand whether those inhibitors can inhibit the effect of $PM_{2.5}$ on cells. As seen in Figure 3.24, for 100 µg/ml $PM_{2.5}$ treatment (mean=66.90; *p<0.05), there was a significant reduction in cell viability compared to the control (mean=100). It was reversed with the L-NMMA treatment together with $PM_{2.5}$. There was a significant escalation in 100 µg/ml PM2.5 +10 µM L-NMMA (mean=102.22; *p<0.05), 100 µg/ml $PM_{2.5}$ +100 µM L-NMMA (mean=127.80; ****p<0.0001), 100 µg/ml $PM_{2.5}$ +300 µM L-NMMA (mean=131.78; ****p<0.0001) compared to only 100 µg/ml $PM_{2.5}$ treatment. There was a significant decrease in 200 µg/ml $PM_{2.5}$ application (mean=70.32; *p<0.05) compared to control (mean=100). It was a similar result with 100 µg/ml $PM_{2.5}$ application. Due to that, 100 µg/ml $PM_{2.5}$ was determined for the experiment setup. Since the 100 µM and 300 µM L-NMMA concentrations gave almost the same results, 100 µM was chosen for further analysis.

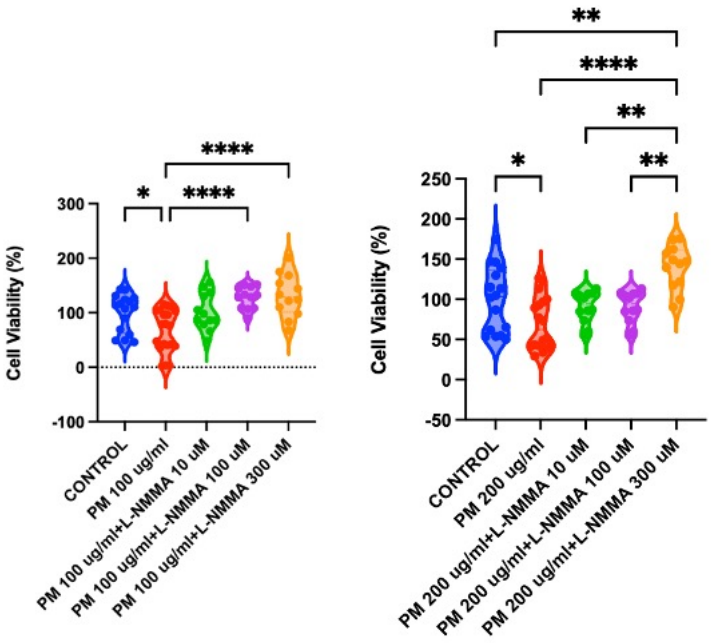

Figure 3. 24 MTT results of BEAS-2B cells $PM_{2.5}$ (100 ug/ml) (A)/ $PM_{2.5}$ (200 ug/ml) (B)+ L-NMMA (10-100-300 uM) treatment. *p<0.05, **p<0.01, ****p<0.0001. $PM_{2.5}$, particulate matter; L-NMMA, N^G-Methyl-L-arginine acetate salt.

As seen in Figure 3.25, when 100 µg/ml $PM_{2.5}$ (mean= 75.76; *p<0.05) was applied to the cells, as expected, it decreased the viability significantly compared to the control (mean=100). This $PM_{2.5}$-induced decrease was reversed by simultaneous exposure to 8 mM NAC (mean=102.99; **p<0.01) treatment. So, 8 mM NAC was chosen for further experiments. Lastly, $PM_{2.5}$ and inhibitors were applied to the cells simultaneously. As seen in Figure 3.25, 100 µg/ml $PM_{2.5}$ (mean=75.76; **p<0.01) decreased the viability compared to the control (mean=100). 8 mM NAC increased the viability (mean=102.99; ***p<0.001) compared to $PM_{2.5}$ treatment, while 8 mM NAC and 100 µM L-NMMA increased viability more significantly compared to $PM_{2.5}$ treatment (mean=113.71; ****p<0.0001).

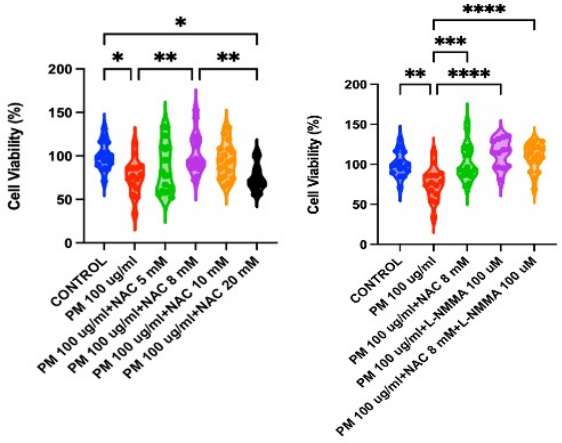

Figure 3. 25 MTT results of BEAS-2B cells treated with 100 ug/ml $PM_{2.5}$ + NAC (5,8,10,20 mM) and only 100 µg/ml $PM_{2.5}$, 100 µg/ml $PM_{2.5}$ +8 mM NAC, 100 µg/ml $PM_{2.5}$ +8 mM NAC+100µM L-NMMA. **p<0.01, ***P<0.001, ****p<0.0001. $PM_{2.5}$, particulate matter; NAC, N-Acetyl-L-cysteine; -NMMA, N^G-Methyl-L-arginine acetate salt.

3.3 SARS-CoV-2 infection of hBEOs

3.3.1 ACE2, TMPRSS2, and FURIN gene expression analysis of hBEOs

Before starting SARS-CoV-2 infection trials, organoids were used to demonstrate ACE2, TMPRSS2, and FURIN gene expression, which makes them able to be infected with SARS-CoV-2. For this aim, organoids obtained from smokers, shown in Table 2.5, were used. qPCR was repeated 3 times for 2 patients and 2 times for 1 patient (n=8). As seen in Figure 3.26 below, organoids expressed ACE2, TMPRRS2, and FURIN genes.

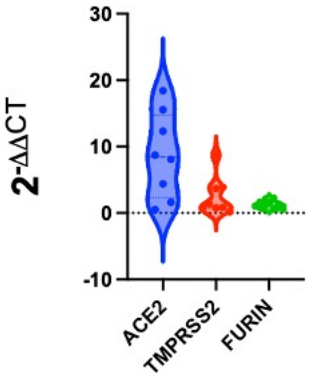

Figure 3. 26 Smoker hBEOs' gene expression analysis of ACE2, TMPRSS2, and FURIN.

3.3.2 SARS-CoV-2 dose and duration optimization with IF by labeling Spike protein.

In the first infection trial, hBEO were directly taken to the BSL3-lab after matrigel dissolvent while still in an inward position, and infection was tested for MOI 0.1, 0.5, and 1 for 24 hours. At the end of 24 hours, it was seen that keeping hBEO with the virus for that long caused the morphological disruption and death of most hBEO. However, the desired infection images still needed to be obtained. Several ones with minimum damage were used for immunofluorescence, and their confocal microscope images were taken. Spike antibody (ab273433, Abcam) was used with 1:333 dilution together with 1:100 diluted Alexa Fluor 594 (Goat anti-Mouse IgG (H+L) Highly Cross-Adsorbed Secondary Antibody, Invitrogen, A32742). Hoechst dye was used as nuclei staining. As seen in Figure 3.27 with arrows below, MOI 0.5 intensity was higher than MOI 0.1. However, there was a deficient expression of spike protein in Figure 3.27D, which was MOI 1. Therefore, new experiments were conducted because it was unclear whether the hBEO were inward or because the highest MOI value caused more deaths and inhibited the infection.

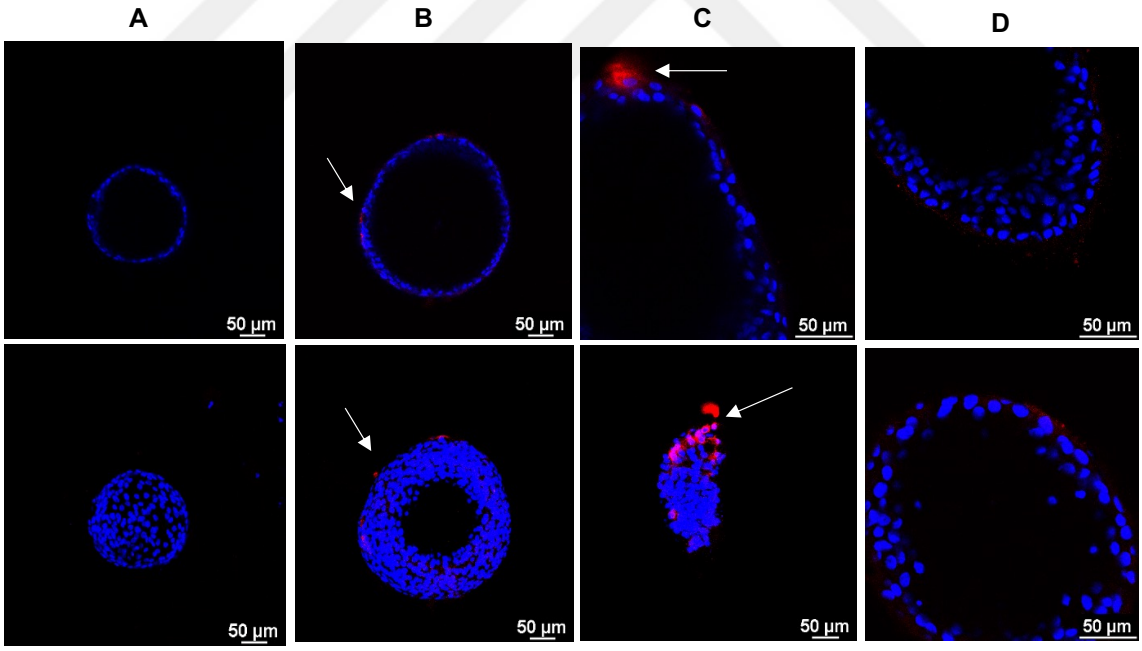

Figure 3. 27 Confocal microscopy images of negative control inward hBEOs (A); inward hBEO infected with SARS-CoV-2 for 24h with MOI 0.1 (B), 0.5 (C) and 1 (D). Red dots represent spike protein; Hoechst (blue) is used for nuclear staining.

Secondly, the hBEOs were placed outward and incubated with a MOI of 0.5 for 2 hours, followed by post-infection incubation for 24 and 48 hours. The mortality rate significantly decreased when the infection lasted 2 hours, and the virus rate in the hBEOs increased as the post-infection time increased. White arrows point to the spike proteins in Figure 3.28.

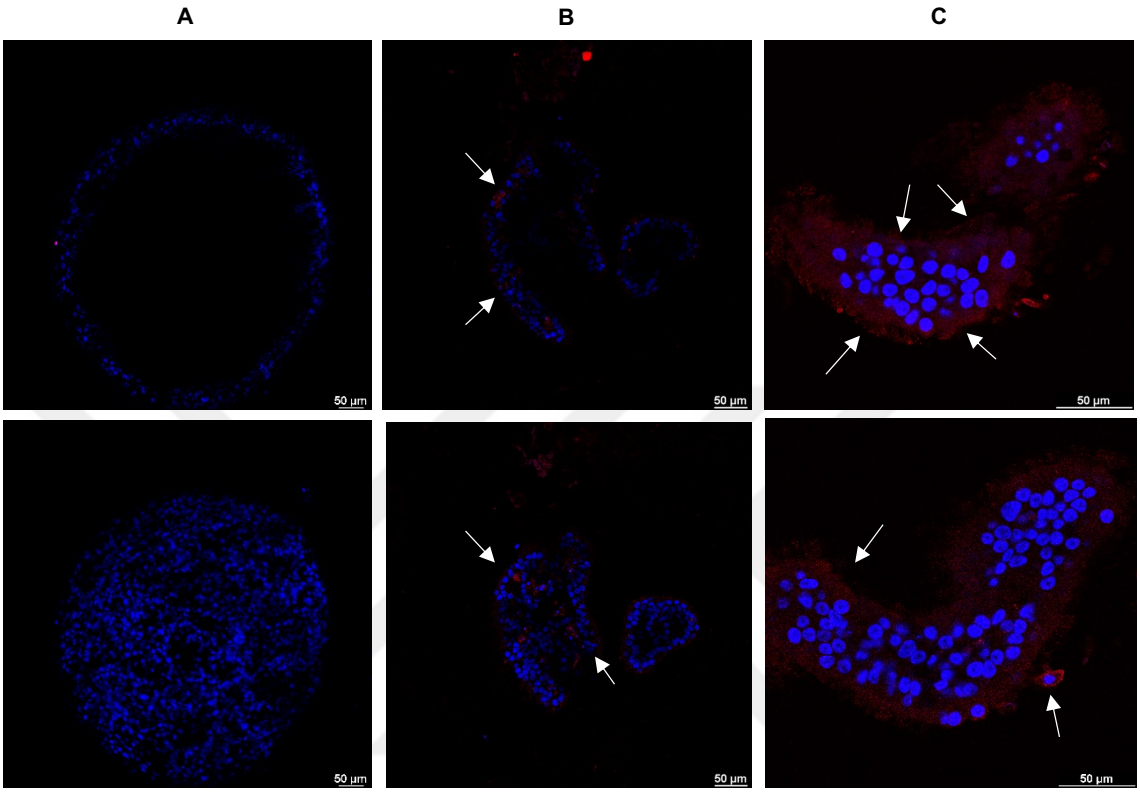

Figure 3. 28 Confocal microscopy images of negative control outward hBEOs (A), outward hBEOs infected with SARS-CoV-2 for 24h with MOI 0.5 (B) and for 48h with MOI 0.5 (C). Red dots represent spike protein; Hoechst (blue) is used for nuclear staining.

Then, due to the increased matrigel prices, it was checked whether the hBEOs could be kept on a low attachment plate instead of being seeded into matrigel during the post-infection period. hBEOs were infected with MOI 0.5 for 2h and incubated for 48h and 72 h as a post-infection period. Alexa Fluor Plus 488(Goat anti-Rabbit IgG (H+L) Highly Cross-Adsorbed Secondary Antibody, Invitrogen, A32731) was used as a secondary antibody. Viral proliferation appears more clearly in matrigel at both 48 and 72 hours. Morphological disorders and clump formations were observed more in the hBEO remaining in the low attachment plate for 2-3 more days, especially in the ones with 72h post-infection incubation, as seen in Figures 3.29 and 3.30. Finally, it was observed that

72 hours post-infection gave better results than 48 hours and did not harm the hBEO in matrigel.

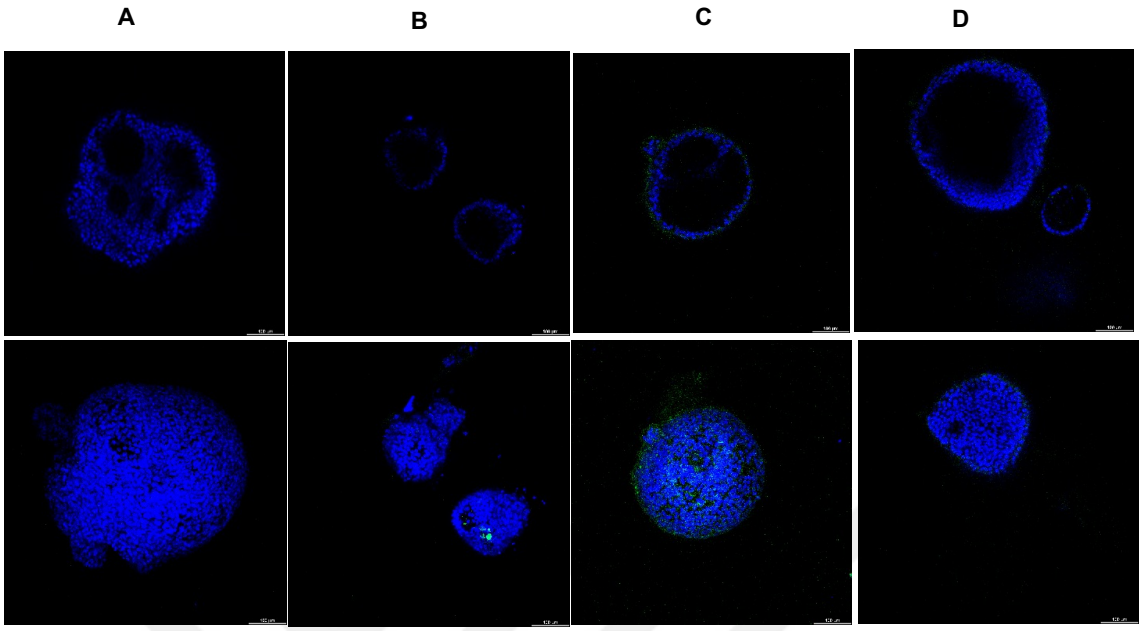

Figure 3. 29 Confocal microscopy images of negative control outward hBEOs incubated 48h in matrigel (A), in low attachment plate (B), outward hBEO infected with SARS-CoV-2 for 2h with MOI 0.5, incubated 48h post-infection in matrigel (C), in low attachment plate (D). Green dots represent spike protein; Hoechst (blue) is used for nuclear staining.

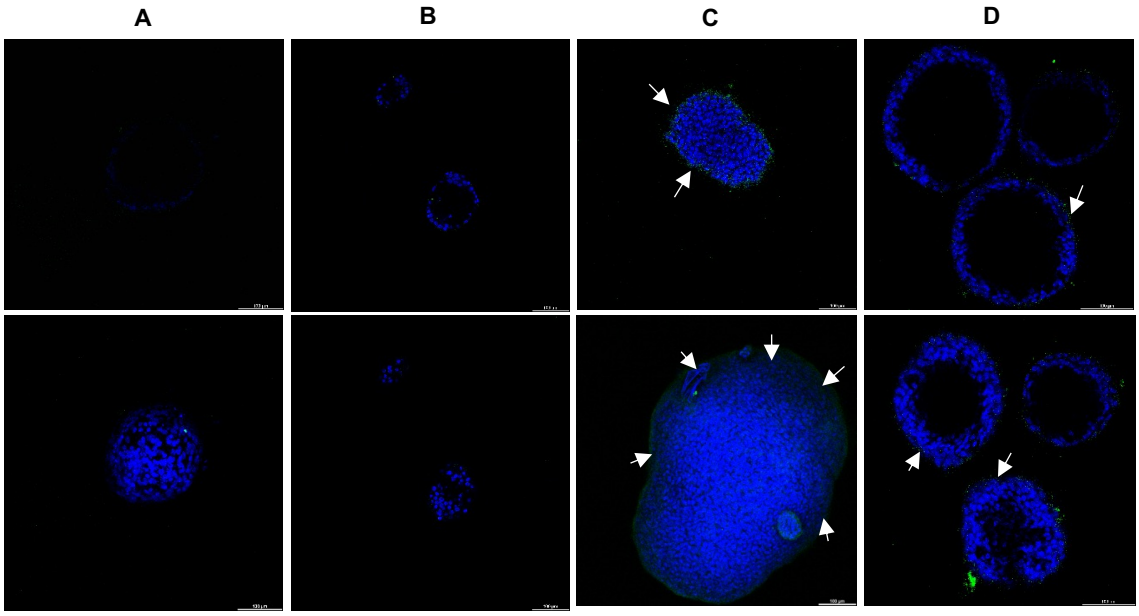

Figure 3. 30 Confocal microscopy images of negative control outward hBEOs incubated for 72h in matrigel (A), in low attachment plate(B), outward hBEOs infected with SARS-CoV-2 for 2h with MOI 0.5, incubated 72h post-infection in matrigel (C), in low

attachment plate (D). Green dots represent spike protein; Hoechst (blue) is used for nuclear staining.

Finally, staining was performed with cytokeratin (CK) 5, a cytoplasmic marker, to find out where spike proteins appear in the cells infected by the virus, whether they only appear at attachment points outside the cell or they also multiply in the cytoplasm. CK5 (ab53121, Abcam) antibody was used 1:500 diluted together with 1:100 diluted Alexa Fluor 594 (Goat anti-Mouse IgG (H+L) Highly Cross-Adsorbed Secondary Antibody, Invitrogen, A32742). Spike ab (ab273433, Abcam) was used 1:333 together with 1:100 diluted Alexa Fluor Plus 488(Goat anti-Rabbit IgG (H+L) Highly Cross-Adsorbed Secondary Antibody, Invitrogen, A32731). Post-incubation was repeated for 24,48, and 72h, and it was concluded that 72h in matrigel is the best incubation period after 2h MOI 0.5 infection. As seen in Figure 3.31 below, especially in 72h, viral replication was observed inside the cells, too. Lastly, the same protocol was applied to different patients' hBEOs for 72 hours post-infection for double check. As seen in Figure 3.32, similar results were obtained.

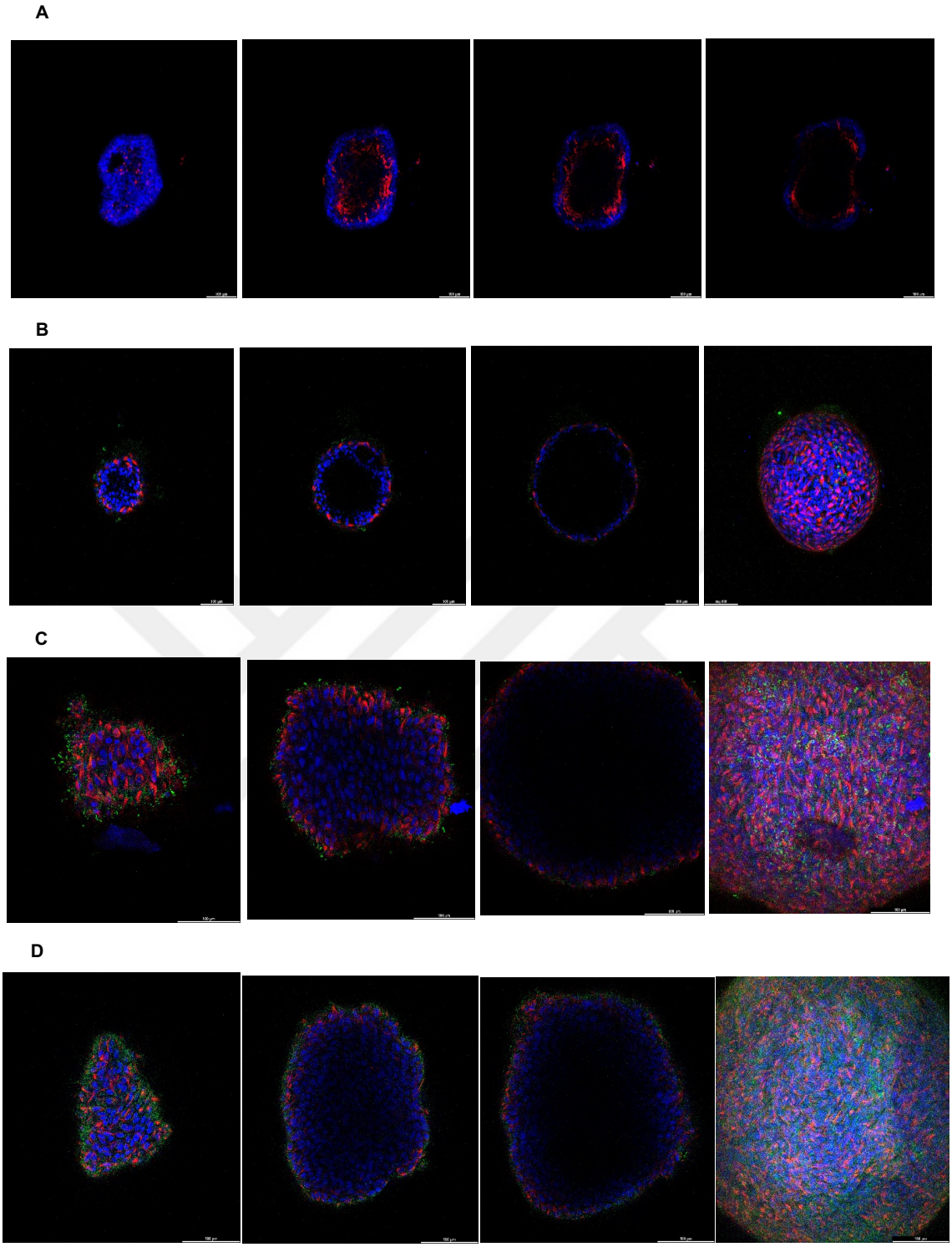

Figure 3. 31 Confocal microscopy images of CK5 (red) in negative control outward hBEOs incubated for 72h in matrigel (A), Confocal microscopy images of CK5 (red) and spike protein (green) in outward hBEO infected with SARS-CoV-2 for 2h with MOI 0.5, incubated 24h post-infection in matrigel (B), 48h post-infection in matrigel (C), 72h post-infection in matrigel (D). Hoechst (blue) is used for nuclear staining.

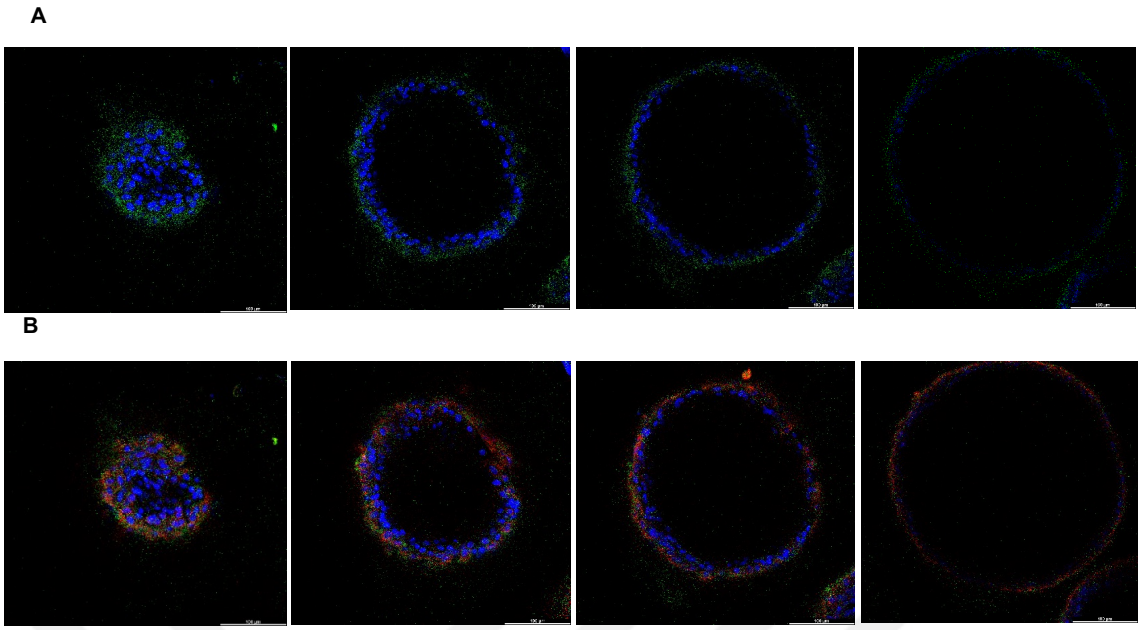

Figure 3. 32 Confocal microscopy images of spike protein (green) replicated in outward hBEOs incubated as post-infection for 72h in matrigel (A), Confocal images of CK5 (red) and spike protein (green) replicated in outward hBEO incubated as post-infection for 72h in matrigel (B). Hoechst (blue) is used for nuclear staining.

3.3.3 N1 gene expression analysis in SARS-CoV-2 infected hBEOs and their supernatants

qPCR was applied to the Wuhan variant of the SARS-CoV-2 virus with serial dilutions (10^7 to 10^1) to obtain an equation for CT values conversion to PFU/ml calculation. So that viral load was determined for each group. The amplification curve and CT values were obtained for each dilution. Based on these standards, the equation was calculated, as seen in Figure 3.33 below.

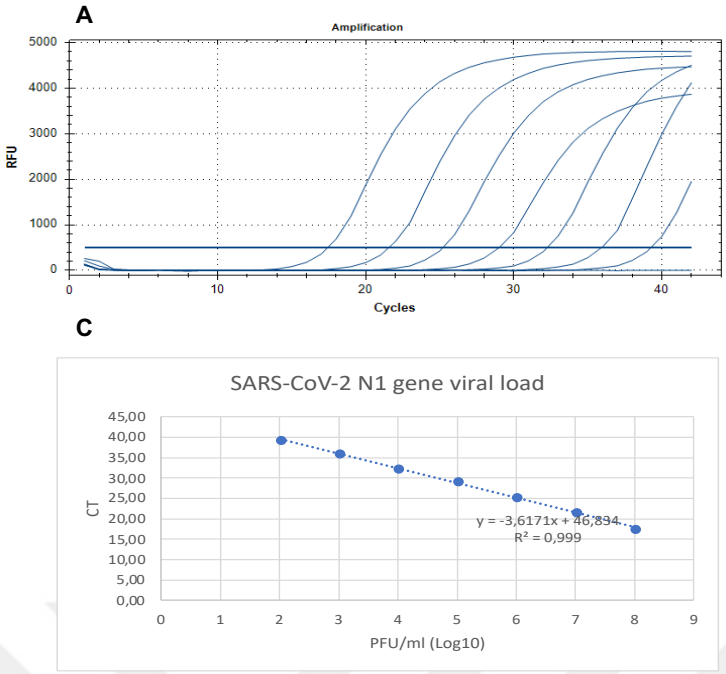

Sample	Cq
wuhan 10*7	17,43
wuhan 10*6	21,56
wuhan 10*5	25,21
wuhan 10*4	29,01
wuhan 10*3	32,26
wuhan 10*2	35,93
wuhan 10*1	39,26
NC	

Figure 3. 33 SARS-CoV-2 N1 gene expression qPCR results represented as amplification curve (A), CT values (B), and viral load equation as PFU/ml (Log10) (C).

Based on these results, CT values over 35,93 corresponding 10^2 viral load are accepted as negative results in terms of the presence of SARS-CoV-2 in the samples.

Organoids demonstrated in Table 2.5 were treated with $PM_{2.5}$ and ROS/RNS inhibitors. Also, SARS-CoV-2 infection-optimized dose and duration were determined as MOI 0.5 for 2h infection and 72h post-infection. Optimum infection was presented with confocal images above. Lastly, qPCR was done with hBEOs and their supernatants treated with this dose and duration of SARS-CoV-2 to prove the infection as a second method. For this aim, 2h viral infection media was used as a positive control, and organoid media not infected with the virus were used as a negative control. The nucleocapsid 1 (N1) gene expression was analyzed for the presence of SARS-CoV-2 in organoids after 72h post-infection, as suggested by the Centers for Disease Control and Prevention (CDC). For supernatant analysis, qPCR was repeated 3 times with triplicates for 3 non-smoker and 3 smoker samples. 2h infection media and 72 hours post-infection organoids itself CT values varied between 30-35. PFU (Plaque Forming Unit)/ml values were between 3-6. There were no CT values for negative controls.

As shown in Figure 3.34, 2h infection non-smoker organoid supernatant samples demonstrated that $PM_{2.5}$ (mean=4.410) significantly increased the viral load in the

supernatant in terms of PFU/ml compared to the control (median=3.986). Also, when the ROS/RNS inhibitors were added to the culture media together with $PM_{2.5}$, N1 gene expression was decreased (mean=3.8) significantly compared to the only $PM_{2.5}$-treated samples (mean=3.986).

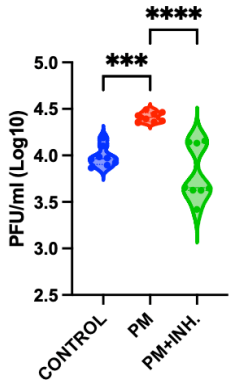

Figure 3. 34 Comparison of PFU/ml values of N1 gene expression between control, $PM_{2.5}$, and $PM_{2.5}$ inhibitors treated non-smoker organoids' supernatants which are infected with SARS-CoV-2 for 2 hours. ***p<0.001, ****P<0.0001.

On the other hand, there was no significant difference in viral load between smokers' organoids supernatant samples, as shown in Figure 3.35 below.

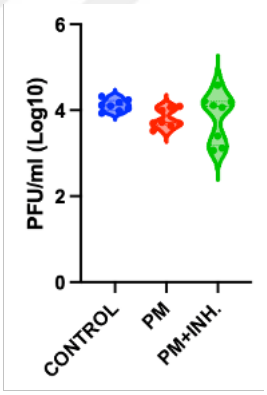

Figure 3. 35 Comparison of PFU/ml values of N1 gene expression between control, $PM_{2.5}$, and $PM_{2.5+}$ inhibitors treated smoker organoids' supernatants which are infected with SARS-CoV-2 for 2 hours.

After 72 hours post-infection incubation, non-smoker organoids obtained from HBECs were also used to determine the viral load inside the organoids and to prove that these organoids were infected by SARS-CoV-2 with this dose and duration. The experiment was conducted 2 times (containing 2 PCR setups with duplicates as a technical replicate, n=8). As seen in Figure 3.46, N1 gene expression was elevated in the $PM_{2.5}$ (mean=4.471)

group compared to the control (mean=3.86) significantly, while it was reversed with the addition of inhibitors (mean=3.341) to the treatment.

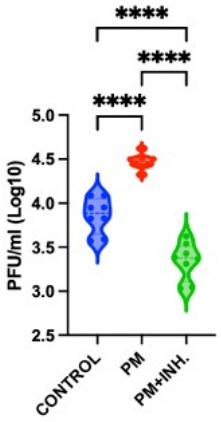

Figure 3. 36 Comparison of PFU/ml values of N1 gene expression between control, $PM_{2.5}$, and $PM_{2.5}$ + inhibitors treated non-smoker organoids infected with SARS-CoV-2 for 2 hours and incubated as the post-infection period for 72 hours. ****p<0.0001.

Also, a 2-way ANOVA analysis was done for 2h infection supernatant groups to determine whether there are differences between smoker and non-smoker organoid supernatants. It can be seen from Figure 3.37 at the end of 2h infection that non-smoker organoids treated with $PM_{2.5}$ (mean=4.410) were significantly expressing a higher amount of N1 gene, and higher PFU/ml values compared to the smoker organoids treated with $PM_{2.5}$ (mean=3.805).

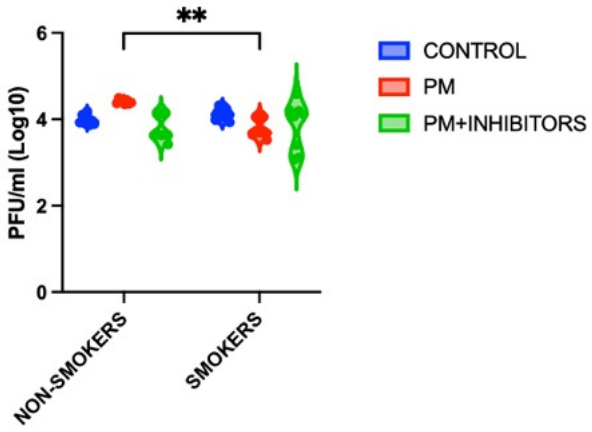

Figure 3. 37 Comparison of PFU/ml values of N1 gene expression between control, $PM_{2.5}$, and $PM_{2.5}$ + inhibitors treated non-smoker organoids' supernatants with smoker organoids' supernatants which are infected with SARS-CoV-2 for 2 hours. **p<0.01.

3.5 Gene expression analysis of hBEOs treated with $PM_{2.5}$ and $PM_{2.5}$+inhibitors with or without SARS-CoV-2 infection

3.5.1 qPCR analysis of hBEOs treated with $PM_{2.5}$ and $PM_{2.5}$+inhibitors with or without SARS-CoV-2 infection

Figure 3.38 below demonstrates qPCR analysis of non-smoker organoids treated with $PM_{2.5}$ and $PM_{2.5}$ + inhibitors without SARS-CoV-2 infection. As shown in Table 2.5, 3 different patients non-smoker organoids were used. qPCR was repeated 2 times with 2 technical replicates (n=12). SOD1 expression was significantly higher in the PM+inhibitors group (median=1.912) compared to the control (median=1.072). NQO1 gene expression was significantly elevated with $PM_{2.5}$ (median=5.941) treatment compared to the control (median=1.07), which is partly considerably reversed by the addition of inhibitors (median=3.94). For the NF2EL2 gene, $PM_{2.5}$ (median=2.055) treatment increased the expression compared to the control (median=0.9985), and $PM_{2.5}$ +inhibitors (median=0.954) treatment decreased it compared to only $PM_{2.5}$ group (median=2.055). ACSL4 gene expression was elevated in the PM group (median=3.036) compared to the control (median=1.127). $PM_{2.5}$ + inhibitors (median=0.915) reduced the expression compared to the only $PM_{2.5}$ -treated group (median=3.036). It can be seen that for CASP1 and CASP9, $PM_{2.5}$ elevated the expression (median=2.198; 1.515) compared to the control (median=1.045; 0.926), which was attenuated together with $PM_{2.5}$ +inhibitor treatment (median=0.516; 0.269) compared to the only $PM_{2.5}$ treated ones. BCL2 expression was higher in the $PM_{2.5}$ +inhibitors group(median=2.354) compared to the only $PM_{2.5}$ treatment (median=1.1995). No significant change was observed for HMOX1, CYGB, KEAP1, and GPX4.

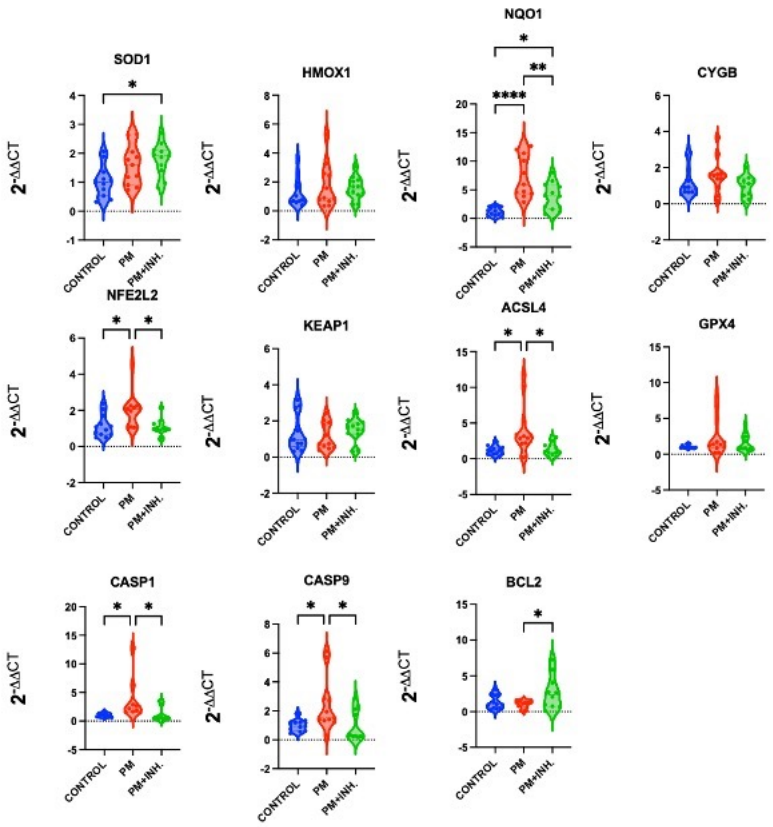

Figure 3. 38 qPCR analysis of non-smoker organoids treated with $PM_{2.5}$ and PM+ inhibitors without infection. *p<0.05, **p<0.01, ****p<0.0001.

Figure 3.39 below demonstrates qPCR analysis of smoker organoids treated with $PM_{2.5}$ and PM+ inhibitors without SARS-CoV-2 infection. As shown in Table 2.5, 3 different patients smoker organoids were used. qPCR was repeated 2 times with 2 technical replicates (n=12). SOD1 gene expression SOD1 expression was significantly higher in the $PM_{2.5}$ +inhibitors group (median=6.652) compared to the control (median=0.7085), similar to the non-smoker results explained in Figure 3.11. HMOX1 expression was elevated in the $PM_{2.5}$ group (median=2.1755) significantly compared to the control group (median=0.882), while it was reduced with $PM_{2.5}$ +inhibitor treatment (median=0.6445) compared to the only $PM_{2.5}$ group (median=2.1755). For NQO1, there was an increase with $PM_{2.5}$ treatment (median=28.4855) compared to the no-treatment group (median=0.698). $PM_{2.5}$ +inhibitors treatment (median=18.797) was significantly higher than no treatment group. Also, there was a decreasing trend when compared with only $PM_{2.5}$ treatment; however, it was not significant. NFE2L2 expression was elevated with $PM_{2.5}$ treatment (median= 2.499) compared to the control (median=0.9215), which was reversed with the addition of inhibitors compared to the only $PM_{2.5}$ treatment (median=0.8705). KEAP1 was higher control group (median=22.264) compared to the

$PM_{2.5}$ treatment (median=0.2415) and $PM_{2.5}$ inhibitors group (median=1.226). CASP9 was higher in the $PM_{2.5}$ treatment group (median= 4.02) than the control group (median=0.978). $PM_{2.5}$ +inhibitors treatment (median=0.386) decreased the CASP9 expression significantly compared to the only $PM_{2.5}$ treatment (median=4.02) BCL-2 expression was increased in $PM_{2.5}$ +inhibitors group (median=2.404) compared to the control (median=1.196) and $PM_{2.5}$ group (median=2.005) significantly. There was no significant change for CYGB, ACSL4, GPX4, or CASP1 genes. For the ACSL4 gene, there was an increasing trend with $PM_{2.5}$ treatment compared to the control, which decreased with the addition of inhibitors; however, it was not statistically significant.

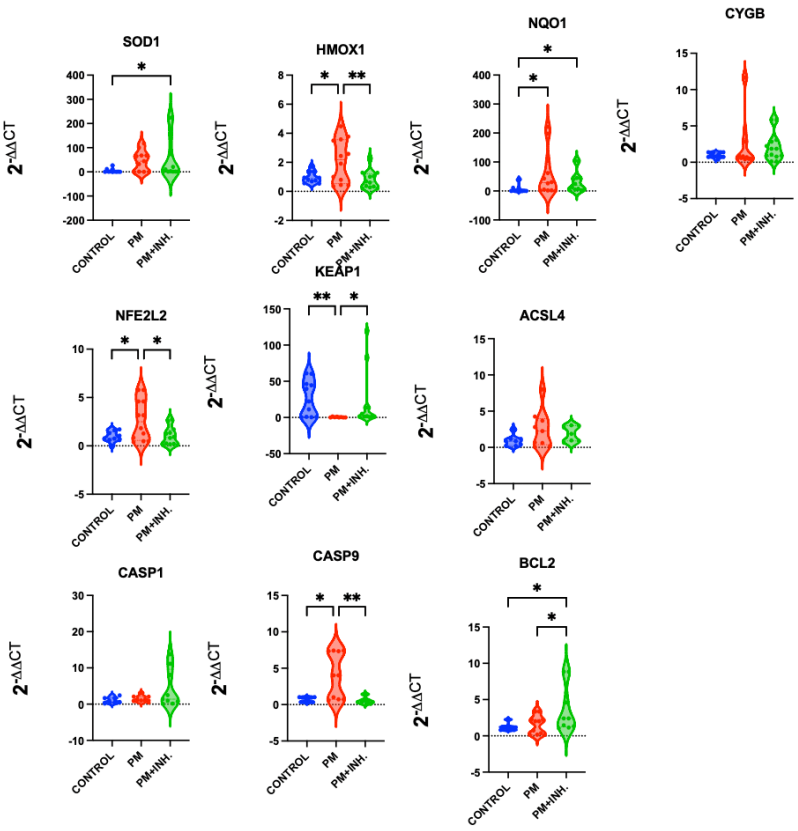

Figure 3. 39 qPCR analysis of smoker organoids treated with $PM_{2.5}$ and $PM_{2.5}$ + inhibitors without infection. *p<0.05, **p<0.01.

Figure 3.40 below demonstrates qPCR analysis of non-smoker organoids treated with $PM_{2.5}$ and $PM_{2.5}$ + inhibitors with SARS-CoV-2 infection. A healthy bronchial epithelial cell line was used as a non-smoker organoid. The experimental setup was repeated 2 times. For NQO1, qPCR was repeated 2 times containing triplicates (n=12); for NFE2L2, ACSL4, SOD1, GPX4, HMOX1, CYGB, and KEAP1 qPCR was repeated 2 times with duplicate technical replicates (n=8), for CASP1, CASP9, and BCL2, qPCR was repeated

2 times one with duplicate one with single technical replicates (n=6). SOD1 gene expression SOD1 expression was significantly higher in the PM+inhibitors group (median=4.191) compared to the control (median=2.2715), similar to the non-smoker and smoker results without infection, which is explained in Figures 3.13 and 3.14, respectively. HMOX1 expression was elevated in the $PM_{2.5}$ group (median=1.1555) significantly compared to the control group (median=0.947), while it was reduced with $PM_{2.5}$ +inhibitors treatment (median=0.308) compared to the only PM group (median=1.1555) similar to the smoker organoids without infection as shown in Figure 3.14. CYGB expression was augmented when those organoids were treated with $PM_{2.5}$ (median=4.2985) compared to the control (median=1.218), while it was decreased in the $PM_{2.5}$ +inhibitors group (median=1.7635) compared to the only $PM_{2.5}$ treatment (median=4.2985) similar to non-smoker organoids without infection. NFE2L2 gene was expressed at a lower level in the $PM_{2.5}$ group compared to the control (however, it was not significant, while it was significantly increased in the $PM_{2.5}$ +inhibitors group (median=1.628) compared to only $PM_{2.5}$ treatment (median=0.944) and control (median=1.281). KEAP1 gene expression was significantly reduced in $PM_{2.5}$ (median=0.4665) compared to the control (median=1.13) and $PM_{2.5}$ inhibitors group (median=1.22). ACSL4 gene was significantly higher in $PM_{2.5}$ (median=1.5945) compared to the control (median=1.0475) and $PM_{2.5}$ +inhibitors treated group (median=1.035). CASP1 and CASP9 were more expressed in $PM_{2.5}$ groups (medians=1.217, 1.659, respectively) than in controls (medians=0.989, 1.0285, respectively). For BCL2 expression, there was a decrease in the $PM_{2.5}$ treatment group (median=1.05) compared to the control (median= 1.6395). There was no significant change for NQO1 and GPX4.

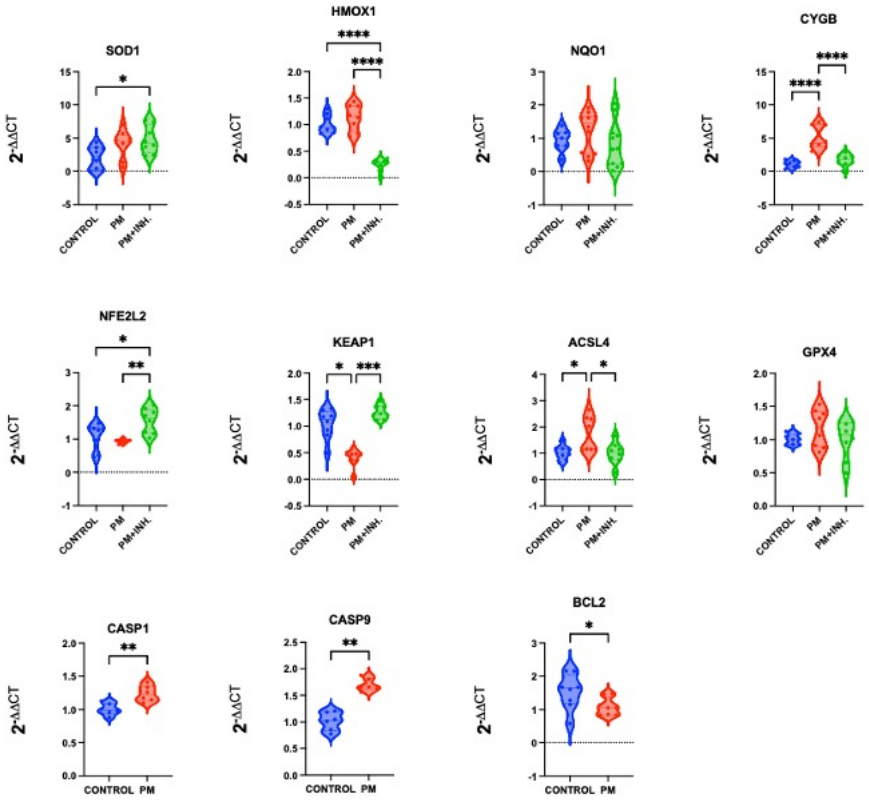

Figure 3. 40 qPCR analysis of non-smoker organoids treated with $PM_{2.5}$ and $PM_{2.5}$ + inhibitors with infection. *p<0.05, **p<0.01, ***p<0.001, ****p<0.0001.

As seen in Figure 3.41 below, when non-smoker vs. smoker results without infection were compared, there were significant differences between SOD1, NQO1, KEAP1, and CASP1. Smokers' SOD1 expression was significantly greater than non-smokers' in terms of the $PM_{2.5}$ + inhibitors group (median=6.652; 1.912). Smokers' NQO1 expression was significantly higher in terms of the $PM_{2.5}$ group (median=28.4855; 5,941). For KEAP1, there was a significant increase in smokers' results for controls (median=22.264; 0.94). For CASP1, there was an increase in smokers with $PM_{2.5}$ + inhibitors treatment compared to the non-smokers. (median=1.393; 0.516).

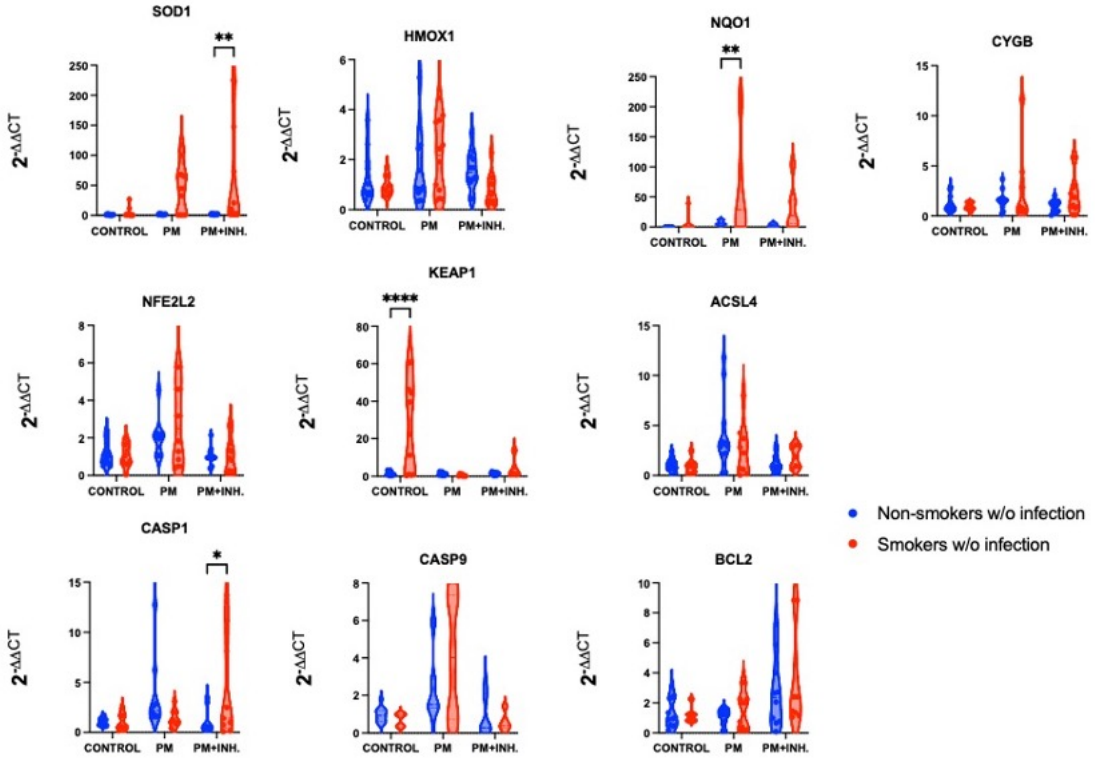

Figure 3. 41 qPCR analysis comparison between non-smoker and smoker organoids treated with $PM_{2.5}$ and $PM_{2.5}$ + inhibitors without (w/o) infection. *p<0.05, **p<0.01.

As seen in Figure 3.42 below, SOD1, HMOX1, NQO1, CYGB, NFE2L2, KEAP1, ACSL4, and CASP1 genes were significantly changed between non-smoker organoids with or without infection. SOD1 gene expression was significantly higher in the infected group compared to the non-infected group in terms of PM (median=4.5035; 1.599) and $PM_{2.5}$ + inhibitors treatment (median=4.191; 1.192). Non-smoker organoids infected with SARS-CoV-2 had significantly lower expression of HMOX1 compared to the non-infected ones when treated with $PM_{2.5}$ + inhibitors (median=0.2845; 1.496). Non-smoker organoids not infected with SARS-CoV-2 had significantly higher expression of NQO1 compared to the infected ones when treated with both only $PM_{2.5}$ (median= 5.941; 1.438) $PM_{2.5}$ +inhibitors (median=3.94; 0,6785). CYGB expression was significantly greater in infected organoids regarding $PM_{2.5}$ treatment (median=4.2985; 1.556). NFE2L2 expression was lower in the infected group (median=0.944) compared to the non-infected ones (median=2.055) in terms of $PM_{2.5}$ treatment. KEAP1 gene expression was higher in the without infection group when organoids were treated with $PM_{2.5}$ (median=0.734, 0.4665). Non-smoker organoids treated with only $PM_{2.5}$ and not infected with SARS-CoV-2 had higher ACSL4 levels than the infected ones (median=3.036, 1.035). CASP1

was greater in non-infected $PM_{2.5}$ -treated organoids (median= 2.198) than in infected $PM_{2.5}$ -treated ones (median= 1.217).

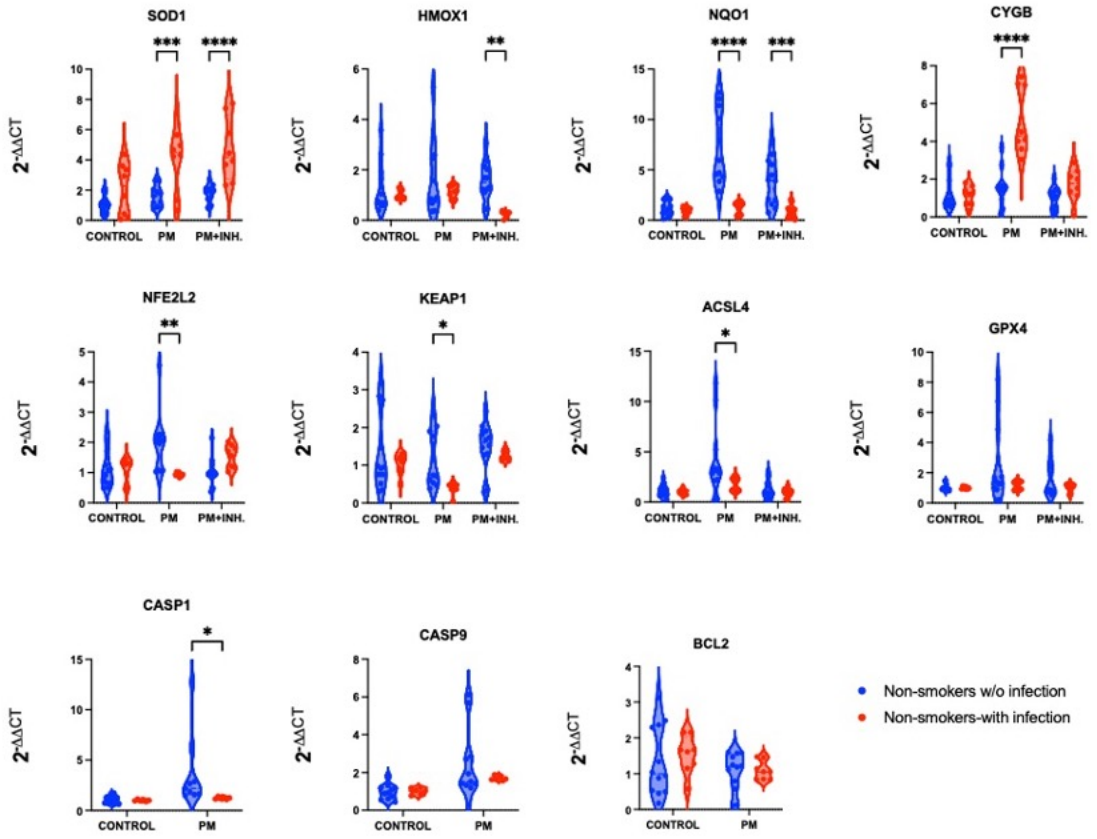

Figure 3. 42 qPCR analysis comparison between non-smoker organoids treated with $PM_{2.5}$ and $PM_{2.5}$ inhibitors with and without(w/o) SARS-CoV-2 infection. **p<0.01, ***p<0.001, ****p<0.0001.

3.6 RNA sequencing analysis of hBEOs treated with $PM_{2.5}$ and $PM_{2.5}$+inhibitors with SARS-CoV-2 infection

For the RNA sequencing, SARS-CoV-2 infected organoids obtained from a healthy human bronchial epithelial cell line treated with $PM_{2.5}$ and $PM_{2.5}$ + inhibitors together with the control group were used. The sample size was 3 for each group. Table 3.2 below show the quantity and quality of each RNA sample.

Table 3. 2 Quantity and quality measurements of sequenced RNA samples.

No.	Sample Name	Sample Number	Tube No.	Concen-tration(ng/μL)	Volume(μL)	Total Mass(μg)	RIN	28S/ 18S	Library Type	Test Result	Remark
1	1a	8522402000715	1	12.835	14	0.1797	9.3	2.4	DNBSEQ Transcriptome	Level B	m<0.2μg
2	1b	8522402000716	1	16.915	14	0.2368	9.2	2.1	DNBSEQ Transcriptome	Level A	
3	1c	8522402000717	1	15.94	14	0.2232	9.3	2.3	DNBSEQ Transcriptome	Level A	
4	2a	8522402000718	1	9.805	12	0.1177	9.5	2	DNBSEQ Transcriptome	Level B	c<10.0ng/μL. m<0.2μg
5	2b	8522402000719	1	14.125	13	0.1836	9.4	2.3	DNBSEQ Transcriptome	Level B	m<0.2μg
6	2c	8522402000720	1	11.29	14	0.1581	9.1	1.5	DNBSEQ Transcriptome	Level B	m<0.2μg
7	3a	8522402000721	1	6.171	14	0.0864	9.2	1.9	DNBSEQ Transcriptome	Level C	c<10.0ng/μL. m<0.2μg
8	3b	8522402000722	1	3.415	17	0.0581	7.9	1.2	DNBSEQ Transcriptome	Level C	c<10.0ng/μL. m<0.2μg
9	3c	8522402000723	1	1.866	20	0.0373	6.8	1.3	DNBSEQ Transcriptome	Level C	c<10.0ng/μL. m<0.2μg. RIN<7.0

All groups were compared as follows: SARS-CoV-2 infected hBEOs (G1 group) versus those also infected with SARS-Cov2 and exposed to $PM_{2.5}$ (G2 group) and those exposed to both $PM_{2.5}$ and ROS/RNS inhibitors (G3 group). The comparisons were “G1 vs. G2”, “G1 vs. G3”, and “G2 vs. G3”. The list of genes associated with the viral entry, oxidative stress, cell death mechanisms, epithelial barrier, and bronchial epithelial cell markers that had been investigated are listed in Table 3.3 below.

Table 3. 3 The list of genes associated with viral entry, oxidative stress, cell death mechanisms; epithelial barrier, and bronchial epithelial cell markers investigated by using RNA sequencing data.

Viral Entry	Oxidative stress	Apoptosis	Apoptosis	Ferroptosis	Epithelial barrier	Bronchial epithelial cell markers
ANPEP	NOS3	BCL2A1	HRAS	TF	CLDN10	LYPD2
C1R	AOC2	JUN	BAD	STEAP3	CLDN9	KRT4
CTSD	MAOB	FOS	ATM	SLC39A8	TJP1	SCGB1A1
TMPRSS2	NCF2	CTSD	CTSS	SLC11A2	CLDN3	KRT13
FURIN	MAOA	ITPR1	MCL1	ALOX15	CLDN12	MKI67
CLTRN	DDO	BCL2L1	PDPK1	CYBB	CLDN4	KRT14
PCSK9	SMOX	DFFB	CFLAR	SLC3A2	CLDN7	KRT5
CTSB	CYBA	TP53	CASP2	GPX4	CLDN23	MUC5B
CTSC	QSOX1	DAXX	CASP6	TP53	CLDN16	TP63
ACE	AOC1	BCL2L11	CASP7	HMOX1	CLDN18	SPDEF
PSMB4	MPO	IKBKB	TRADD	SLC39A14	CLDN1	DAPL1
CTSS	CYP1A1	NFKBIA	BCL2	SLC7A11	CLDN8	MUC5AC
CFI	S100A8	CTSH	DDIT3	GCLC	F11R	CDK1
PSMB2	S100A9	CTSK	NRAS	VDAC3	CTNNA1	MLF1
PSMB5	PDLIM1	CTSZ	CASP9	SLC40A1	JAM3	FOXJ1
CTSL	MT1X	CTSF	BBC3	GCLM	TJP2	POU2F3
TMPRSS4	DUSP1	CASP8	ITPR3	ATG5	OCLN	CCDC113
PCSK7	DHCR24	ERN1	HTRA2	TFRC	CTNND1	TOP2A
PCSK4	GLRX2	CASP10	APAF1	SPEG	CLDN5	CCDC153
PCSK5	MSRA	CASP3	DFFA	FTL	EPCAM	LZTFL1
ACE2	NFE2L2	CTSB	AIFM1	FADD	CLDN15	AVIL
PCSK6	GCLM	BID	FADD	FTH1	CTNNB1	CFTR
C2	MGST1	PMAIP1	XIAP	NCOA4	TJP3	KRT15
DPP4	ATOX1	CTSC	ENDOG	PCBP2	CDH1	ASCL3
PCSK1	SRXN1	DAB2IP	TNFSF10	CP	CLDN11	TRPM5
	FOS	PARP1	CTSL	ATG7	CLDN14	
	JUNB	MAP3K14	TRAF2	PCBP1	CLDN2	
	SOD2	BIRC5	NFKB1	VDAC2	CLDN20	
	TXN	TRAF1	MAP2K1	PRNP	CLDN34	
	SESN2	CAPN1	CAPN2	GSS	CLDN6	
	DRD2	PTPN13	ATF4	LPCAT3	JAM2	
	ERCC3	IKBKG	EIF2AK3			
	GCLC	BAX	ITPR2			
	MAPK14	TNFRSF1A	TP53AIP1			
	GSTM3	RELA	RAF1			
	GSR	KRAS	CTSO			
		HRK	MAP2K2			
		MAP3K5	EIF2S1			
		LMNA	CTSW			
		DIABLO	TNF			
		RIPK1				

25 viral entry-related genes (Table 3.3) were identified through literature reviews to analyze their expression changes in our transcription dataset and to perform group comparisons. According to the comparison results, the alanyl aminopeptidase (ANPEP) gene was upregulated in both the G2 and G3 hBEOs compared to the G1 hBEOs. Additionally, the Complement Component 1 (C1R) gene was upregulated in the G3 group compared to the G1 group. No other genes showed significant changes between groups as seen in Table 3.4.

Table 3. 4 List of viral entry-related DEGs during SARS-COV-2 infection in response to $PM_{2.5}$ and $PM_{2.5}$+inhibitor treatments.

Viral entry related DEGs											
G1 vs G2				G1 vs. G3				G2 vs. G3			
Gene	*logFC*	*p-value*	*Expression status*	*Gene*	*logFC*	*p-value*	*Expression status*	*Gene*	*logFC*	*p-value*	*Expression status*
ANPEP	**1,458720773**	**1,20E-18**	**Upregulated**	**ANPEP**	**1,701480981**	**1,16E-25**	**Upregulated**	ANPEP	0,242760208	0,646999562	Not changed
C1R	0,798038777	6,26E-08	Not changed	**C1R**	**1,713014238**	**2,20E-34**	**Upregulated**	C1R	0,914975461	1,14E-08	Not changed

11 pro-oxidant, 14 oxidative response-related, and 11 antioxidant genes were identified through literature reviews to analyze their expression (Table 3.3). DEGs were identified based on criteria of padj < 0.05 and log2FC < 1. Our analysis revealed a significant change in the nitric oxide synthase 3 (NOS3) gene among the pro-oxidant genes examined. Specifically, NOS3 gene expression was upregulated in the group exposed to both the virus and $PM_{2.5}$ (G2) compared to the group exposed only to SARS-CoV-2 (G1). No significant changes were observed in the comparisons of "G2 vs G3" and "G1 vs G3" for this gene as seen in Table 3.5.

Table 3. 5 List of oxidative stress-related DEGs during SARS-COV-2 infection in response to $PM_{2.5}$ and $PM_{2.5}$+inhibitor treatments.

Pro-oxidant DEGs											
G1 vs G2				G1 vs G3				G2 vs G3			
Gene	*logFC*	*p-value*	*Expression status*	*Gene*	*logFC*	*p-value*	*Expression status*	*Gene*	*logFC*	*p-value*	*Expression status*
NOS3	**1,012553091**	**5,55E-06**	**Upregulated**	NOS3	0,980398292	4,75E-06	Not changed	NOS3	-0,032154799	0,991274418	Not changed

Using the dataset containing 81 apoptotic genes from the KEGG PATHWAY (map04210), we analyzed the expression changes within our transcription dataset (Table 3.7). Our analysis revealed significant differences in the BCL2-related protein A1 (BCL2A1) expression, an anti-apoptotic gene. In the G2 group compared to the G1, the BCL2A1 gene was downregulated. In the G3 group compared to, the BCL2A1 gene did not show a significant change. No significant differences in the expression of this gene were observed in G2 vs. G3 as seen in Table 3.6.

Table 3. 6 List of apoptosis-related DEGs during SARS-COV-2 infection in response to $PM_{2.5}$ and $PM_{2.5}$+inhibitor treatments.

Anti-apoptotic DEGs											
G1 vs G2				G1 vs G3				G2 vs G3			
Gene	*logFC*	*p-value*	*Expression status*	*Gene*	*logFC*	*p-value*	*Expression status*	*Gene*	*logFC*	*p-value*	*Expression status*
BCL2A1	**-1,027648033**	**2,51E-10**	**Downregulated**	BCL2A1	-0,768983197	4,39E-06	Not changed	BCL2A1	0,258664836	0,467836278	Not changed

Using the dataset of 31 ferroptotic genes from the KEGG PATHWAY (map04216), we examined the expression changes of these genes in our transcription dataset (Table 3.3). The analysis revealed that the only gene with a significant expression change in our group comparisons was transferrin (TF). This gene was upregulated in both the G1 vs. G2 and G1 vs. G3 comparisons. However, no significant change was observed in the TF gene expression in the G3 compared to the G2 as seen in Table 3.7.

Table 3. 7 List of ferroptosis-related DEGs during SARS-COV-2 infection in response to $PM_{2.5}$ and $PM_{2.5}$+inhibitor treatments.

Ferroptosis related genes											
G1 vs G2				G1 vs G3				G2 vs G3			
Gene	*logFC*	*p-value*	*Expression status*	*Gene*	*logFC*	*p-value*	*Expression status*	*Gene*	*logFC*	*p-value*	*Expression status*
TF	**1,947261236**	**1,98E-60**	**Upregulated**	**TF**	**2,132027522**	**5,49E-73**	**Upregulated**	TF	0,184766287	0,609720383	Not changed

We examined the expression changes of bronchial epithelial cell marker genes identified by (Ravindra et al., 2021) through single-cell longitudinal analysis of SARS-CoV-2 in human airway epithelial cells, using the data obtained from our study (Table 3.3). Among the total of 25 genes, we displayed the genes with significant changes in our group comparisons in Table 3.8 below. According to our analysis, the expression of the club cell marker gene LY6/PLAUR domain containing 2 (LYPD2) was significantly upregulated in both the G2 and G3 groups compared to the G1 group. Additionally, another club cell marker gene, *SCGB1A1*, was upregulated in the G3 group compared to the G1 group. Furthermore, in the G1 vs. G3 comparison, the proliferative basal cell marker gene marker of proliferation Ki-67 (MKI67) was upregulated. In the G3 compared to the G2, the expression levels of LYPD2, and SCGB1A1, remained unchanged, whereas MKI67 expression was upregulated.

Table 3. 8 List of bronchial epithelial cell marker-related DEGs during SARS-COV-2 infection in response to $PM_{2.5}$ and $PM_{2.5}$+inhibitor treatments.

Bronchial epithelial cell markers related DEGs											
G1 vs G2				G1 vs G3				G2 vs G3			
Gene	*logFC*	*p-value*	*Expression status*	*Gene*	*logFC*	*p-value*	*Expression status*	*Gene*	*logFC*	*p-value*	*Expression status*
LYPD2	**1,164629314**	**1,24E-45**	**Upregulated**	**LYPD2**	**1,695861908**	**2,19E-96**	**Upregulated**	LYPD2	0,531232594	1,66E-08	Not changed
SCGB1A1	0,529108149	7,37E-05	Not changed	**SCGB1A1**	**1,302925073**	**3,60E-30**	**Upregulated**	SCGB1A1	0,773816924	5,47E-10	Not changed
MKI67	0,80478814	0,000215428	Not changed	**MKI67**	**1,844930854**	**1,59E-21**	**Upregulated**	**MKI67**	**1,040142714**	**5,16E-06**	**Upregulated**

Additionally, we used the epithelial barrier gene set (31 genes) from the study by (Zhou et al., 2023) to determine the effects of the virus, $PM_{2.5}$, and ROS/RNS inhibitors on the expression of epithelial barrier-related genes in our dataset. The gene list examined is presented in Table 3.3. The analysis showed no significant changes in the expression of epithelial barrier-related genes in any of the group comparisons.

3.4 Measurement of ROS (8-isoprostane)/RNS (nitrate+nitrite, nitrate, nitrite) and inflammatory cytokines (IL1β, TNFα, GM-CSF, IL-6 and IL-8) from COVID-19 patients and healthy individuals plasma samples and hBEOs' supernatants

3.4.1 Measurement of RNS (nitrate+nitrite, nitrate, nitrite) from COVID-19 patients and healthy individuals plasma samples

The objective of RNS analysis was to examine the association between plasma nitrate+nitrite, nitrate, and nitrite levels and the severity of COVID-19. Firstly, a comparison between controls and all COVID-19 patients was performed for RNS measurements. According to that analysis, nitrite and nitrite/nitrate concentrations, respectively, were significantly higher in patients (median=1.21 and 0.029; ****p<0.0001) compared to controls (median=0.53; and 0.022), as seen in Figure 3.44.

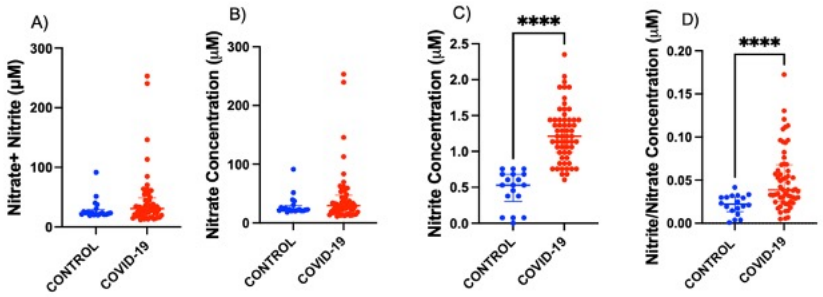

Figure 3. 43 Plasma Nitrate+nitrite levels (A), nitrate levels (B), nitrite (C), and nitrite/nitrate (D) levels in healthy controls and COVID-19 patients. ****p<0.0001. Data are expressed as median ± interquartile range.

After that, whether COVID-19 severity affects the RNS level was checked as seen in Figure3.45. Nitrate+nitrite and nitrate concentrations were respectively higher in severe patients (median=34.37 and 33.43; *p<0.05) compared to the mild (median= 22.25 and 20.62) ones. Nitrite concentration was lower in controls (median= 0.53; ****p<0.0001) compared to mild, moderate, and severe patients (median= 1.56, 1.17 and 0.83; ****p<0.0001 and *p<0.05). Also, there was a gradual decrease in nitrite concentration with the increase in the severity of patients. Nitrite /nitrate concentration was significantly lower in the control group (median=0.022; ****p<0.0001) compared to mild patients (median=0.073). Further, there was a gradual decrease from mild to moderate (median=0.034; *p<0.05) and severe (median=0.029; ****p<0.0001) patients.

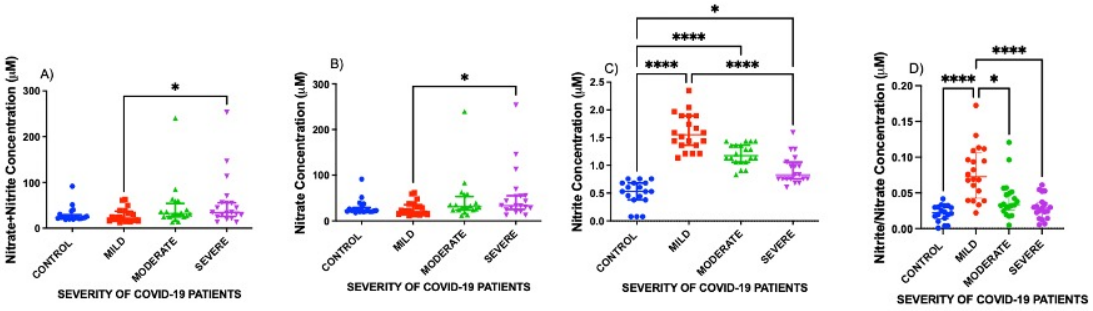

Figure 3. 44 Plasma Nitrate+nitrite levels (A), nitrate levels (B), nitrite (C), and nitrite/nitrate (D) levels in healthy controls and mild, moderate, and severe patients. *p <0.05, ****p<0.0001. Data are expressed as median ± interquartile range.

ROC analysis of RNS (nitrate+nitrite, nitrate, nitrite) level in COVID-19 patients

ROC was conducted to assess the predictive accuracy in correlating Nitrate+nitrite, nitrate, and nitrite levels with COVID-19 infection. There was a significant result for nitrite levels in the control vs. all COVID-19 groups (area under the curve (AUC) was 0.9765 to distinguish COVID-19 patients and controls with a p-value smaller than 0.0001) as seen in Figure 3.46 below. For the control vs. mild and moderate groups, the area was 1 with a p-value smaller than 0.0001, which means that a 100% nitrite level is a predictor for mild and moderate COVID patients. While the area was 0.9228 with p value smaller than 0.0001 for control vs. severe groups.

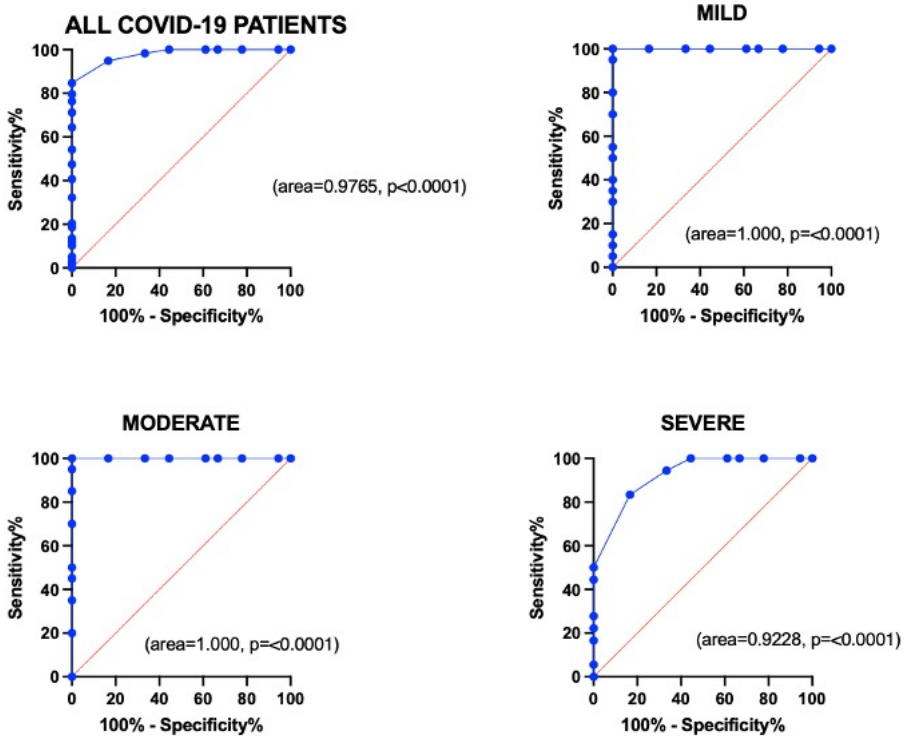

Figure 3. 45 ROC analysis of nitrite in the control vs all COVID-19 groups together and control vs. mild, moderate, and severe groups separately.

3.4.2 Measurement of ROS (8-isoprostane) in COVID-19 patients and healthy individuals' plasma samples

The objective of ROS analysis was to investigate the association between ROS level and the severity of COVID-19. 8-isoprostane is formed by the lipid peroxidation of arachidonic acid. It is one of the reliable oxidative stress markers used to measure ROS in plasma samples. As seen in Figures 3.47 and 3.48, 8-isoprostane levels were significantly higher in COVID-19 patients (median= 2990.983; **p<0.01) compared to the controls (median=278.745). A significant increase has been observed in the severe group (median=4073.15; **p<0.01).

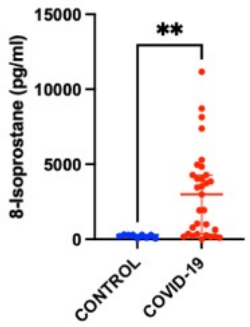

Figure 3. 46 Plasma 8-isoprostane level in healthy controls and COVID-19 patients. **p<0.01. Data are expressed as median ± interquartile range.

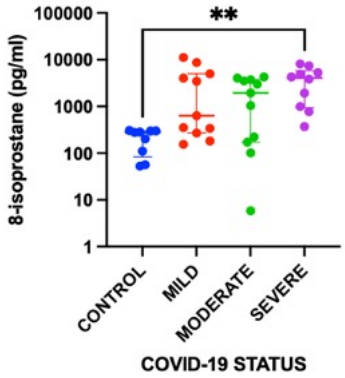

Figure 3. 47 Plasma 8-isoprostane level in healthy controls and mild, moderate, and severe patients. **p<0.01. Data are expressed as median ± interquartile range.

ROC analysis of ROS (8-isoprostane) level in COVID-19 patients

ROC analysis was conducted to assess the predictive accuracy of correlating 8-isoprostane levels with COVID-19 infection as seen in Figure 3.49. AUC was 0.8472 to distinguish COVID-19 patients and controls with a p-value of 0.0016. For the control vs. mild patients' area, it was 0.8283 with a p-value equal to 0.0135; for the control vs. moderate group area, it was 0.7273 with a p-value of 0.874; for the severe group area, it was 1 with a p-value of 0.0002 which means that 8-isoprostane level is best for distinguishing severe COVID-19 patients from control group as a biomarker.

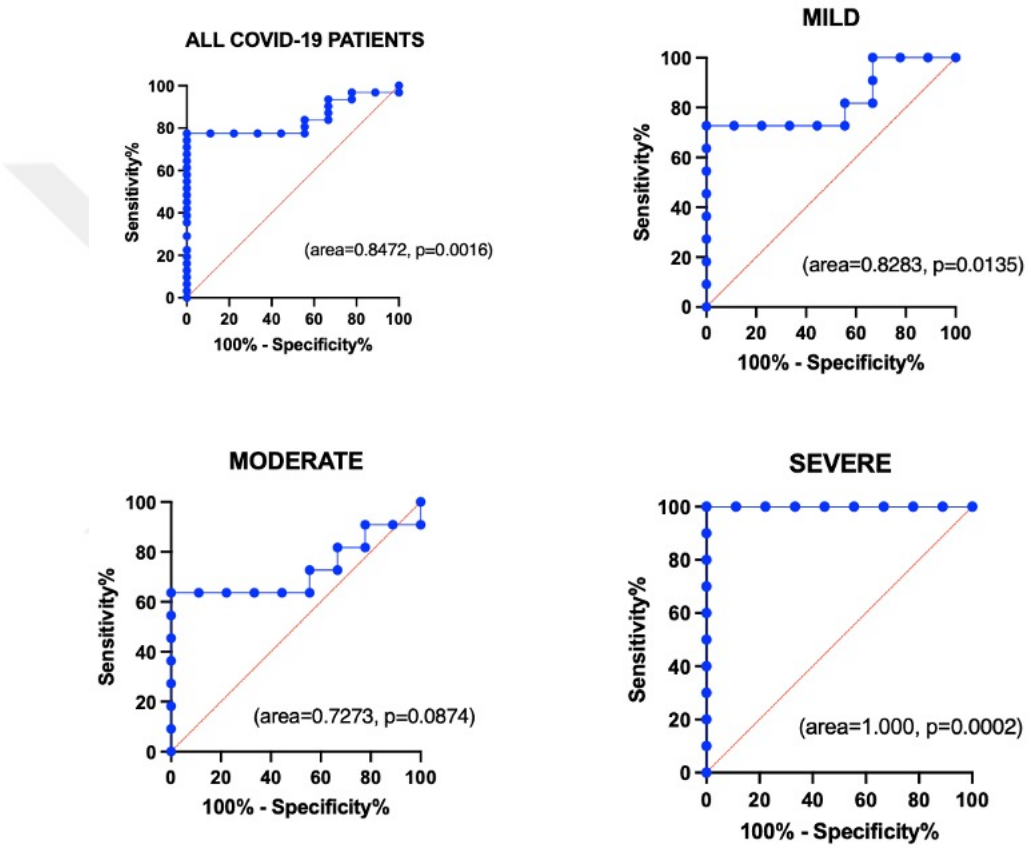

Figure 3. 48 ROC analysis of 8-isoprostane concentration in the control vs all COVID-19 groups together and control vs. mild, moderate, and severe groups separately.

Figures 3.46 and 3.49 show that RNS and ROS levels were significant determinants of COVID-19 status.

3.4.3 Measurement of inflammatory cytokines (IL1β, TNFα, GM-CSF, IL-6 and IL-8) in COVID-19 patients and healthy individuals plasma samples

The objective of inflammatory cytokine analysis was to investigate the association between plasma IL-6, IL-8, IL-1β, GM-CSF and TNF-α, levels and the severity of

coronavirus disease. As shown in Figure 3.50 below, there was no significant difference between groups in IL-1β, TNF-α, and GM-CSF analysis.

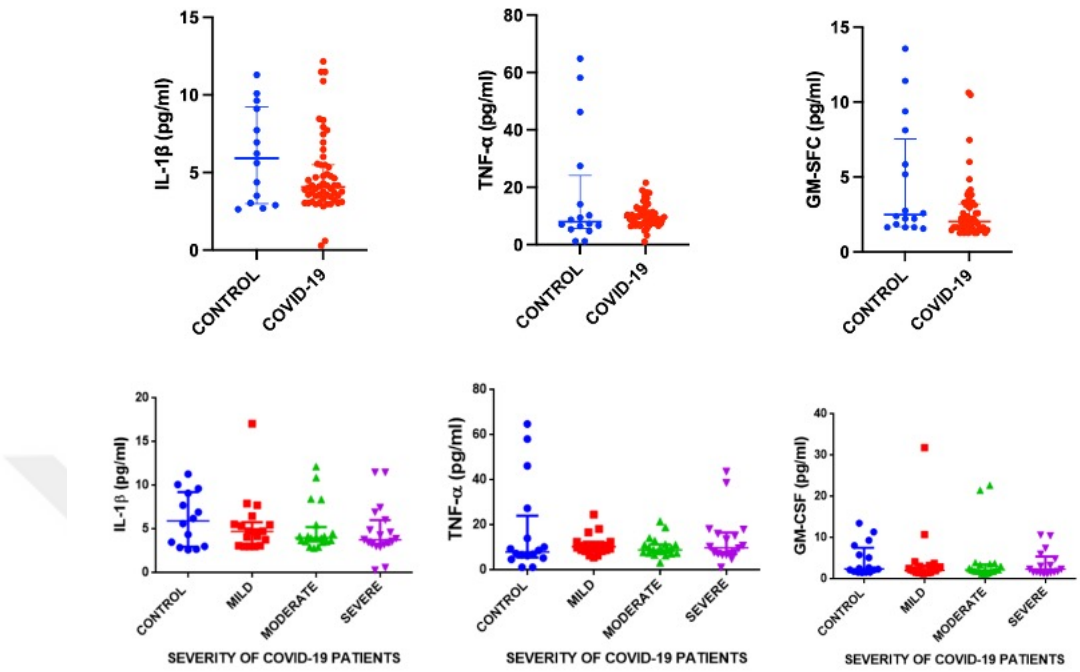

Figure 3. 49 IL1β, TNF-α, and GM-CSF levels in plasma samples of control vs. COVID-19 groups and control vs. mild, moderate, and severe groups, respectively. Data are expressed as median ± interquartile range).

In our ELISA experiments, we found that IL-6 levels were significantly greater in the COVID-19 group (median= 18.5615; ****p<0.0001) compared to the control (median=2.729), as seen in Figure 3.51. There was no gradual increase from mild patients (median=23.744; ****p<0.0001) to moderate (median=15.683; ***p<0.001) and severe ones (median=22.531; ****p<0.0001). Each patient group was significantly higher than healthy individuals as seen in Figure 3.51.

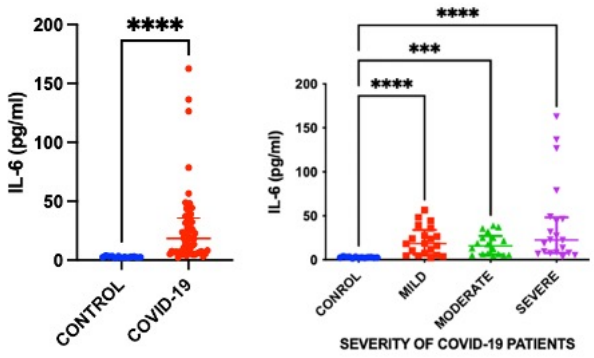

Figure 3. 50 Plasma IL-6 level in healthy controls and COVID-19 patients. ***p<0.001, ****p<0.0001. Data are expressed as median ± interquartile range.

In our ELISA experiments, we found that IL-8 levels were significantly greater in the COVID-19 group (median=36.786; *p<0.05) compared to the control group (median=27.7275) as seen in Figure 3.52. Control (median=27.7275; **p<0.01), mild (median=34.4935; *p<0.05), and moderate (median=31.009; *p<0.05), groups were significantly lower than severe cases (median=48.128).

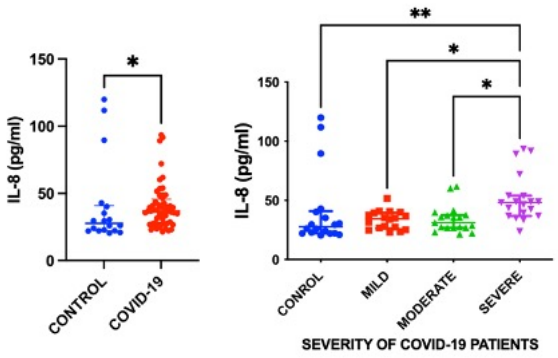

Figure 3. 51 Plasma IL-8 level in healthy controls and COVID-19 patients. *p<0.05, **p<0.01. Data are expressed as median ± interquartile range.

ROC analysis of inflammatory cytokines (IL-6 and IL-8) in COVID-19 patients

ROC analysis was performed to understand whether using IL-6 level to distinguish healthy people from COVID-19 patients is possible. AUC was 0.9801 with a p-value smaller than 0.0001 for all patient groups together, while the area was 0.9596 with a p-value smaller than 0.0001 for mild vs. control. AUC was 1 for the moderate vs. control group with a p-value smaller than 0.0001. Lastly, for severe vs. control analysis, the area was 0.9827 with a p-value smaller than 0.0001. As seen in Figure 3.53 below IL-6 is a good predictor for all COVID-19 patients' groups.

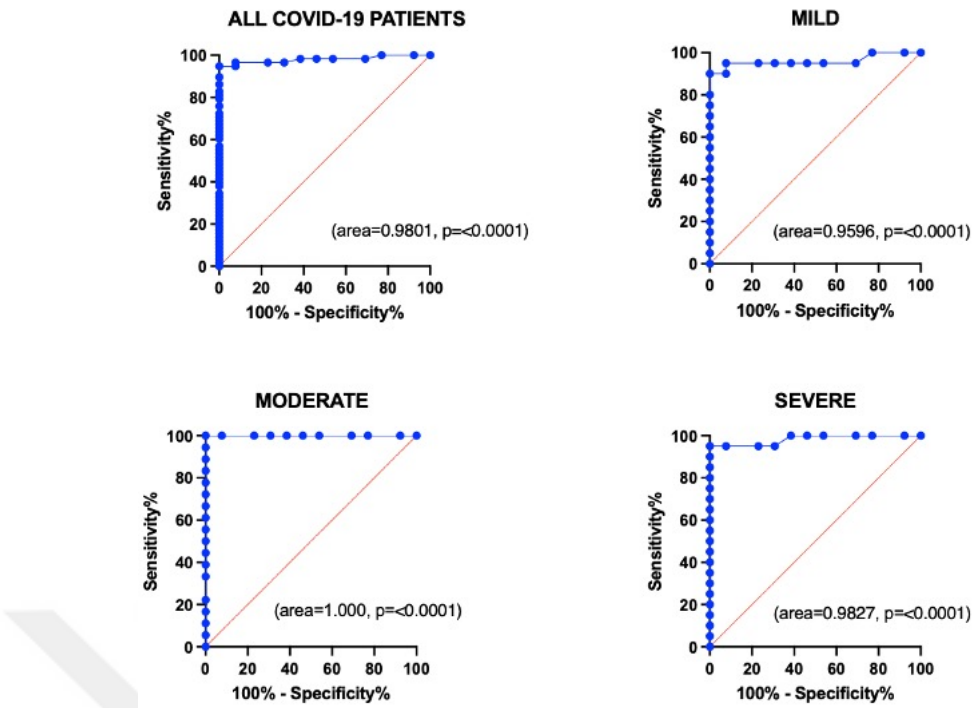

Figure 3. 52 ROC analysis of IL-6 concentration in the control vs all COVID-19 groups together and control vs. mild, moderate, and severe groups separately.

Lastly, ROC analysis was performed to understand whether it is possible to use IL-8 level to distinguish healthy people from COVID-19 patients as seen in Figure 3.54. AUC the curve was 0.6572, with a p-value of 0.0458 for all patients. It was 0.6080 with a p-value of 0.2681 for mil vs control, while the area was 0.5863 with a value of 0.3700 in the moderate group. Lastly, AUC was 0.07749, and the p-value was 0.043 for severe vs. control. These results demonstrate that IL-8 is not a better biomarker than IL-6, but still, it can be used especially for severe patients.

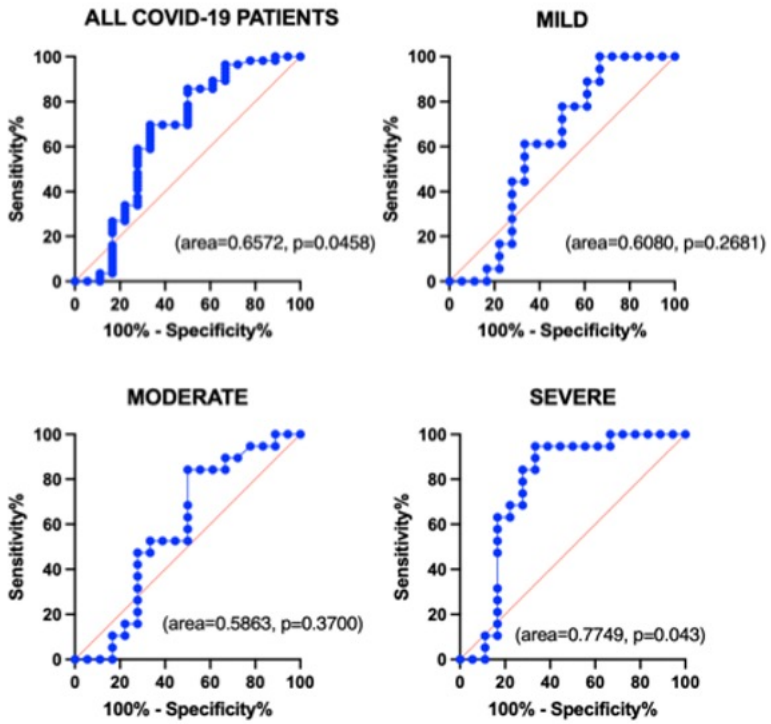

Figure 3. 53 ROC analysis of IL-8 concentration in the control vs all COVID-19 groups together and control vs. mild, moderate, and severe groups separately.

3.4.4 Measurement of inflammatory cytokines (IL-6 and IL-8) in hBEO supernatants

IL-6 and IL-8 measurements were done using supernatants of organoids infected or not infected with SARS-CoV-2, which are the control group, treated with $PM_{2.5}$ and $PM_{2.5}$ + inhibitors. A supernatant of organoids obtained from healthy bronchial epithelial cell lines was used as a non-smoker sample in without-infection groups, 2h infection groups, and 72h post-infection groups. Also, there were 3 different smokers' organoids supernatants in the without infection group, while there was one smoker' organoids' supernatant for 2h infection groups and 72h post-infection groups. Each measurement was repeated twice with 3 technical replicates.

Figure 3.55 represents the results of supernatants of organoids only exposed to the treatments without viral infection. As seen in Figure 3.55A, when the non-smokers' organoids were treated with $PM_{2.5}$ and $PM_{2.5}$ +inhibitors without infection, it was observed that $PM_{2.5}$ +inhibitors (median=83.278) decreased the IL-6 level compared to the control (median=193.147) and only $PM_{2.5}$ (median=202.559) treated group. As seen in Figure 3.55B, when the smokers' organoids were treated with $PM_{2.5}$ (median=129.39), IL-6 levels increased significantly compared to the control (median=43.3), $PM_{2.5}$

+inhibitors (median=54,523) treatment decreased the IL-6 level compared to the $PM_{2.5}$ (median=129.39) treated group significantly.

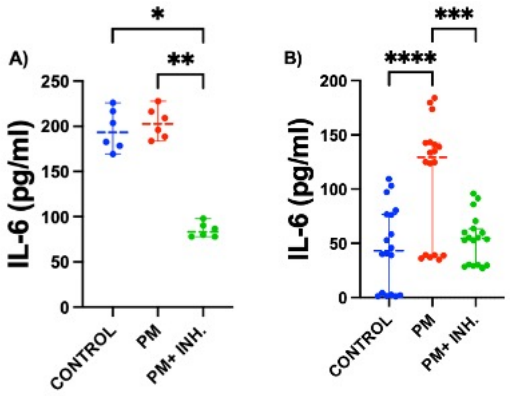

Figure 3. 54 Comparison of IL-6 levels in supernatants of organoids obtained from non-smokers (A) and smokers (B) between control, $PM_{2.5,}$ and $PM_{2.5}$ + inhibitors treated groups without SARS-CoV-2 infection. *p<0.05, **p<0.01, ***p<0.001, ****p<0.0001. Data are expressed as median ± interquartile range.

Figure 3.56 represents the results of supernatants of organoids exposed to the treatments before the 2h infection. As seen in Figure 3.56A, when the non-smokers' organoids were treated with $PM_{2.5}$ and $PM_{2.5}$ +inhibitors without infection, it was observed that $PM_{2.5}$ (median=23.484) increased the IL-6 level significantly compared to the control (median=8.411) while $PM_{2.5}$ +inhibitors (median=9.021) decreased the IL-6 level compared to the only $PM_{2.5}$ (median=23.484) treated group. As seen in Figure 3.56B, when the smokers' organoids were treated with $PM_{2.5}$. IL-6 levels did not change significantly compared to the control; $PM_{2.5}$+inhibitors (median=382.685) treatment increased the IL-6 level compared to the only $PM_{2.5}$ (median=123.185) treated group significantly, which was unexpected. Also, there were significant differences between non-smokers' and smokers' IL-6 levels after treatment with SAR-CoV-2 for 2 hours, which can be seen in Figure 3.58.

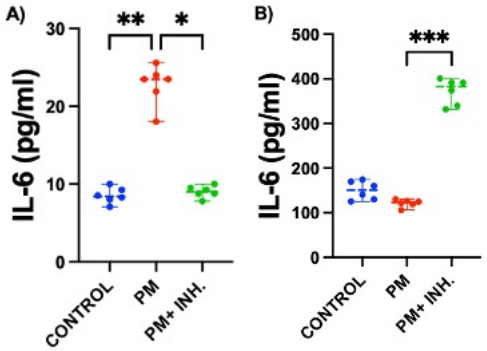

Figure 3. 55 Comparison of IL-6 levels in supernatants of organoids obtained from non-smokers (A) and smokers (B) in between control, $PM_{2.5}$, and $PM_{2.5}$ + inhibitors treated groups with 2h SARS-CoV-2 infection. *p<0.05, **p<0.01, ***p<0.001. Data are expressed as median ± interquartile range.

Figure 3.57 represents the results of supernatants of organoids exposed to the treatments prior to the 2h infection and 72-post infection incubation. As seen in Figure 3.57A, when the non-smokers' organoids were treated with $PM_{2.5}$ and $PM_{2.5}$ + inhibitors there were no significant changes in IL-6 levels. As seen in Figure 3.57B, when the smokers' organoids were treated with $PM_{2.5}$+ inhibitors (median=17.408), IL-6 levels were increased compared to the control (median=2.398),). Also, the drastic difference between non-smoker and smoker's IL-6 levels, after treatment with SAR-CoV-2 for 2 hours reduced after 72h post-infection incubation which can be seen in Figure 3.58.

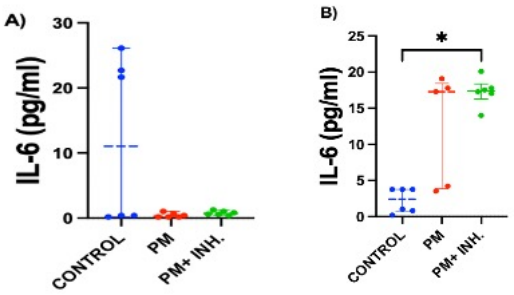

Figure 3. 56 Comparison of IL-6 levels in supernatants of organoids obtained from non-smokers (A) and smokers (B) in between control, $PM_{2.5}$, and $PM_{2.5}$ + inhibitors treated groups with 72h SARS-CoV-2 infection. *p<0.05. Data are expressed as median ± interquartile range.

In Figure 3.58 below, a 2-way ANOVA analysis was done to compare non-smokers vs. smokers. IL-6 levels of all non-smoker and smoker groups without infection can be seen. In control and $PM_{2.5}$-treated groups, non-smokers' IL-6 expression (median=193.147; 195.964) was significantly higher than smokers (median=43.3; 129.39). IL-6 levels of all non-smoker and smoker groups 2h infection supernatants can be seen. In controls, $PM_{2.5}$ treated groups, and $PM_{2.5}$+inhibitors treated groups, smokers IL-6 levels (median= 150.442; 123.185; 382.685) were higher than the non-smokers (median=8.411; 23.484;9.021). IL-6 levels in all non-smoker and smoker groups 72h post-infection supernatants can be seen. There was still a significant IL-6 level increase in smokers in terms of $PM_{2.5}$ (median=17.28; 0.294) and $PM_{2.5}$+ inhibitors (median=17.408; 0.715) compared to non-smokers.

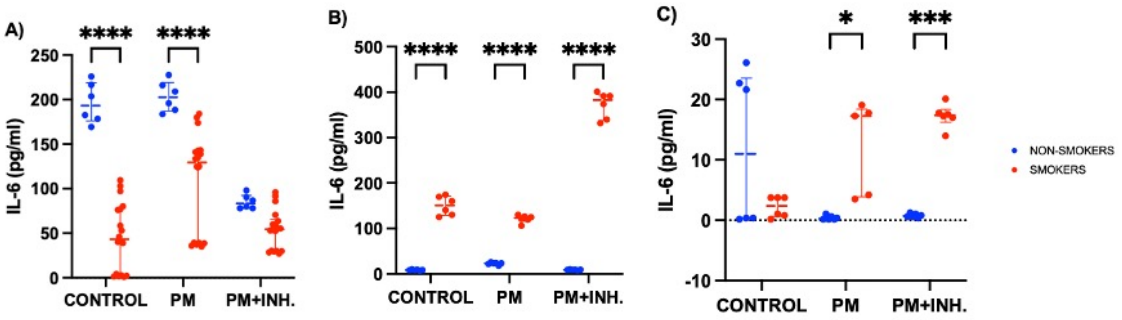

Figure 3. 57 Comparison of IL-6 levels in supernatants of organoids treated with $PM_{2.5}$ and $PM_{2.5}$+ inhibitors obtained from non-smokers vs. smokers without infection (A), with 2h infection (B) and 72h post-infection (C). *p<0.05, ***p<0.001, ****p<0.0001. Data are expressed as median ± interquartile range.

In Figure 3.59 below, all non-smoker data collected in 1 graph and 2-way ANOVA analysis were done to compare w/o infection, 2h infection, and 72h post-infection groups. For controls, there was a significant decrease in 2h infected (median=8.411) and 72h (median=11.027) post-infected groups compared to the w/o infection group (median= 193.147). For $PM_{2.5}$ treatment, there was a significant decrease in 2h infected (median=23.484) and 72h (median=0.294) post-infected groups compared to the w/o infection group (median= 195.964). For $PM_{2.5}$+ inhibitors treatment, there was a significant decrease in 2h infected (median=9.021) and 72h (median=0.715) post-infected groups compared to the w/o infection group (median= 83.278).

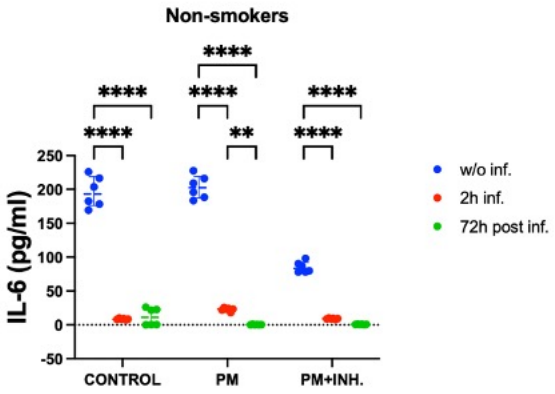

Figure 3. 58 Comparison of IL-6 levels in supernatants of organoids treated with $PM_{2.5}$ and $PM_{2.5}$ + inhibitors obtained from non-smokers without infection, 2h infection, and 72h post-infection groups. **p<0.01, ****p<0.0001. Data are expressed as median ± interquartile range.

In Figure 3.60 below, all smoker data collected in 1 graph and 2-way ANOVA analysis were done to compare w/o infection, 2h infection, and 72h post-infection groups. For controls, there was an increase in 2h infection (median=150.442 compared to the not infected group (median=43.3), which was attenuated with 72h post-infection (median=2.398). For $PM_{2.5}$ -treated ones, 72h post-infected group (median=17.535) was significantly lower than 2h infected (median=123.185) and not-infected groups (median=129.39). For $PM_{2.5}$ +inhibitors treated ones, there was an increase in 2h infection (median=382.685) compared to the not infected group (median=54.523), which was attenuated with 72h post-infection (median=17.408).

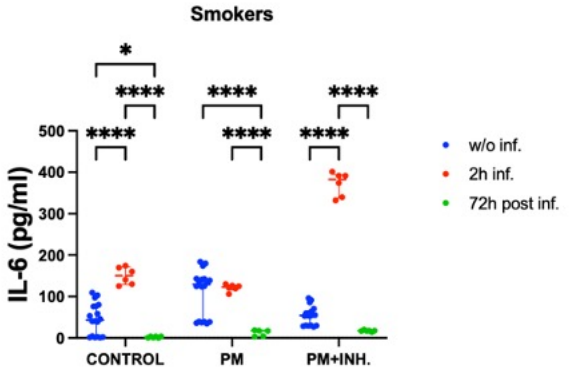

Figure 3. 59 Comparison of IL-6 levels in supernatants of organoids treated with $PM_{2.5}$ and $PM_{2.5}$ + inhibitor obtained from smokers without infection, 2h infection, and 72h post-infection groups. *p<0.05, ****p<0.0001. Data are expressed as median ± interquartile range.

Figure 3.61 represents the IL-8 results of supernatants of organoids only exposed to the treatments without viral infection. As seen in Figure 3.61A, when the non-smokers' organoids were treated with $PM_{2.5}$ + inhibitors without infection, it was observed that $PM_{2.5}$ + inhibitors (median=4879.8) decreased the IL-8 level compared to the control (median=12358). As seen in Figure 3.61B, there were no significant differences for smoker groups.

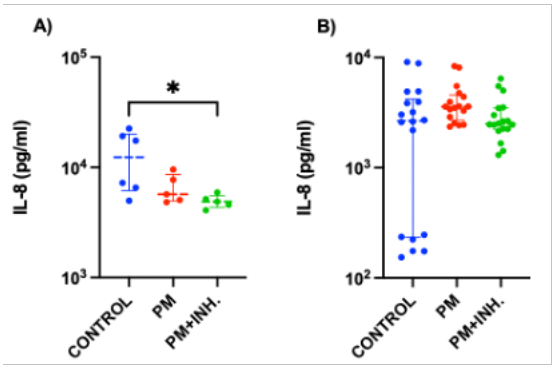

Figure 3. 60 Comparison of IL-8 levels in supernatants of organoids obtained from non-smokers (A) and smokers (B) between control, $PM_{2.5}$, and $PM_{2.5}$ + inhibitors treated groups without SARS-CoV-2 infection. *p<0.05. Data are expressed as median ± interquartile range.

Figure 3.62 represents the results of supernatants of organoids exposed to the treatments prior to the 2h infection. As seen in Figure 3.62A, when the non-smokers' organoids were treated with $PM_{2.5}$ and $PM_{2.5}$ +inhibitors, it was observed that $PM_{2.5}$ (median=1035.57) increased the IL-8 level significantly compared to the control (median=682.254) while $PM_{2.5}$ +inhibitors (median=1038.31) increased the IL-8 level significantly compared to the control (median=682.254) too. As seen in Figure 3.62B, there was no significant change for smoker groups.

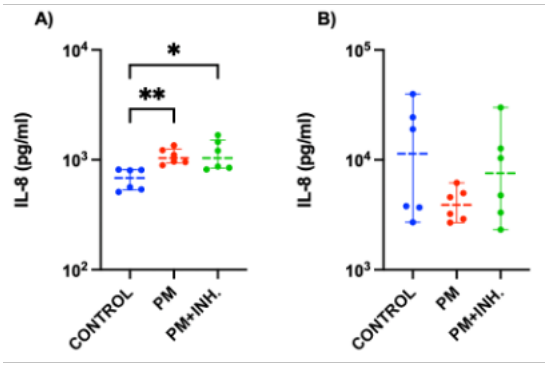

Figure 3. 61 Comparison of IL-8 levels in supernatants of organoids obtained from non-smokers (A) and smokers (B) between control, $PM_{2.5,}$ and $PM_{2.5}$ + inhibitors treated groups with 2h SARS-CoV-2 infection. *p<0.05, **p<0.01. Data are expressed as median ± interquartile range.

Figure 3.63 represents the results of supernatants of organoids exposed to the treatments prior to the 2h infection—and 72-post infection incubation. As seen in Figure 3.63A, when the non-smokers' organoids were treated with $PM_{2.5}$ inhibitors (median=88.943), a significant change in IL-8 levels was observed compared to the control (median=30.567).

$PM_{2.5}$+ inhibitors (median=88.943) group was significantly higher than only the $PM_{2.5}$ (median=41.894) group. As seen in Figure 3.63B, when the smokers' organoids were treated with $PM_{2.5}$ + inhibitors (median=698,387), the treatment also increased the IL-8 level compared to the control group (median=274.191). Also, there was a significant difference between non-smokers' and smokers' IL-8 levels after 72h post-infection incubation, which can be seen in Figure 3.64.

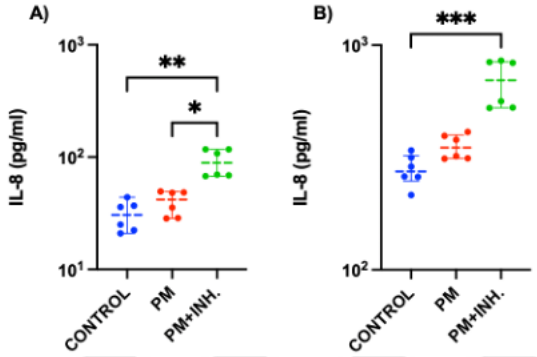

Figure 3. 62 Comparison of IL-8 levels in supernatants of organoids obtained from non-smokers (A) and smokers (B) between control, $PM_{2.5,}$ and $PM_{2.5}$ + inhibitors treated groups with 72h SARS-CoV-2 infection. *p<0.05, **p<0.01, **p<0.01. Data are expressed as median ± interquartile range.

In Figure 3.64 below, a 2-way ANOVA analysis was done to compare non-smokers vs. smokers. IL-8 levels of all non-smoker and smoker groups without infection can be seen in Figure 3.64A. In the controls, smokers without infection group, IL-8 level (median=2661.47) was lower compared to the non-smokers (median=12358). The opposite situation was observed for 2h infected groups (Figure 3.64B), with IL-8 levels higher in control smokers (median=11393.5) vs control non-smokers (median=682.254). For 72h post-infection (Figure 3.64C), IL-8 levels were elevated in smokers for control (median=274.191), $PM_{2.5}$ treatment (median=349.997), and $PM_{2.5}$ +inhibitors treatment (median=698.387) compared to the non-smoker (median=30.567; 41.894; 88.943) respectively.

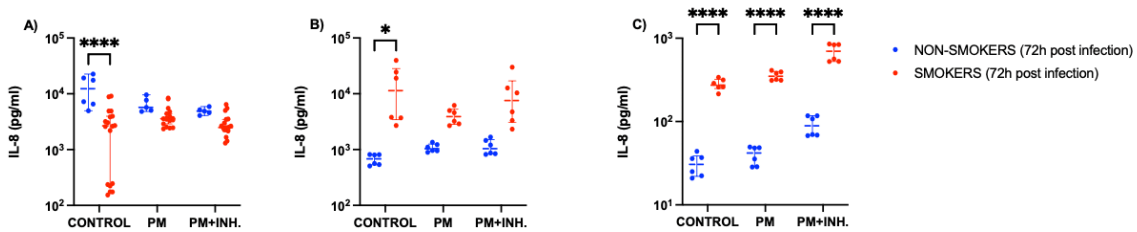

Figure 3. 63 Comparison of IL-8 levels in supernatants of organoids treated with $PM_{2.5}$ and $PM_{2.5}$ + inhibitors obtained from non-smokers vs. smokers without infection (A), with 2h infection (B) and 72h post-infection (C). *p<0.05, **p<0.01, ****p<0.0001. Data are expressed as median ± interquartile range.

In Figure 3.65 below, all non-smoker data collected in 1 graph and 2-way ANOVA analysis were done to compare w/o infection, 2h infection, and 72h post-infection groups. For controls, there was a significant decrease in 2h infected (median=682.254) and 72h (median=30.567) post-infected groups compared to the w/o infection group (median= 12358). For $PM_{2.5}$ treatment, there was a significant decrease in 2h infected (median=1035.57) and 72h (median=1038.31) post-infected groups compared to the w/o infection group (median=5706). For $PM_{2.5}$ + inhibitors treatment, there was no significant change.

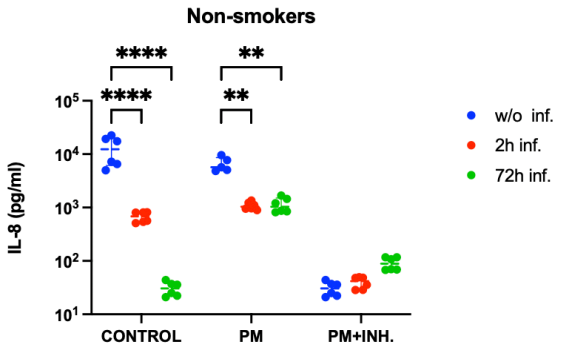

Figure 3. 64 Comparison of IL-8 levels in supernatants of organoids treated with $PM_{2.5}$ and $PM_{2.5}$ + inhibitors obtained from non-smokers without infection, 2h infection, and 72h post-infection groups. **p<0.01, ****p<0.0001. Data are expressed as median ± interquartile range.

In Figure 3.66 below, all smoker data collected in 1 graph and 2-way ANOVA analysis were done to compare w/o infection, 2h infection, and 72h post-infection groups. For controls, there was an increase in 2h infection (median=11393.5) compared to the not infected group (median=2661.47), which was attenuated with 72h post-infection (median=271.191). For $PM_{2.5}$ treated ones, no significant change between groups was observed. For $PM_{2.5}$+inhibitors treated ones, there was an increase in 2h infection (median=7571.56) compared to the not infected group (median=2496.18), which was attenuated with 72h post-infection (median=698.387).

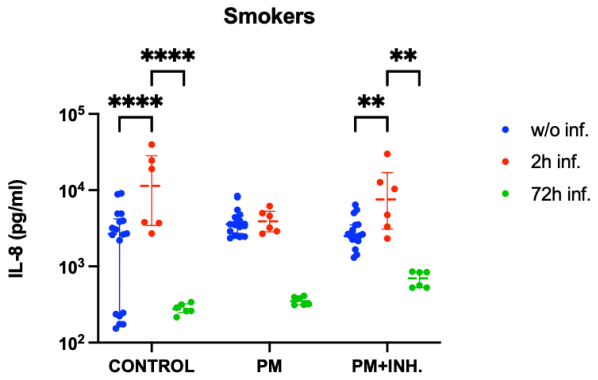

Figure 3. 65 Comparison of IL-8 levels in supernatants of organoids treated with $PM_{2.5}$ and $PM_{2.5}$ + inhibitors obtained from smokers without infection, 2h infection, and 72h post-infection groups. **p<0.01, ****p<0.0001. Data are expressed as median ± interquartile range.

CHAPTER 4

DISCUSSION

In this study, we investigated the role of reactive oxygen and nitrogen species in the pathogenesis and severity of COVID-19 and, the interaction between $PM_{2.5}$ and SARS-CoV-2 by using human bronchial epithelial organoids. We demonstrated increased viral load due to $PM_{2.5}$ which was partially possible to prevent by using ROS/RNS inhibitors. $PM_{2.5}$ created oxidative and nitrosative stress together with SARS-CoV-2 infection in terms of increased pro-oxidant expression and antioxidant mechanism activation, so elevated antioxidant expression. ROS/RNA inhibitors were relatively effective in the suppression of increased oxidative/nitrosative stress. Also, cell death mechanism activation was shown due to air pollutants. These molecular analyses were conducted by using qPCR, and RNA sequencing methods. Moreover, elevated ROS/RNS was shown in patients' plasma samples with spectrophotometric measurements. 8-isoprostane, ROS indicator, and nitrite, RNS indicator were determined as prognostic biomarkers for COVID-19 severity. Lastly, we established that IL-6 is a better biomarker than IL-8 for COVID-19 patients based on ELISA analysis.

SARS-CoV-2 infection is mostly associated with cytokine production, inflammation, and cell death, which might further lead to organ failure. Besides pneumonia, COVID-19 can damage many organs, including the liver, kidney, heart, immune system, and blood. Therefore, it is significant to pay attention to the molecular mechanism underlying the infection for protection and treatment methods (T. Wang et al., 2020). Oxidative stress is crucial in the pathophysiology of various acute and chronic diseases such as cancer, lung diseases, cardiovascular diseases, and viral infections like COVID-19 (Milatovic et al., 2011). Oxidative stress and inflammation reinforce one another, contributing to the systemic hyperinflammatory state (Vollbracht & Kraft, 2022). RNS, produced by local inflammatory and pulmonary cells, plays a role in the development of pulmonary infections and chronic lung conditions (Konyalilar et al., 2022). Moreover, in SARS-CoV-2 infection, RNS has been found to operate as a mediators of systemic inflammation (Ahmed et al., 2023).

The major aim of the study was to elucidate the molecular mechanism of oxidative and nitrosative stress due to SARS-CoV-2 infection and $PM_{2.5}$ in hBEOs and understand whether it might be prevented with ROS/RNS inhibitors. This step contained several objectives. The first one was organoid production. Initially, bronchial tissues obtained

from lobectomy or pneumonectomy surgeries are used to proliferate bronchial epithelial cells and then characterized with epithelial cell markers by immunofluorescence staining for further steps. Those cell cultures were expressing basal, ciliated, goblet, and secretory cells together with epithelial barrier proteins such as E-cadherin and occludin, which means that they are able to be used for bronchial organoid production. Most of the patients who underwent those surgeries were smokers or ex-smokers, which means there was a lack of non-smoker bronchial tissue, to overcome this problem, a human bronchial epithelial cell line was used for non-smoker human bronchial organoid production. The clinical and basic sciences in the field of lung research have been greatly impacted by traditional 2D cell culture methods. In contrast to in vivo and clinical observations and applications, it hasn't been sufficient to address all research questions, particularly in the past few years (Konar et al., 2016). What makes 3D cultures more advantageous than 2D cultures is that they have high heterogeneous tissue complexity and allow better observation of cell-cell and cell-matrix relationships (Joo et al., 2024). Nowadays, lung organoids are used in understanding the mechanism of various diseases and treatment methods (Chan et al., 2022). After the urge of the COVID-19 pandemic, with sequencing analysis, ACE2 and TMPRSS2, major SARS-CoV-2 entrance proteins, were proven to be predominantly expressed in transient secretory cells that are differentiated into goblet and ciliated cells. Therefore, bronchial organoids became one of the most valuable models to study SARS-CoV-2 infection (Lukassen et al., 2020). For these reasons, in our study, we conducted main cell culture experiments with hBEOs. Although COVID studies have accelerated very quickly due to the pandemic, mechanistic studies on the relationship between COVID and air pollution, especially those using 3D cultures, are still quite limited, so we believe that our study will make a significant contribution to the literature. Differentiated human bronchial epithelial organoids were obtained from proliferated human bronchial epithelial cells in 3-4 weeks; their characterization was done with epithelial cell markers before treatments. For organoid imaging, Dekkers et al.'s protocol was used as a reference (Dekkers et al., 2019). Also, characterized organoids were used to show ACE2, TMPRSS2, and Furin expression with qPCR analysis to be sure that these organoids could be infected with SARS-CoV-2.

The second objective was the collection, isolation, and dose optimization of $PM_{2.5}$ samples. As indicated previously, air pollution is one of the most important health and environmental issues worldwide (Comunian et al., 2020). PMs are one of the major components of this pollution presented indoors and outdoors, especially in crowded and

traffic-heavy areas (Boogaard et al., 2022). They have a role as a crucial risk factor for various diseases like heart diseases, lower respiratory tract infections, COPD, asthma, lung cancer, and diabetes (Ritchie, 2024). Due to its small size, $PM_{2.5}$ is one of the most dangerous ones that can be transported through alveoli and enter the circulation, leading to pulmonary inflammation together with increased oxidative, nitrosative stress that might lead to and further (Donaldson et al., 2001; Pu et al., 2022). Due to these reasons, we collected $PM_{2.5}$ samples from the city center for approximately 7 months to have a heterogeneous mixture that represents inhaled $PM_{2.5}$ pollutants by individuals better. Teflon filters were preferred instead of quartz ones to eliminate the filter fiber contamination. In recent years, studies have been published from all around the world, establishing a linear correlation between COVID-19 cases, hospitalization and mortality, and air pollution in terms of $PM_{2.5}$ (Andrée, 2020; Aykaç & Etiler, 2022; Conticini et al., 2020; Travaglio et al., 2021; Wu et al., 2020; Yao et al., 2020; Zhu et al., 2020). In our previous study, we demonstrated that SARS-CoV-2 is present on those PMs, especially in busy locations, which makes the transportation of the virus for longer time periods and distances (Kayalar et al., 2021). Moreover, SARS-CoV-2 occupies ACE2 receptors, which causes the shift of the RAS system from an anti-inflammatory to an inflammatory pathway, while PM has an inhibitory effect on the release of some antiviral cytokines (Frontera et al., 2020; B. Wang et al., 2020). Also, some research showed an increased expression of the SARS-CoV-2 entrance-related genes and proteins with the elevated PM concentration in different models (Sagawa et al., 2021). It has been demonstrated that PM impairs epithelial barrier integrity, causing more virus uptake (Fiorito et al., 2022). Bayram and colleagues have demonstrated reduced ciliary beating frequency and elevated inflammatory stimulators due to the pollutants in primary human epithelial cells, which has an impact on defective immune response to infection and augmented cell death (Bayram et al., 1998; Bayram et al., 2013; Bayram et al., 2006). Research conducted with the PMs collected in London has shown increased ACE2 expression in primary human nasal epithelial cell line due to exposure to PM_{10} while it was attenuated by co-treatment of cells with PM_{10} and NAC (Miyashita et al., 2023).

Prior to the SARS-CoV-2 infection, organoids were treated with $PM_{2.5}$ to create oxidative/nitrosative stress and to check whether it influences the infection. Also, NAC and L-NMMA are used as reactive oxygen and nitrogen species inhibitors, respectively. NAC is a significant stimulator for antioxidant GSH production, a precursor in synthesizing reduced GSH. It has mucolytic effects and reveals a wide range of

antioxidant and anti-inflammatory activities by scavenging free radicals. It is an FDA-approved drug recommended for various disease treatments, such as pneumonia, ARDS, and COPD (Liu et al., 2024). Moreover, previously, anti-thrombotic effects had been presented with an inhibitory effect on the NF-KB pathway in response to infections such as influenza and respiratory syncytial virus. Therefore, elevated scientific attention on NAC has prompted the evaluation of its efficacy in COVID-19 research (Alam et al., 2023; Chen et al., 2023). Some randomized trials demonstrated that NAC treatment decreased the C-reactive protein and D-dimer levels in COVID-19 patients compared to the control group, which may have a reducing effect on the severity of the disease (Assimakopoulos et al., 2021; Avdeev et al., 2022; de Alencar et al., 2021). Also, few studies demonstrated the attenuated mortality rates due to the NAC treatment (Assimakopoulos et al., 2021; de Alencar et al., 2021; Faverio et al., 2022; Izquierdo et al., 2022). L-NMMA is a nonspecific NOS inhibitor, effective for all types of NOS such as eNOS (endothelial NOS), iNOS (inducible NOS) and nNOS (neuronal NOS) (Joneschild et al., 1999). The anti-inflammatory effect of L-NMMA in various diseases such as renal, neurodegenerative, and cardiovascular diseases has been presented (Haşimi et al., 2023). Reports have demonstrated higher levels of blood NO^-_3 and NO^-_2, which are metabolites of NO, in COVID-19 patients, especially in the severe ones, compared to the healthy controls. One of the reasons for this might be the higher iNOS synthesis during the inflammation (W. Fang et al., 2021). So, inhibition of NOS may be a treatment option to prevent the disease from worsening.

NAC and L-NMMA were used simultaneously with $PM_{2.5}$ and couldn't be applied separately to check their individual effect on organoids, since it was necessary to keep the number of groups limited because of the high cost of 3D culture production. Dose optimization of $PM_{2.5}$, NAC, and L-NMMA was conducted with bronchial epithelial cell line BEAS-2B cell by cell viability assay. 100 μg/ml for 24h was the most effective dose higher than the IC50 value for $PM_{2.5}$ to create oxidative/nitrosative stress while not causing the death of the cell population. 8 mM NAC and 100 μM L-NMMA, 24h were chosen as the optimum concentrations and duration due to the increasing effect on cell viability compared to the control separately and in the presence of $PM_{2.5}$ (100 μg/ml). Moreover, they had a higher protective effect when they were applied together.

As the third objective, the SARS-CoV-2 infection dose and duration were optimized with the help of Chan and colleagues' study (Chan et al., 2022). At the end of

the differentiation period, organoids were transferred to ultra-low attachment plates for 3 days to change the inward position to the outward position. When organoids are obtained in matrigel mostly ciliated, goblet cells face the lumen while basal cells cover the outer layer. Since ciliated and goblet cells are the major cells in bronchial tissue expressing ACE2 and TMPRRS2, flip-flopping those cells outward raises the possibility of binding and getting into cells of SARS-CoV-2 so that the infection efficacy too (Chan et al., 2022; Lukassen et al., 2020). Since a longer stay without an extracellular matrix may cause deterioration in the organoid conformation and the flip-flop could be clearly observed in 3 days, organoids were incubated at ultra-low attachment plates for 3 days. On the last day of 3 days, organoids were treated with $PM_{2,5}$ and $PM_{2,5}$+ inhibitors for 24h. At the end of those treatments, organoids were infected with SARS-CoV-2 in the BSL3 lab. MOI 0.5 for 2h was chosen as the optimum dose and duration of the infection with immunofluorescence staining of SARS-CoV-2 spike a structural protein facilitating viral entry (V'kovski et al., 2021). Lower doses were not enough for the infection while increasing infection periods such as 24 and 48h led to cell death and deformed organoid structure. To overcome these problems and increase the infection efficacy, it was decided to infect cells in an ultra-low attachment plate for 2h and incubate them 72h in matrigel as a post-infection period so that viruses taken into cells can be proliferated inside. Post-infection periods of more than 72h were also detrimental for cells even in the matrigel. Furthermore, qPCR for the SARS-CoV-2 N1 gene, encoding a structural protein bounded to the viral RNA and forming the nucleocapsid, was applied to the 2h infection media as a positive control and to the organoids after the 72h post-infection to check whether the organoids are infected with the virus and also to check if the $PM_{2.5}$ and inhibitors have any effect on infection (V'kovski et al., 2021). Before that, for viral load calculation, SARS-CoV-2 N1 gene qPCR was applied to the serial dilutions (10^7 to 10^1) to create a standard equation of the virus sample itself. According to qPCR results, it was shown that CT values above 35,93 were negative. In our samples of non-smoker organoids 2h infection media, which has CT values between 30-35, corresponding to 3-5 PFU/ml, there was a significant increase in viral load in the $PM_{2.5}$- treated group compared to the controls while it was decreased with the addition of inhibitors. Viral load was similar between non-smoker and smoker organoids supernatants. Only smokers had a lower amount of virus in the $PM_{2.5}$ treated group. Viral load was parallel in the 72h post-infected organoids itself. There was a significantly increased viral load after the $PM_{2.5}$ treatment compared to the control, and it was reduced when the organoids were treated with $PM_{2.5}$+

inhibitors compared to the control and only the $PM_{2.5}$-treated group. These results support the phenomena of increased viral infection due to air pollution, which is explained above. On the other hand, smoker organoids 2h infection media showed no differences between $PM_{2.5}$ and inhibitor treatment. It can be speculated that smoker organoid susceptibility to SAR-CoV-2 was not altered with air pollution.

At the end of treatment and infection protocols, organoid qPCR analyses were conducted to investigate the oxidative/nitrosative stress-related mechanisms. Redox homeostasis in infected cells and lung inflammation are hallmarks of infections caused by respiratory viruses (Komaravelli & Casola, 2014) Firstly, the antioxidant mechanism NFE2L2 pathway was checked. NFE2L2 is a transcription factor bound to KEAP1 protein in the cytosol in physiological conditions while transported to the nucleus and activating the expression of antioxidant genes such as HMOX1, and NQO1 in the presence of oxidative stress (Gain & Kelesidis, 2023). It has been demonstrated that NFE2L2 activation contributes to the preservation of lung architecture in response to inflammatory stimuli. Additionally, NFE2L2 activation has been found to have therapeutic benefits in animal models of ARDS and respiratory infections, among other lung illnesses (Cuadrado et al., 2020). In our analysis, we demonstrated the increased NFE2L2 gene expression in non-smoker and smoker organoids treated with $PM_{2.5}$ without infection, showing the sufficiency of $PM_{2.5}$ to create an oxidative stress that activates this pathway. Also, it was reversed in both groups when the organoids were exposed to the inhibitors which present that inhibitors were effective on this mechanism in suppressing oxidative/nitrosative stress. On the other hand, in the SARS-CoV-2 infected groups, $PM_{2.5}$ was not enough by itself to create transcriptional difference while $PM_{2.5}$+ inhibitors were increasing the expression of the NFE2L2 gene. Based on 2-way ANOVA results, $PM_{2.5}$ treated organoids expressed lower levels of NFE2L2 when infected. A study conducted with COVID-19 lung biopsies revealed the suppression of this pathway while NFE2L2 inducer drugs prevent the replication of SARS-CoV-2 and inflammation (Olagnier et al., 2020). So based on our result, we can speculate that $PM_{2.5}$ might cause an extra burden to those cells in terms of stress in which the antioxidant mechanism was not able to reverse this situation, with the activation of the antioxidant pathway by NFE2L2 transcription factor. When it was reversed with oxidative/nitrosative stress inhibitors, the organoids were able to create an antioxidant answer for the virus. For KEAP1 expression, the non-infected smoker group represented the opposite results of NFE2L2 which was expected since KEAP1 acts as an inhibitor of NFE2L2 in the cytosol.

There were no changes for the non-smoker, not-infected groups. The level of the KEAP1 gene was significantly higher in control groups of smokers compared to non-smokers, the low amount of KEAP1 gene in non-smokers might be the reason not to see any changes in transcription level, a relatively significant difference might be observed in translational level. Furthermore, an antiviral response against numerous viruses, such as HIV, influenza virus, RSV, and Ebola virus, has been linked to upregulation of the NFE2L2-transcriptional target HMOX1 (Espinoza et al., 2017). HMOX1 can initiate an antiviral response by activating the interferon response (Koliaraki & Kollias, 2011). In our results, it was increased in the smoker, non-infected group, and non-smoker, infected group with the $PM_{2.5}$ treatment while reversed with the addition of inhibitors. In contrast, non-smoker, not-infected groups were not affected in terms of HMOX1 expression after $PM_{2.5}$ and $PM_{2.5}$ inhibitors treatments while NQO1 expression was significantly increased with the $PM_{2.5}$ exposure and attenuated with the inhibitors. According to these results, it can be said that in non-smoker groups without infection, there might be increased oxidative stress by $PM_{2.5,}$ activating NQO1 antioxidant first instead of HMOX1, while it was the opposite for non-smokers, SARS-CoV-2 infected groups. In smoker groups without infection, both were activated. Remarkably, the antioxidant and cytoprotective effects of NFE2L2/KEAP1 axis activation are long-term persistent, due to enzyme-mediated mechanisms instead of small molecules and longer half-lives, in contrast to direct antioxidants like vitamin C, which are extrinsic, short-lived (minutes to hours) and depleted during the process of ROS scavenging, (Gao et al., 2001; Schmidt et al., 2015). So, pharmacological activation of this pathway in the context of SARS-CoV-2 infection might be a better solution in the treatment by protecting the host cell more consistently, promoting an anti-inflammatory response, and inhibiting the viral proliferation (Cuadrado et al., 2020). Olagnier et al. demonstrated decreased expression of HMOX1 and NQO1 with SARS-CoV-2 infected Vero-6 cells (Olagnier et al., 2020). In our analysis, we observed reduced HMOX1 levels in the $PM_{2.5}$+inhibitors treated group and attenuated NQO1 in $PM_{2.5}$, $PM_{2.5}$+inhibitors treated groups in the infected organoids compared to the non-infected ones. These results will contribute greatly to the knowledge on this subject, as they contain 3D culture data that support the results obtained in 2D studies in the literature. GPX4 and SOD1 are other antioxidant enzymes induced by the NFE2L2/KEAP1 pathway (Emanuele et al., 2021). However, there were no significant differences in any circumstances for GPX4 in our 3D cultures, while SOD1 was elevated in $PM_{2.5}$+ inhibitors groups compared to the controls in each condition. CYGB, a

scavenger of NO that decreases the production of peroxynitrite so RNS, was measured to assess nitrosative stress due to air pollution and SARS-CoV-2 infection. Thuy and colleagues established increased nitrate+nitrite levels in CYGB knockout mice compared to the wildtype (Thuy et al., 2016). Also, CYGB level elevates in hypoxic conditions (Burmester et al., 2007; Huang et al., 2006). Based on our analysis, in the SARS-CoV-2 infected groups, $PM_{2.5}$ elevated CYGB expression which means nitrosative stress was created by air pollution, so the anti-nitrosative mechanism activated in contrast to non-infected groups. Moreover, this nitrosative stress was reversed by the addition of ROS/RNS inhibitors.

Furthermore, cell death mechanisms ferroptosis and apoptosis were investigated. ACSL4, the main indicator of ferroptosis was significantly elevated due to $PM_{2.5}$ compared to the control group; $PM_{2.5}$+ inhibitors decreased the expression compared to the only $PM_{2.5}$ treated group in non-smoker groups both SARS-CoV-2 infected and not infected ones. As mentioned previously, HMOX1 catalyzes heme degradation causing an iron release to the cytosol, accumulation of the iron leads to the induction of ROS production through the Fenton reaction which initiates ferroptosis. So, the NFE2L2 pathway has a regulatory role in ferroptosis too. (Ju et al., 2021). In our infected groups both HMOX1 and ACSL4 expression was increased with the $PM_{2.5}$ and reversed with the inhibitor addition which supports the literature. Since NFE2L2 partly modulates ferroptosis and ferroptosis may take part in organ damage during COVID-19, targeting the NFE2L2 pathway combating SARS-CoV-2 infection might be a more efficient than directly inhibiting cell death when the antioxidant system considered (Fratta Pasini et al., 2021).

As an intrinsic apoptotic pathway marker CASP9, as an anti-apoptotic marker BCL-2 expression was investigated. In all groups (non-smoker, smoker not infected, and non-smoker, infected ones) apoptosis was induced by $PM_{2.5}$ as CASP9 expression was raised compared to the control while decreased with the inhibitors. As supporting data, inhibitors increased BCL-2 expression in not-infected groups even the PM had no effect. On the other hand, PM decreased the BCL-2 expression in infected ones which means there might be higher apoptotic activation in infected organoids. Lastly, CASP1, an inflammatory cell death pyroptosis marker was measured. It was significantly higher in $PM_{2.5}$ treatment groups for non-smokers both infected and not-infected ones while inhibitors reversed it in not-infected non-smokers indicating the importance of prevention

of ROS/RNS on the inflammatory cascade. Due to insufficient mRNA isolation, the infected organoids had no $PM_{2.5}$+ inhibitor groups for CASP1, CASP9, and BCL-2.

Furthermore, SARS-CoV-2 infected and not-infected organoids' culture supernatants were collected to investigate inflammatory mediators released due to $PM_{2.5}$, $PM_{2.5}$+ inhibitors, and SARS-CoV-2 from organoids. Since a significant difference was observed in IL-6 and 8 in the in vivo setup, these cytokines were also examined in the in vitro setup too. Numerous studies using cell lines, human samples, and animal models demonstrated increased IL-6 levels due to air pollution. For instance, Quay et al., showed elevated IL-6 mRNA in BEAS-2B cells due to fine particles (Quay et al., 1998). Thompson and colleagues presented strong correlation with air pollutants and IL-6 in healthy adults blood samples (Thompson et al., 2010). Liu et al. presented increased IL-6 levels in lung tissue and plasma of wild-type mice due to intratracheal exposure to PMs (Liu et al., 2018). Moreover, cigarette smoke's effect on cytokine release was investigated in different models. Higher IL-6 level was observed in breath condensate and plasma of smokers (Carpagnano et al., 2003; Elisia et al., 2020; Helmersson et al., 2005). Today, antioxidant therapy is a subject being researched for use in the treatment of inflammation-related problems. Recently, NAC's reducing effect on IL-6 release was demonstrated in different meta-analyses of randomized clinical trials with blood samples (Askari et al., 2020; Faghfouri et al., 2020). It is known that normal physiologic concentration of NO stimulates IL-6 release and pharmacological inhibition of NO was found to attenuate IL-6 mRNA (Siednienko et al., 2011; Steensberg et al., 2007). We used L-NMMA as an inhibitor agent of NO synthase together with NAC as an antioxidant. In our results, for the not-infected organoids, there was an escalation of IL-6 level with air pollutant in the smoker group, which was not significant for non-smokers. Inhibitors decreased the IL-6 release compared to only $PM_{2.5}$ exposure in both smokers and non-smokers. So, these finding supports the literature.2h SARS-CoV-2 infection, increased the IL-6 level in non-smoker organoids which were treated with $PM_{2.5}$ while inhibitors reversed it. However similar results were not obtained for smokers, there was an increase in IL-6 levels with the treatment of $PM_{2.5}$+ inhibitors. But still, IL-6 level was significantly higher in smoker groups compared to the non-smokers. After 72h post-infection, the smoker graph represented a significant increase in $PM_{2.5}$+ inhibitors compared to only $PM_{2.5}$ exposure. However, the drastic difference between non-smokers' and smokers' IL-6 levels after treatment with SAR-CoV-2 for 2 hours reduced after 72h post-infection incubation. But still significantly higher than non-smokers.

IL-8 expression in not-infected groups did not change with $PM_{2.5}$ exposure. It could be explained as short-term exposure to this pollutant was not sufficient for IL-8 stimulation. A study conducted with 251 COPD patients' blood samples showed that short-term exposure to $PM_{2.5}$ was not associated with IL-8 level (Dadvand et al., 2014). A randomized cross-over study established an insignificant change in IL-8 levels due to short-term exposure to $PM_{2.5}$ too (Kumarathasan et al., 2018). Moreover, studies investigating long-term PM exposure and IL-8 levels are very limited in performing meta-analysis (Tang et al., 2020).SARS-CoV-2 infection for 2h and increase the IL-8 level in $PM_{2.5}$ and $PM_{2.5}$+ inhibitors treated non-smokers. However, the significance was higher for only $PM_{2.5}$ exposure which can be speculated as inhibitors were relatively effective in the suppression of IL-8 due to pollutant. In the 72h post-infection group, opposite results were obtained for both non-smokers and smokers. Inhibitors stimulated IL-8 release. After the post-infection period, IL-8 levels were significantly greater in smokers compared to non-smokers. Different studies reveal the association of increased IL-8 levels with cigarette smoke exposure too (Caruso et al., 2021; Cui et al., 2021).

Another objective of the study was to investigate the transcriptional alterations in SARS-CoV-2 infected hBEOs treated with air pollutants and ROS/RNS inhibitors. For this objective, oxidative stress and cell death-related genes were investigated. Moreover, bronchial epithelial cell markers, epithelial barrier markers, and viral entry-related genes were examined. RNA sequencing was done to the hBEOs which were SARS-CoV-2 infected. Before the infection, organoids were treated with $PM_{2.5}$ and $PM_{2.5}$+ROS/RNS inhibitors. Only the virus-infected group without treatment was used as their control. RNA sequencing offers a comprehensive analysis of cellular gene expression profiles, playing a significant role in the investigation of biological processes and elucidation of the molecular mechanisms of diseases. This methodology significantly provides new targets for the diagnosis and treatment of diseases (Stark et al., 2019; Wang et al., 2009). Our findings indicate that in SARS-CoV-2 infected hBEOs, exposed to $PM_{2.5}$, the expression of major viral entry genes such as ACE2, and TMPRSS2, did not change, whereas the expression of the ANPEP gene was increased. Similar elevation was observed in the $PM_{2.5}$+inhibitors group too. There was no significant difference between only $PM_{2.5}$ and $PM_{2.5}$+inhibitors treated groups. ANPEP gene encodes an alanyl aminopeptidase that serves as a receptor for certain coronaviruses. Specifically, ANPEP is known to be the primary receptor for HCoV-229E, an alpha coronavirus. While its direct involvement in the entry of SARS-CoV, MERS-CoV, and SARS-CoV-2 has not

been established, studies suggest that different coronaviruses utilize distinct receptors and co-receptors for cell entry. For example, the entry of SARS-CoV and SARS-CoV-2 predominantly relies on the ACE2 receptor, while MERS-CoV uses Dipeptidyl peptidase-4 (DPP4) as its receptor (Kratzel et al., 2021; Murgolo et al., 2021). So based on this data, it can be said that air pollutant $PM_{2.5}$ increased the virus receptor ANPEP in hBEOs while ROS/RNS inhibitors were not effective in suppressing this elevation. C1R gene encodes a member of the peptidase S1 protein family which is part of the complement system and plays a crucial role in the immune response. Although C1R is not a direct receptor for coronavirus entry, the complement system's overall state can influence viral pathogenesis and the host's inflammatory response. Dysregulation of the complement system can exacerbate disease severity, as seen in severe COVID-19 cases where complement activation contributes to hyperinflammation and tissue damage (Kulasinghe et al., 2022; Yu et al., 2022). Yan and colleagues presented that complement pathways were among the most greatly enriched of all pathways due to SARS-CoV-2 infection by examining the transcriptome of primary human bronchial epithelial cells and the alveolar epithelial cell line A549. They have demonstrated increased C1R in the SARS-CoV-2 infected cell line compared to the control (Yan et al., 2020). Another sequencing research conducted with autopsy patient samples revealed upregulation of C1R in the lungs of COVID-19 patients compared with those from patients who died of non-viral causes (Kulasinghe et al., 2022). In our dataset, C1R was upregulated in the $PM_{2.5}$+ inhibitors group after the virus infection. Usually, complement activity is defensive during viral infections and critically essential to control the pathogen however there are few exceptions (Stoermer & Morrison, 2011). The mechanism that alters this usually protective system into a dangerous one during COVID-19 is still not clear. It might be due to the virus's overwhelming combined local and systemic complement activation. Another unique aspect of our study is that it proves the altered expression of these two genes related to virus entry, due to air pollutants and ROS/RNS inhibitors, which are not widely covered in the literature and especially not shown in 3D cultures.

Oxidative stress association with SARS-CoV-2 infection and the impact of $PM_{2.5}$ and ROS/RNS inhibitors were studied at the transcriptomic level. NOS3 is critical for producing NO, a molecule that modulates vascular tone and oxidative stress used as a marker of pro-oxidant. In the lungs, primarily pulmonary endothelial cells, also bronchial and alveolar epithelial cells express NOS3. It is localized at the basal membrane of ciliary microtubules which has a role in CBF along with induction of epithelial inflammatory

mediators (Bove & van der Vliet, 2006). According to our analysis, NOS3 was upregulated in the $PM_{2.5}$ group compared to the control which indicates oxidative stress mechanism activation due to pollutant. There were no significant changes between the $PM_{2.5}$+inhibitor group versus the control so it can be speculated that ROS/RNS inhibitors were effective in suppressing the activation of oxidative stress which is induced in only the $PM_{2.5}$ treated group. Since we used L-NMMA, a nonspecific NOS inhibitor as an RNS inhibitor, it was expected to see inhibition of NOS.

Apoptosis related genes were also included in the transcriptomic analysis. There was downregulation of the anti-apoptotic BCL2A1 gene in the $PM_{2.5}$-treated group compared to the control. Even though there was no significant difference between only $PM_{2.5}$ exposed and $PM_{2.5}$+inhibitors exposed groups it can be speculated that ROS/RNS inhibitors partly affected the inhibition of apoptosis since there were also no changes between control and $PM_{2.5}$+inhibitors group. This gene encodes a member of the BCL-2 protein family which can reduce the release of pro-apoptotic cytochrome c from mitochondria that prevents caspase activation (Vogler, 2012). Goel et al. revealed induction of BCL2A1 due to SARS-CoV-2 infection in nasopharyngeal swab samples of COVID-19 patients (Goel et al., 2021). The bioinformatic analysis demonstrated the upregulation of BCL2A1 in human lung epithelial cells within 24 hours too (Ramana, 2021). Studies suggest that viruses can manipulate apoptotic pathways to enhance their replication (Thomson, 2001). For instance, upregulation of BCL2A1 can prevent apoptosis of infected cells, allowing the virus more time to replicate before the host cell dies. Unfortunately, since we do not have a control group without SARS-CoV-2 infection in sequence data it was not possible to confirm these results. However, we can contribute to the literature by providing a clue for altered host metabolism due to $PM_{2.5}$'s apoptotic effect after the SARS-CoV-2 infection. Moreover, it supports our qPCR results too. In the SARS-CoV-2 infected setup, $PM_{2.5}$ decreased the expression of the anti-apoptotic BCL2 gene which was not altered in the non-infected groups by only $PM_{2.5}$ stimulation. So, we can conclude that due to air pollutants' overwhelming induction of different signaling pathways, such as inflammation and oxidative stress-related ones may switch the viral survival mechanism in the host to cell death activation. Furthermore, there was a TF gene upregulation in $PM_{2.5}$ and $PM_{2.5}$+ inhibitors groups compared to the only SARS-CoV-2 infected controls refers to the induction of ferroptosis in the treated groups. Also, it can be said that inhibitors were not effective in the prevention of ferroptosis activation since there were no significant differences between $PM_{2.5}$ treated and

$PM_{2.5}$+inhibitor treated ones. Transferrin is the main protein in charge of iron transport found in serum that can be transported into the cell via transferrin receptor (TFR1) mediated endocytosis. Increased transferrin inside of the cell, means augmented iron ions creating oxidant radicals which causes lipid peroxidation further, ferroptosis. (Yan et al., 2021). Gao et. al discovered that transferrin is an essential extracellular component of ferroptosis (M. Gao et al., 2015). Moreover, increased expression of TFR1 has been associated with viral entry and replication, suggesting that viruses like SARS-CoV-2 might exploit the TF-TFR1 axis to modulate iron availability and induce ferroptosis (Li et al., 2023). Sequencing results related to ferroptosis were supportive of qPCR analysis making our work more comprehensive. As mentioned above ACSL4, and HO-1 were upregulated in $PM_{2.5}$ treated SARS-CoV-2 infected hBEOs setup.

SARS-CoV-2 infected, $PM_{2.5}$ and $PM_{2.5}$+inhibitors treated hBEOs were also used to identify DEGs related to bronchial epithelial cell markers. Based on these analyses it was found that $PM_{2.5}$ increased the expression of the LYPD2 gene, in virus-infected hBEOs. Upregulation was also observed in the $PM_{2.5}$+inhibitors group. Moreover, there was an upregulation of the SCGB1A gene in the $PM_{2.5}$+ inhibitors group compared to the control. LYPD2 and SCGB1A are mainly expressed in cell populations intermediate between basal cells to club cells and club cells and are also found in ciliated cells in lower amounts (Ravindra et al., 2021). Moreover, there was an upregulation of MKI67 gene, a proliferative basal cell marker, in the $PM_{2.5}$+inhibitor group compared to only $PM_{2.5}$ treated ones and controls. These findings suggest that $PM_{2.5}$ exposure increases the expression of LYPD2 and SCGB1A1 genes, markers of secretory club cells, indicating cell differentiation while the addition of ROS/RNS inhibitors leads to an increase in proliferative basal cells. It is known that major SARS-CoV-2 entrance-related proteins such as ACE2, and TMPRSS2, are mainly expressed in transient secretory cells which may differentiate into ciliated cells (Lukassen et al., 2020). As mentioned above viral load was higher in $PM_{2.5}$-treated hBEOs, so, we can hypothesize that air pollutants facilitate the virus entry indirectly by causing the differentiation of cells that express higher amounts of viral entry proteins in the host organism. On the other hand, ROS/RNS inhibitors may have a protective effect by inducing proliferative basal cells with a relatively lower amount of virus entry-related protein expression. Moreover, increased expression of viral entry receptor ANPEP due to exposure to $PM_{2.5}$ in hBEOs might be one of the reasons for higher SARS-CoV-2 infection too.

As explained above, studies have shown oxidative and nitrosative stress together with the cytokine storm, influences the pathogenesis and severity of SARS-CoV-2 infections (Ahmed et al., 2023; Bastin et al., 2023; Coronel et al., 2023; Wieczfinska et al., 2022; Wolszczak-Biedrzycka et al., 2024). Due to that, it is very significant to determine prognostic biomarkers related to oxidative and nitrosative stress to aid in identifying high-risk patients and predicting major outcomes such as ARDS or mortality (Semiz, 2022). Rapid identification of potential critical patients will help to prioritize healthcare resources, which were under strain during the pandemic (Zhao et al., 2020). The second aim of this study was to validate ROS/RNS markers and inflammatory cytokines in blood plasma samples of COVID-19. For this aim, mild, moderate, and severe COVID-19 patient samples were used with healthy control samples who had never had a COVID-19 infection. The severity of patients was categorized based on NIH guideline (*NIH, COVID-19 Treatment Guidelines* 2024).

Firstly, nitrosative stress was determined by quantifying RNS using nitrite (NO^-_2) and nitrate (NO^-_3) measurement kit, which are physiological metabolites of NO, one of the key signaling molecules, in multiple systems such as host defense, vascular homeostasis, and neurotransmission (Hidaka et al., 2016). The very limited half-life (2-6 sec.) of NO presents unique challenges for quantification. It is a lipophilic molecule that can diffuse rapidly through cells (Griendling et al., 2016). NO^-_2 and NO^-_3 are relatively stable reservoirs of NO, facilitating the determination of the nitrosative stress in the biological samples (Möller et al., 2019). Most of the studies conducted with blood samples concentrate on only oxidative stress and the COVID-19 relationship; the impact of nitrosative stress on disease is not well elucidated. Few studies demonstrated increased nitrosative stress in patients compared to the healthy controls. For instance, in a study conducted with 110 COVID-19 patients and 50 healthy controls, terms of RNS, NO•, ONO−, and ONOO− were measured from serum samples, and all three of them were significantly higher in the patient group. Moreover, ICU patients exert a higher amount of RNS compared to the ones not admitted to the ICU (Ahmed et al., 2023). Wang and colleagues quantified serum nitrate levels in 109 recovered adults and 166 uninfected individuals. Nitrate concentration was higher in recovered patients compared to the non-infected ones, indicating that nitrate might be a long-term biomarker for irreversible outcomes of COVID-19 (Wang et al., 2021). A prospective study including 11 non-survivor and 42 survivor patients found greater serum nitrate levels in non-survivors,

representing that nitrosative stress might be a marker for COVID-19 mortality (Lorente et al., 2022).

In our quantification, we measured nitrate+nitrite as a representative of total RNS and nitrite separately. So, the nitrate level was calculated by subtraction. Based on our results, there was a significant increase in the COVID-19 group compared to the controls in terms of nitrite levels. Also, whether COVID-19 severity affects the RNS level was checked. We demonstrated that nitrite concentration was significantly higher in the mild, moderate, and severe patient groups, while the concentration decreased with the severity. For total RNS and nitrate levels, there were significant elevations in severe patients compared to the mild ones. According to ROC analysis of nitrite concentration, there were significant results for all COVID-19 patients and each subgroup separately, indicating the novelty of our analysis. AUC was 0.9765 for all COVID-19 patients, while it was 1 for mild and moderate ones and 0.922 for severe groups. Based on these results, we can speculate that nitrite measurement can be used as a biomarker for COVID-19, especially for mild and moderate patients, which is a perspective not yet in the literature.

Secondly, oxidative stress was determined by quantifying ROS using an 8-isoprostane kit, which is one of the emerging gold standard methods for ROS measurement (Kitano et al., 2006). In the cells, ROS oxidize lipids, causing structural changes that might stimulate or inhibit different mechanisms. Lipid peroxidation is one of the major estimators of oxidative stress in biological samples. It creates hydroperoxides subsequently converted to relatively more stable molecules such as prostaglandin F2α isomer 8-isoprostane (also known as 8-isoPGF2α) (Graille et al., 2020). It is produced by the peroxidation of arachidonic acids, presenting detectable amounts in all tissues and biological fluids even in the exhaled breath condensate; elevated oxidative injury makes them more advantageous over other detection methods, together with chemical stability (Milne, 2017; Stathopoulos et al., 2014). It has been used as a disease marker in tissue fibrosis, prostate, and lung cancer; however, there are limited studies using this method for COVID-19, especially in blood plasma samples. (Meera et al., 2020). This is one of the major novelties of our study. Soto and colleagues measured increased levels of 8-isoprostane in blood plasma samples of moderate and severe COVID-19 patients compared to the healthy controls. However, there was a lack of mild patient group in that study (Soto et al., 2022). A cross-sectional comparative study in which 50 COVID-19 symptomatic patients and 21 controls were included showed a higher serum 8-isoprostane

level in the patient group. Conversely, this time, the majority of the patients were mild, and there were no subgroup comparisons (Muhammad et al., 2021).

According to our results, the 8-isoprostane (pg/ml) level was significantly higher in the patient group compared to the controls. When the patient group was divided based on the severity of the disease as mild, moderate, and severe, a significant increase was observed in severe patients. ROC analysis was conducted to assess the predictive accuracy in correlating 8-isoprostane level with COVID-19 infection. Based on that analysis, it was possible to detect COVID-19 patients by 8-isoprostane level with 84,7% accuracy from healthy individuals, while this ratio was 100% for severe ones. So, it can be speculated that 8-isoprostane measurement from plasma samples can be used as a COVID-19 biomarker, especially in severe patients. Since 8-isoprostane was more sensitive and specific for severe patients, while nitrite was more specific to mild and moderate ones, it would be better to quantify both ROS and RNS to obtain more consistent results. These results, which support the literature in this respect, are one of the original parts of our study. As explained above, most studies concentrate on reactive oxygen or nitrogen species measured in blood independently. Even if all of them present possible prognostic factors, what makes our work unique from others is that it includes patients from each severity stage and suggests the measurement of both ROS/RNS to have more accurate results giving an opportunity to use them as indicators of disease severity and might influence patient survival.

In a manner of cytokine quantification, there were no significant differences between patients and healthy individuals in terms of IL-1β, TNF-α and GM-CSF. IL-6 and 8 were found to be elevated in COVID-19 groups compared to the healthy individuals. Since these inflammatory mediators (IL-1β, TNF-α , and GM-CSF) have pro-inflammatory properties, they might have been produced and depleted before blood samples were taken from patients and stimulated other epithelial and immune cells, causing the release of other inflammatory cytokines such as IL-6 and 8. They may not have been observed in plasma samples due to their short half-lives. For IL-6, mild, moderate, and severe patients presented higher values compared to controls, while it was only severe ones for IL-8. According to ROC analysis of IL-6, AUC was almost 1 for all patients and the severe group too, while it was 1 for the moderate group, which indicates the power of IL-6 as a biomarker. On the other hand, the accuracy of IL-8 as a biomarker was between 58-78% for all patients and separately for each group, representing that IL-8 by itself is not sufficient and accurate as IL-6 as a prognostic factor.

Limitations of this study are a restricted number of patients included for biomarker validations. For the results obtained to be useful in the clinic, the sample size needed to be expanded. Due to the small number of non-smoker patients who undergo surgery in which we obtain bronchial tissue, part of the virus infection experiments was conducted with the primary human bronchial epithelial cell line. Moreover, the proliferation of bronchial cells from tissue and hBEO production by using these cells requires long periods and high costs. It could be better if the experimental setup repeated more than 3 times however due to the time and budget restrictions it was not possible. Lastly, as conducted in the in vivo part, it was planned to check ROS/RNS level in organoid supernatants too. Unfortunately, since the kits coming from abroad were unavailable at this time interval, it is intended to be held in the future. In future directions, for statistically more significant results, all experiments can be repeated by increasing the number of samples. The effects of ROS and RNS inhibitors on organoids can also be examined separately. Due to the low amount and quality of RNAs treated with $PM_{2.5}$ and $PM_{2.5}$+ inhibitors without infection, sequencing could not be conducted for these groups. It would be best at least to have control without infection or any treatment to make more relevant comparisons in the sequencing part. Moreover, significant results at the mRNA level can also be checked at the protein level.

In summary, we can divide this study into two parts in vitro and in vivo. The in vitro part contains hBEOs production, $PM_{2.5}$ sampling, and treatment of hBEOs with $PM_{2.5}$, $PM_{2.5}$+ inhibitors, and their infection with SARS-CoV-2. Elucidation of the molecular mechanisms by qPCR and RNA sequencing analysis, underlying the relationship of SARS-CoV-2, $PM_{2.5,}$ and ROS/RNS production revealed that $PM_{2.5}$ increased the viral load in hBEOs. Moreover, $PM_{2.5}$ created oxidative/nitrosative stress in hBEOs that activated the antioxidant NFE2L2/KEAP1 pathway which was partly or completely reversed with inhibitors showing the effectiveness of NAC+L-NMMMA as a protective agent. $PM_{2.5}$ elevated the antioxidant genes while $PM_{2.5}$+inhibitors had the opposite effect in terms of HMOX1 in SARS-CoV-2 infected hBEO and in terms of NQO1 in not-infected hBEOs. Moreover, pro-oxidant NOS3 was upregulated in SARS-CoV-2 infected $PM_{2.5}$ treated samples which was reversed with the ROS/RNS inhibitors. Also, cell death mechanisms apoptosis and ferroptosis were activated due to pollutant exposure. Lastly, IL-6 and 8 levels were lower in smokers in the presence or absence of pollutants and inhibitors without infection while non-smokers had higher IL-6 and 8 levels after the SARS-CoV-2 infection. Even though many studies investigate COVID-

19, air pollution, and oxidative/nitrosative stress relationship; most of them are conducted with 2D cell culture methods and do not contain mechanistic results covering all 3 subheadings. The in vivo part contains ROS/RNS and inflammatory cytokine measurements from plasma samples. Based on these analyses, as supporting literature, we concluded that ROS/RNS and inflammatory cytokine levels are higher in COVID-19 patients compared to the controls, especially in severe ones. IL-6 is a better biomarker than IL-8 to distinguish COVID-19 cases and healthy individuals. The novel results are explained below. 8-isoprostane as ROS indicator and nitrite as RNS indicator are potential biomarkers for COVID-19, that should be tested in larger study groups for routine clinical tests. 8-isoprostane was more accurate for severe patients while nitrite was more accurate for mild and moderate patients, measurement of both would be more convenient. This study will make a significant contribution to the literature as it contains both in vivo and in vitro setups that support each other. The in vitro part, conducted with a 3D cell culture model, reveals novel data covering antioxidant mechanisms, inflammatory response, cell death pathways, and viral host cell entry markers, bronchial epithelial cell markers associated with SARS-CoV-2 infection, and air pollution. In vivo part conducted with patients' plasma samples revealed novel biomarkers for severity detection in COVID-19 cases. For these reasons, this study has the potential to reveal predictive, preventive, and therapeutic contributions to COVID-19.

BIBLIOGRAPHY

Ahmed, S. A., Alahmadi, Y. M., & Abdou, Y. A. (2023). The impact of serum levels of reactive oxygen and nitrogen species on the disease severity of COVID-19. *International Journal of Molecular Sciences*, *24*(10), 8973.

Alam, M. S., Hasan, M. N., Maowa, Z., Khatun, F., Nazir, K. N. H., & Alam, M. Z. (2023). N-acetylcysteine reduces severity and mortality in COVID-19 patients: A systematic review and meta-analysis. *Journal of advanced veterinary and animal research*, *10*(2), 157.

Alipoor, S. D., Jamaati, H., Tabarsi, P., & Mortaz, E. (2020). Immunopathogenesis of Pneumonia in COVID-19. *Tanaffos*, *19*(2), 79.

Alysandratos, K.-D., Herriges, M. J., & Kotton, D. N. (2021). Epithelial stem and progenitor cells in lung repair and regeneration. *Annual review of physiology*, *83*, 529-550.

Andrée, B. P. J. (2020). Incidence of COVID-19 and connections with air pollution exposure: evidence from the Netherlands. *MedRxiv*, 2020.2004. 2027.20081562.

Askari, M., Faryabi, R., Mozaffari, H., & Mofrad, M. D. (2020). The effects of N-Acetylcysteine on serum level of inflammatory biomarkers in adults. Findings from a systematic review and meta-analysis of randomized clinical trials. *Cytokine*, *135*, 155239.

Assimakopoulos, S. F., Aretha, D., Komninos, D., Dimitropoulou, D., Lagadinou, M., Leonidou, L., Oikonomou, I., Mouzaki, A., & Marangos, M. (2021). N-acetylcysteine reduces the risk for mechanical ventilation and mortality in patients with COVID-19 pneumonia: a two-center retrospective cohort study. *Infectious Diseases*, *53*(11), 847-854.

Avdeev, S. N., Gaynitdinova, V. V., Merzhoeva, Z. M., & Berikkhanov, Z. G.-M. (2022). N-acetylcysteine for the treatment of COVID-19 among hospitalized patients. *The Journal of Infection*, *84*(1), 94.

Aykaç, N., & Etiler, N. (2022). COVID-19 mortality in Istanbul in association with air pollution and socioeconomic status: an ecological study. *Environmental Science and Pollution Research*, *29*(9), 13700-13708.

Barkauskas, C. E., Chung, M.-I., Fioret, B., Gao, X., Katsura, H., & Hogan, B. L. (2017). Lung organoids: current uses and future promise. *Development*, *144*(6), 986-997.

Bastin, A., Abbasi, F., Roustaei, N., Abdesheikhi, J., Karami, H., Gholamnezhad, M., Eftekhari, M., & Doustimotlagh, A. (2023). Severity of oxidative stress as a hallmark in COVID-19 patients. *European Journal of Medical Research*, *28*(1), 558.

Bayram, H., Devalia, J. L., Khair, O. A., Abdelaziz, M. M., Sapsford, R. J., Sagai, M., & Davies, R. J. (1998). Comparison of ciliary activity and inflammatory mediator release from bronchial epithelial cells of nonatopic nonasthmatic subjects and atopic asthmatic patients and the effect of diesel exhaust particles in vitro. *Journal of allergy and clinical immunology*, *102*(5), 771-782.

Bayram, H., Fakili, F., Gögebakan, B., Bayraktar, R., Öztuzcu, S., Dikensoy, Ö., & Chung, K. F. (2013). Effect of serum on diesel exhaust particles (DEP)-induced apoptosis of airway epithelial cells in vitro. *Toxicology letters*, *218*(3), 215-223.

Bayram, H., Ito, K., Issa, R., Ito, M., Sukkar, M., & Chung, K. F. (2006). Regulation of human lung epithelial cell numbers by diesel exhaust particles. *European respiratory journal*, *27*(4), 705-713.

Białas, A. J., Sitarek, P., Miłkowska-Dymanowska, J., Piotrowski, W. J., & Górski, P. (2016). The role of mitochondria and oxidative/antioxidative imbalance in

pathobiology of chronic obstructive pulmonary disease. *Oxidative medicine and cellular longevity*, *2016*.

Bitko, V., & Barik, S. (2001). An endoplasmic reticulum-specific stress-activated caspase (caspase-12) is implicated in the apoptosis of A549 epithelial cells by respiratory syncytial virus. *Journal of cellular biochemistry*, *80*(3), 441-454.

Bolger, A. M., Lohse, M., & Usadel, B. (2014). Trimmomatic: a flexible trimmer for Illumina sequence data. *Bioinformatics*, *30*(15), 2114-2120.

Boogaard, H., Patton, A., Atkinson, R., Brook, J., Chang, H., Crouse, D., Fussell, J., Hoek, G., Hoffmann, B., & Kappeler, R. (2022). Long-term exposure to traffic-related air pollution and selected health outcomes: A systematic review and meta-analysis. *Environment international*, *164*, 107262.

Bove, P. F., & van der Vliet, A. (2006). Nitric oxide and reactive nitrogen species in airway epithelial signaling and inflammation. *Free Radical Biology and Medicine*, *41*(4), 515-527.

Burmester, T., Gerlach, F., & Hankeln, T. (2007). Regulation and role of neuroglobin and cytoglobin under hypoxia. *Hypoxia and the Circulation*, 169-180.

Bustamante-Marin, X. M., & Ostrowski, L. E. (2017). Cilia and mucociliary clearance. *Cold Spring Harbor perspectives in biology*, *9*(4), a028241.

Cao, J. Y., & Dixon, S. J. (2016). Mechanisms of ferroptosis. *Cellular and Molecular Life Sciences*, *73*, 2195-2209.

Carneiro, B. A., & El-Deiry, W. S. (2020). Targeting apoptosis in cancer therapy. *Nature reviews Clinical oncology*, *17*(7), 395-417.

Carpagnano, G. E., Kharitonov, S., Foschino-Barbaro, M., Resta, O., Gramiccioni, E., & Barnes, P. (2003). Increased inflammatory markers in the exhaled breath condensate of cigarette smokers. *European respiratory journal*, *21*(4), 589-593.

Caruso, M., Distefano, A., Emma, R., Di Rosa, M., Carota, G., Rust, S., Polosa, R., Zuccarello, P., Ferrante, M., & Raciti, G. (2021). Role of cigarette smoke on angiotensin-converting enzyme-2 protein membrane expression in bronchial epithelial cells using an air-liquid interface model. *Frontiers in pharmacology*, *12*, 652102.

Cascella, M., Rajnik, M., Aleem, A., Dulebohn, S. C., & Di Napoli, R. (2023). Features, evaluation, and treatment of coronavirus (COVID-19). *Statpearls [internet]*.

Chan, L. L., Anderson, D. E., Cheng, H. S., Ivan, F. X., Chen, S., Kang, A. E., Foo, R., Gamage, A. M., Tiew, P. Y., & Koh, M. S. (2022). The establishment of COPD organoids to study host-pathogen interaction reveals enhanced viral fitness of SARS-CoV-2 in bronchi. *Nature Communications*, *13*(1), 7635.

Chen, B., Raja, K., Pierre-Louis, F., Patel, M., Patel, R., Kang, S., Daniel, N., Attalla, M., & Philips, M. (2023). Intravenous N-acetylcysteine in management of COVID-19: a case series. *Journal of Pharmacy Practice*, *36*(4), 1008-1014.

Chen, C., Arjomandi, M., Balmes, J., Tager, I., & Holland, N. (2007). Effects of chronic and acute ozone exposure on lipid peroxidation and antioxidant capacity in healthy young adults. *Environmental health perspectives*, *115*(12), 1732-1737.

Chen, S., Zhou, Y., Chen, Y., & Gu, J. (2018). fastp: an ultra-fast all-in-one FASTQ preprocessor. *Bioinformatics*, *34*(17), i884-i890.

Chen, Y., Guo, Y., Pan, Y., & Zhao, Z. J. (2020). Structure analysis of the receptor binding of 2019-nCoV. *Biochemical and biophysical research communications*, *525*(1), 135-140.

Chiu, M. C., Li, C., Liu, X., Song, W., Wan, Z., Yu, Y., Huang, J., Xiao, D., Chu, H., & Cai, J.-P. (2022). Human nasal organoids model SARS-CoV-2 upper respiratory

infection and recapitulate the differential infectivity of emerging variants. *MBio*, *13*(4), e01944-01922.

Choi, J., Iich, E., & Lee, J.-H. (2016). Organogenesis of adult lung in a dish: Differentiation, disease and therapy. *Developmental biology*, *420*(2), 278-286.

Chowdhury, S. D., & Oommen, A. M. (2020). Epidemiology of COVID-19. *Journal of digestive endoscopy*, *11*(01), 03-07.

Comunian, S., Dongo, D., Milani, C., & Palestini, P. (2020). Air pollution and COVID-19: the role of particulate matter in the spread and increase of COVID-19's morbidity and mortality. *International journal of environmental research and public health*, *17*(12), 4487.

Conticini, E., Frediani, B., & Caro, D. (2020). Can atmospheric pollution be considered a co-factor in extremely high level of SARS-CoV-2 lethality in Northern Italy? *Environmental pollution*, *261*, 114465.

Copat, C., Cristaldi, A., Fiore, M., Grasso, A., Zuccarello, P., Santo Signorelli, S., Conti, G. O., & Ferrante, M. (2020). The role of air pollution (PM and NO2) in COVID-19 spread and lethality: a systematic review. *Environmental Research*, *191*, 110129.

Coronel, P. M. V., Pereira, I. C., Basilio, D. C. L. S., Espinoça, I. T., de Souza, K. F. S., Ota, R. S. N., de Almeida, E. B., Paredes-Gamero, E. J., Wilhelm Filho, D., & Perdomo, R. T. (2023). Biomarkers of oxidative stress and inflammation in subjects with COVID-19: Characterization and prognosis of the disease. *Microbial Pathogenesis*, *184*, 106339.

Cortez, V., & Schultz-Cherry, S. (2021). The role of goblet cells in viral pathogenesis. *The FEBS journal*, *288*(24), 7060-7072.

Cuadrado, A., Pajares, M., Benito, C., Jiménez-Villegas, J., Escoll, M., Fernández-Ginés, R., Yagüe, A. J. G., Lastra, D., Manda, G., & Rojo, A. I. (2020). Can activation of NRF2 be a strategy against COVID-19? *Trends in pharmacological sciences*, *41*(9), 598-610.

Cui, Y., Liang, Y., Ip, M. S., & Mak, J. C. (2021). Cigarette smoke induces apoptosis via 18 kDa translocator protein in human bronchial epithelial cells. *Life sciences*, *265*, 118862.

Dadvand, P., Nieuwenhuijsen, M. J., Agustí, À., De Batlle, J., Benet, M., Beelen, R., Cirach, M., Martinez, D., Hoek, G., & Basagaña, X. (2014). Air pollution and biomarkers of systemic inflammation and tissue repair in COPD patients. *European respiratory journal*, *44*(3), 603-613.

Davis, J. D., & Wypych, T. P. (2021). Cellular and functional heterogeneity of the airway epithelium. *Mucosal immunology*, *14*(5), 978-990.

de Alencar, J. C. G., Moreira, C. d. L., Müller, A. D., Chaves, C. E., Fukuhara, M. A., da Silva, E. A., Miyamoto, M. d. F. S., Pinto, V. B., Bueno, C. G., & Lazar Neto, F. (2021). Double-blind, randomized, placebo-controlled trial with N-acetylcysteine for treatment of severe acute respiratory syndrome caused by coronavirus disease 2019 (COVID-19). *Clinical infectious diseases*, *72*(11), e736-e741.

Dekkers, J. F., Alieva, M., Wellens, L. M., Ariese, H. C., Jamieson, P. R., Vonk, A. M., Amatngalim, G. D., Hu, H., Oost, K. C., & Snippert, H. J. (2019). High-resolution 3D imaging of fixed and cleared organoids. *Nature protocols*, *14*(6), 1756-1771.

Delgado-Roche, L., & Mesta, F. (2020). Oxidative stress as key player in severe acute respiratory syndrome coronavirus (SARS-CoV) infection. *Archives of medical research*, *51*(5), 384-387.

Demchenko, A., Lavrov, A., & Smirnikhina, S. (2022). Lung organoids: Current strategies for generation and transplantation. *Cell and Tissue Research*, *390*(3), 317-333.

Denney, L., & Ho, L.-P. (2018). The role of respiratory epithelium in host defence against influenza virus infection. *biomedical journal*, *41*(4), 218-233.

Devalia, J., Sapsford, R., Wells, C., Richman, P., & Davies, R. (1990). Culture and comparison of human bronchial and nasal epithelial cells in vitro. *Respiratory medicine*, *84*(4), 303-312.

Di Meo, S., Reed, T. T., Venditti, P., & Victor, V. M. (2016). Role of ROS and RNS sources in physiological and pathological conditions. *Oxidative medicine and cellular longevity*, *2016*.

Donaldson, K., Stone, V., Seaton, A., & MacNee, W. (2001). Ambient particle inhalation and the cardiovascular system: potential mechanisms. *Environmental health perspectives*, *109*(suppl 4), 523-527.

Duval, K., Grover, H., Han, L.-H., Mou, Y., Pegoraro, A. F., Fredberg, J., & Chen, Z. (2017). Modeling physiological events in 2D vs. 3D cell culture. *Physiology*, *32*(4), 266-277.

Dye, B. R., Hill, D. R., Ferguson, M. A., Tsai, Y.-H., Nagy, M. S., Dyal, R., Wells, J. M., Mayhew, C. N., Nattiv, R., & Klein, O. D. (2015). In vitro generation of human pluripotent stem cell derived lung organoids. *elife*, *4*, e05098.

Ebrahimi, M., Norouzi, P., Aazami, H., & Moosavi-Movahedi, A. A. (2021). Review on oxidative stress relation on COVID-19: Biomolecular and bioanalytical approach. *International journal of biological macromolecules*, *189*, 802-818.

Elisia, I., Lam, V., Cho, B., Hay, M., Li, M. Y., Yeung, M., Bu, L., Jia, W., Norton, N., & Lam, S. (2020). The effect of smoking on chronic inflammation, immune function and blood cell composition. *Scientific Reports*, *10*(1), 19480.

Elmore, S. (2007). Apoptosis: a review of programmed cell death. *Toxicologic pathology*, *35*(4), 495-516.

Emanuele, S., Celesia, A., D'Anneo, A., Lauricella, M., Carlisi, D., De Blasio, A., & Giuliano, M. (2021). The good and bad of Nrf2: an update in Cancer and New perspectives in COVID-19. *International Journal of Molecular Sciences*, *22*(15), 7963.

Engedal, N., Žerovnik, E., Rudov, A., Galli, F., Olivieri, F., Procopio, A. D., Rippo, M. R., Monsurrò, V., Betti, M., & Albertini, M. C. (2018). From oxidative stress damage to pathways, networks, and autophagy via microRNAs. *Oxidative medicine and cellular longevity*, *2018*.

Erickson, R., Huang, C., Allen, C., Ireland, J., Roth, G., Zou, Z., Lu, J., Lafont, B. A., Garza, N. L., & Brumbaugh, B. (2023). SARS-CoV-2 infection of human lung epithelial cells induces TMPRSS-mediated acute fibrin deposition. *Nature Communications*, *14*(1), 6380.

Espinoza, J. A., González, P. A., & Kalergis, A. M. (2017). Modulation of antiviral immunity by heme oxygenase-1. *The American journal of pathology*, *187*(3), 487-493.

Ewels, P., Magnusson, M., Lundin, S., & Käller, M. (2016). MultiQC: summarize analysis results for multiple tools and samples in a single report. *Bioinformatics*, *32*(19), 3047-3048.

Faghfouri, A. H., Zarezadeh, M., Tavakoli-Rouzbehani, O. M., Radkhah, N., Faghfuri, E., Kord-Varkaneh, H., Tan, S. C., & Ostadrahimi, A. (2020). The effects of N-acetylcysteine on inflammatory and oxidative stress biomarkers: A systematic review and meta-analysis of controlled clinical trials. *European journal of pharmacology*, *884*, 173368.

Fang, K.-Y., Cao, W.-C., Xie, T.-A., Lv, J., Chen, J.-X., Cao, X.-J., Li, Z.-W., Deng, S.-T., & Guo, X.-G. (2021). Exploration and validation of related hub gene

expression during SARS-CoV-2 infection of human bronchial organoids. *Human Genomics*, *15*, 1-13.

Fang, W., Jiang, J., Su, L., Shu, T., Liu, H., Lai, S., Ghiladi, R. A., & Wang, J. (2021). The role of NO in COVID-19 and potential therapeutic strategies. *Free Radical Biology and Medicine*, *163*, 153-162.

Fatehullah, A., Tan, S. H., & Barker, N. (2016). Organoids as an in vitro model of human development and disease. *Nature cell biology*, *18*(3), 246-254.

Faverio, P., Rebora, P., Rossi, E., Del Giudice, S., Montanelli, F., Garzillo, L., Busnelli, S., Luppi, F., Valsecchi, M. G., & Pesci, A. (2022). Impact of N-acetyl-l-cysteine on SARS-CoV-2 pneumonia and its sequelae: results from a large cohort study. *ERJ open research*, *8*(1).

Finkel, T. (2012). Signal transduction by mitochondrial oxidants. *Journal of Biological Chemistry*, *287*(7), 4434-4440.

Fiorito, S., Soligo, M., Gao, Y., Ogulur, I., Akdis, C. A., & Bonini, S. (2022). Is the epithelial barrier hypothesis the key to understanding the higher incidence and excess mortality during COVID-19 pandemic? The case of Northern Italy. *Allergy*, *77*(5), 1408-1417.

Fratta Pasini, A. M., Stranieri, C., Girelli, D., Busti, F., & Cominacini, L. (2021). Is ferroptosis a key component of the process leading to multiorgan damage in COVID-19? *Antioxidants*, *10*(11), 1677.

Frontera, A., Cianfanelli, L., Vlachos, K., Landoni, G., & Cremona, G. (2020). Severe air pollution links to higher mortality in COVID-19 patients: The "double-hit" hypothesis. *Journal of Infection*, *81*(2), 255-259.

Fubini, B., & Hubbard, A. (2003). Reactive oxygen species (ROS) and reactive nitrogen species (RNS) generation by silica in inflammation and fibrosis. *Free Radical Biology and Medicine*, *34*(12), 1507-1516.

Gain, C., & Kelesidis, T. (2023). The role of oxidative stress in the pathogenesis of infections with coronaviruses. *Frontiers in microbiology*, *13*, 1111930.

Ganesan, S., Comstock, A. T., & Sajjan, U. S. (2013). Barrier function of airway tract epithelium. *Tissue Barriers*, *1*(4), e24997.

Gao, M., Monian, P., Quadri, N., Ramasamy, R., & Jiang, X. (2015). Glutaminolysis and transferrin regulate ferroptosis. *Molecular cell*, *59*(2), 298-308.

Gao, W., Li, L., Wang, Y., Zhang, S., Adcock, I. M., Barnes, P. J., Huang, M., & Yao, X. (2015). Bronchial epithelial cells: the key effector cells in the pathogenesis of chronic obstructive pulmonary disease? *Respirology*, *20*(5), 722-729.

Gao, X., Dinkova-Kostova, A. T., & Talalay, P. (2001). Powerful and prolonged protection of human retinal pigment epithelial cells, keratinocytes, and mouse leukemia cells against oxidative damage: the indirect antioxidant effects of sulforaphane. *Proceedings of the National Academy of Sciences*, *98*(26), 15221-15226.

Ge, S. X., Jung, D., & Yao, R. (2020). ShinyGO: a graphical gene-set enrichment tool for animals and plants. *Bioinformatics*, *36*(8), 2628-2629.

Godbole, N. M., Chowdhury, A. A., Chataut, N., & Awasthi, S. (2022). Tight junctions, the epithelial barrier, and Toll-like receptor-4 during lung injury. *Inflammation*, *45*(6), 2142-2162.

Goel, S., Saheb Sharif-Askari, F., Saheb Sharif Askari, N., Madkhana, B., Alwaa, A. M., Mahboub, B., Zakeri, A. M., Ratemi, E., Hamoudi, R., & Hamid, Q. (2021). SARS-CoV-2 switches 'on'MAPK and NFκB signaling via the reduction of nuclear DUSP1 and DUSP5 expression. *Frontiers in pharmacology*, *12*, 631879.

Gonzalez-Garcia, P., Fiorillo Moreno, O., Zarate Peñata, E., Calderon-Villalba, A., Pacheco Lugo, L., Acosta Hoyos, A., Villarreal Camacho, J. L., Navarro Quiroz,

R., Pacheco Londoño, L., & Aroca Martinez, G. (2023). From cell to symptoms: The role of SARS-CoV-2 cytopathic effects in the pathogenesis of COVID-19 and long COVID. *International Journal of Molecular Sciences*, *24*(9), 8290.

Graille, M., Wild, P., Sauvain, J., Hemmendinger, M., Canu, I. G., & Hopf, N. (2020). Urinary 8-isoprostane as a biomarker for oxidative stress. A systematic review and meta-analysis. *Toxicology letters*, *328*, 19-27.

Grant, W. B., Lahore, H., McDonnell, S. L., Baggerly, C. A., French, C. B., Aliano, J. L., & Bhattoa, H. P. (2020). Evidence that vitamin D supplementation could reduce risk of influenza and COVID-19 infections and deaths. *Nutrients*, *12*(4), 988.

Griendling, K. K., Touyz, R. M., Zweier, J. L., Dikalov, S., Chilian, W., Chen, Y.-R., Harrison, D. G., & Bhatnagar, A. (2016). Measurement of reactive oxygen species, reactive nitrogen species, and redox-dependent signaling in the cardiovascular system: a scientific statement from the American Heart Association. *Circulation research*, *119*(5), e39-e75.

Guimbellot, J. S., Leach, J. M., Chaudhry, I. G., Quinney, N. L., Boyles, S. E., Chua, M., Aban, I., Jaspers, I., & Gentzsch, M. (2017). Nasospheroids permit measurements of CFTR-dependent fluid transport. *JCI insight*, *2*(22).

Guo, Y.-R., Cao, Q.-D., Hong, Z.-S., Tan, Y.-Y., Chen, S.-D., Jin, H.-J., Tan, K.-S., Wang, D.-Y., & Yan, Y. (2020). The origin, transmission and clinical therapies on coronavirus disease 2019 (COVID-19) outbreak–an update on the status. *Military medical research*, *7*, 1-10.

Güner, A. E., Sürmeli, A., Kural, K., Şahin, E., Alkan, P., Kocayiğit, E., Hatipoğlu, M., Birinci, Ş., Memişoğlu, K., & MARAL, I. (2021). First known COVID-19 case and contact tracing efforts in İstanbul, Turkey. *Turkish Journal of Medical Sciences*, *51*(4), 1653-1658.

Han, Y., Yang, L., Duan, X., Duan, F., Nilsson-Payant, B. E., Yaron, T. M., Wang, P., Tang, X., Zhang, T., & Zhao, Z. (2020). Identification of candidate COVID-19 therapeutics using hPSC-derived lung organoids. *bioRxiv*, 2020.2005. 2005.079095.

Harrison, A. G., Lin, T., & Wang, P. (2020). Mechanisms of SARS-CoV-2 transmission and pathogenesis. *Trends in immunology*, *41*(12), 1100-1115.

Hartsock, A., & Nelson, W. J. (2008). Adherens and tight junctions: structure, function and connections to the actin cytoskeleton. *Biochimica et Biophysica Acta (BBA)-Biomembranes*, *1778*(3), 660-669.

Haşimi, A., Doğan, Ö., Serdar, C. C., & Serdar, M. A. (2023). Association of serum ADMA, SDMA and L-NMMA concentrations with disease progression in COVID-19 patients. *Biochemia medica*, *33*(1), 21-31.

He, Y., Wang, J., Li, F., & Shi, Y. (2020). Main clinical features of COVID-19 and potential prognostic and therapeutic value of the microbiota in SARS-CoV-2 infections. *Frontiers in microbiology*, *11*, 543205.

Heinemann, U., & Schuetz, A. (2019). Structural features of tight-junction proteins. *International Journal of Molecular Sciences*, *20*(23), 6020.

Helmersson, J., Larsson, A., Vessby, B., & Basu, S. (2005). Active smoking and a history of smoking are associated with enhanced prostaglandin F2α, interleukin-6 and F2-isoprostane formation in elderly men. *Atherosclerosis*, *181*(1), 201-207.

Hidaka, M., Gotoh, A., Shimizu, T., Minamisawa, K., Imamura, H., & Uchida, T. (2016). Visualization of NO3−/NO2− Dynamics in Living Cells by Fluorescence Resonance Energy Transfer (FRET) Imaging Employing a Rhizobial Two-component Regulatory System*♦. *Journal of Biological Chemistry*, *291*(5), 2260-2269.

Hoffmann, M., Kleine-Weber, H., Schroeder, S., Krüger, N., Herrler, T., Erichsen, S., Schiergens, T. S., Herrler, G., Wu, N.-H., & Nitsche, A. (2020). SARS-CoV-2 cell entry depends on ACE2 and TMPRSS2 and is blocked by a clinically proven protease inhibitor. *Cell*, *181*(2), 271-280. e278.

Hu, B., Huang, S., & Yin, L. (2021). The cytokine storm and COVID-19. *Journal of medical virology*, *93*(1), 250-256.

Huang, J., Gao, W., Gao, Y., & Liao, W. (2006). Hypoxia upregulates the expression of cytoglobin in lung cancer cells. *Zhonghua yi xue za zhi*, *86*(5), 321-324.

Huang, J., Hume, A. J., Abo, K. M., Werder, R. B., Villacorta-Martin, C., Alysandratos, K.-D., Beermann, M. L., Simone-Roach, C., Lindstrom-Vautrin, J., & Olejnik, J. (2020). SARS-CoV-2 infection of pluripotent stem cell-derived human lung alveolar type 2 cells elicits a rapid epithelial-intrinsic inflammatory response. *Cell stem cell*, *27*(6), 962-973. e967.

Hynds, R. E., & Giangreco, A. (2013). Concise review: the relevance of human stem cell-derived organoid models for epithelial translational medicine. *Stem cells*, *31*(3), 417-422.

Izquierdo, J. L., Soriano, J. B., González, Y., Lumbreras, S., Ancochea, J., Echeverry, C., & Rodríguez, J. M. (2022). Use of N-Acetylcysteine at high doses as an oral treatment for patients hospitalized with COVID-19. *Science Progress*, *105*(1), 00368504221074574.

Jan, R. (2019). Understanding apoptosis and apoptotic pathways targeted cancer therapeutics. *Advanced pharmaceutical bulletin*, *9*(2), 205.

Joneschild, E. S., Chen, L.-E., Seaber, A. V., Frankel, E. S., & Urbaniak, J. R. (1999). Effect of a NOS inhibitor, L-NMMA, on the contractile function of reperfused skeletal muscle. *Journal of reconstructive microsurgery*, *15*(01), 55-60.

Joo, H., Min, S., & Cho, S.-W. (2024). Advanced lung organoids for respiratory system and pulmonary disease modeling. *Journal of Tissue Engineering*, *15*, 20417314241232502.

Ju, J., Song, Y.-n., & Wang, K. (2021). Mechanism of ferroptosis: a potential target for cardiovascular diseases treatment. *Aging and Disease*, *12*(1), 261.

Kapałczyńska, M., Kolenda, T., Przybyła, W., Zajączkowska, M., Teresiak, A., Filas, V., Ibbs, M., Bliźniak, R., Łuczewski, Ł., & Lamperska, K. (2018). 2D and 3D cell cultures–a comparison of different types of cancer cell cultures. *Archives of Medical Science*, *14*(4), 910-919.

Karekla, E., Liao, W.-J., Sharp, B., Pugh, J., Reid, H., Quesne, J. L., Moore, D., Pritchard, C., MacFarlane, M., & Pringle, J. H. (2017). Ex vivo explant cultures of non–small cell lung carcinoma enable evaluation of primary tumor responses to anticancer therapy. *Cancer research*, *77*(8), 2029-2039.

Katsura, H., Sontake, V., Tata, A., Kobayashi, Y., Edwards, C. E., Heaton, B. E., Konkimalla, A., Asakura, T., Mikami, Y., & Fritch, E. J. (2020). Human lung stem cell-based alveolospheres provide insights into SARS-CoV-2-mediated interferon responses and pneumocyte dysfunction. *Cell stem cell*, *27*(6), 890-904. e898.

Kayalar, Ö., Arı, A., Babuççu, G., Konyalılar, N., Doğan, Ö., Can, F., Şahin, Ü. A., Gaga, E. O., Kuzu, S. L., & Arı, P. E. (2021). Existence of SARS-CoV-2 RNA on ambient particulate matter samples: a nationwide study in Turkey. *Science of the Total Environment*, *789*, 147976.

Khomich, O. A., Kochetkov, S. N., Bartosch, B., & Ivanov, A. V. (2018). Redox biology of respiratory viral infections. *Viruses*, *10*(8), 392.

Kim, J.-H., Kim, J., Kim, W. J., Choi, Y. H., Yang, S.-R., & Hong, S.-H. (2020). Diesel particulate matter 2.5 induces epithelial-to-mesenchymal transition and

upregulation of SARS-CoV-2 receptor during human pluripotent stem cell-derived alveolar organoid development. *International journal of environmental research and public health*, *17*(22), 8410.

Kitano, S., Hisatomi, H., Hibi, N., Kawano, K., & Harada, S. (2006). Improved method of plasma 8-Isoprostane measurement and association analyses with habitual drinking and smoking. *World Journal of Gastroenterology: WJG*, *12*(36), 5846.

Knight, D. A., & Holgate, S. T. (2003). The airway epithelium: structural and functional properties in health and disease. *Respirology*, *8*(4), 432-446.

Koliaraki, V., & Kollias, G. (2011). A new role for myeloid HO-1 in the innate to adaptive crosstalk and immune homeostasis. *Crossroads between Innate and Adaptive Immunity III*, 101-111.

Komaravelli, N., & Casola, A. (2014). Respiratory viral infections and subversion of cellular antioxidant defenses. *Journal of pharmacogenomics & pharmacoproteomics*, *5*(4).

Konar, D., Devarasetty, M., Yildiz, D. V., Atala, A., & Murphy, S. V. (2016). Lung-on-a-chip technologies for disease modeling and drug development: supplementary issue: image and video acquisition and processing for clinical applications. *Biomedical engineering and computational biology*, *7*, BECB. S34252.

Konyalilar, N., Kayalar, Ö., Mortazavi, D., Rajabi, H., Korkunç, S., Erkan, S., Aksoy, T., Gönenli, M., Akyıl, F. T., & Altın, S. (2022). The role of reactive nitrogen species as biomarkers of disease severity in COVID-19. In: Eur Respiratory Soc.

Kozlowski, M. T., Crook, C. J., & Ku, H. T. (2021). Towards organoid culture without Matrigel. *Communications biology*, *4*(1), 1387.

Kratzel, A., Kelly, J. N., V'kovski, P., Portmann, J., Brüggemann, Y., Todt, D., Ebert, N., Shrestha, N., Plattet, P., & Staab-Weijnitz, C. A. (2021). A genome-wide CRISPR screen identifies interactors of the autophagy pathway as conserved coronavirus targets. *PLoS biology*, *19*(12), e3001490.

Krynytska, I., Marushchak, M., Birchenko, I., Dovgalyuk, A., & Tokarskyy, O. (2021). COVID-19-associated acute respiratory distress syndrome versus classical acute respiratory distress syndrome (a narrative review). *Iranian journal of microbiology*, *13*(6), 737.

Kucukural, A., Yukselen, O., Ozata, D. M., Moore, M. J., & Garber, M. (2019). DEBrowser: interactive differential expression analysis and visualization tool for count data. *BMC genomics*, *20*, 1-12.

Kulasinghe, A., Tan, C. W., dos Santos Miggiolaro, A. F. R., Monkman, J., SadeghiRad, H., Bhuva, D. D., Junior, J. d. S. M., de Paula, C. B. V., Nagashima, S., & Baena, C. P. (2022). Profiling of lung SARS-CoV-2 and influenza virus infection dissects virus-specific host responses and gene signatures. *European respiratory journal*, *59*(6).

Kumarathasan, P., Vincent, R., Blais, E., Bielecki, A., Guénette, J., Filiatreault, A., Brion, O., Cakmak, S., Thomson, E. M., & Shutt, R. (2018). Cardiovascular and inflammatory mechanisms in healthy humans exposed to air pollution in the vicinity of a steel mill. *Particle and fibre toxicology*, *15*, 1-17.

Kutuk, O., Aytan, N., Karakas, B., Kurt, A. G., Acikbas, U., Temel, S. G., & Basaga, H. (2017). Biphasic ROS production, p53 and BIK dictate the mode of cell death in response to DNA damage in colon cancer cells. *PLoS ONE*, *12*(8), e0182809.

Lancaster, M. A., & Huch, M. (2019). Disease modelling in human organoids. *Disease models & mechanisms*, *12*(7), dmm039347.

Lauxmann, M. A., Santucci, N. E., & Autrán-Gómez, A. M. (2020). The SARS-CoV-2 coronavirus and the COVID-19 outbreak. *International braz j urol*, *46*, 6-18.

Lescure, F.-X., Bouadma, L., Nguyen, D., Parisey, M., Wicky, P.-H., Behillil, S., Gaymard, A., Bouscambert-Duchamp, M., Donati, F., & Le Hingrat, Q. (2020). Clinical and virological data of the first cases of COVID-19 in Europe: a case series. *The Lancet Infectious Diseases*, *20*(6), 697-706.

Lewandowski, M., & Gwozdzinski, K. (2017). Nitroxides as antioxidants and anticancer drugs. *International Journal of Molecular Sciences*, *18*(11), 2490.

Li, H., Xu, X.-L., Dai, D.-W., Huang, Z.-Y., Ma, Z., & Guan, Y.-J. (2020). Air pollution and temperature are associated with increased COVID-19 incidence: a time series study. *International journal of infectious diseases*, *97*, 278-282.

Li, J., Cao, F., Yin, H.-l., Huang, Z.-j., Lin, Z.-t., Mao, N., Sun, B., & Wang, G. (2020). Ferroptosis: past, present and future. *Cell death & disease*, *11*(2), 88.

Lin, C.-I., Tsai, C.-H., Sun, Y.-L., Hsieh, W.-Y., Lin, Y.-C., Chen, C.-Y., & Lin, C.-S. (2018). Instillation of particulate matter 2.5 induced acute lung injury and attenuated the injury recovery in ACE2 knockout mice. *International journal of biological sciences*, *14*(3), 253.

Lin, L., Lu, L., Cao, W., & Li, T. (2020). Hypothesis for potential pathogenesis of SARS-CoV-2 infection–a review of immune changes in patients with viral pneumonia. *Emerging microbes & infections*, *9*(1), 727-732.

Liu, C.-W., Lee, T.-L., Chen, Y.-C., Liang, C.-J., Wang, S.-H., Lue, J.-H., Tsai, J.-S., Lee, S.-W., Chen, S.-H., & Yang, Y.-F. (2018). PM 2.5-induced oxidative stress increases intercellular adhesion molecule-1 expression in lung epithelial cells through the IL-6/AKT/STAT3/NF-κB-dependent pathway. *Particle and fibre toxicology*, *15*, 1-16.

Liu, T.-H., Wu, J.-Y., Huang, P.-Y., Tsai, Y.-W., Hsu, W.-H., Chuang, M.-H., Tang, H.-J., & Lai, C.-C. (2024). Clinical efficacy of N-acetylcysteine for COVID-19: A systematic review and meta-analysis of randomized controlled trials. *Heliyon*.

Liu, Z., Anderson, J. D., Deng, L., Mackay, S., Bailey, J., Kersh, L., Rowe, S. M., & Guimbellot, J. S. (2020). Human nasal epithelial organoids for therapeutic development in cystic fibrosis. *Genes*, *11*(6), 603.

Loh, C.-Y., Chai, J. Y., Tang, T. F., Wong, W. F., Sethi, G., Shanmugam, M. K., Chong, P. P., & Looi, C. Y. (2019). The E-cadherin and N-cadherin switch in epithelial-to-mesenchymal transition: signaling, therapeutic implications, and challenges. *Cells*, *8*(10), 1118.

Lorente, L., Gómez-Bernal, F., Martín, M., Navarro-Gonzálvez, J., Argueso, M., Perez, A., Ramos-Gómez, L., Solé-Violán, J., y Ramos, J. M., & Ojeda, N. (2022). High serum nitrates levels in non-survivor COVID-19 patients. *Medicina intensiva*, *46*(3), 132-139.

Lukassen, S., Chua, R. L., Trefzer, T., Kahn, N. C., Schneider, M. A., Muley, T., Winter, H., Meister, M., Veith, C., & Boots, A. W. (2020). SARS-CoV-2 receptor ACE 2 and TMPRSS 2 are primarily expressed in bronchial transient secretory cells. *The EMBO journal*, *39*(10), e105114.

Ma, Q. (2010). Transcriptional responses to oxidative stress: pathological and toxicological implications. *Pharmacology & therapeutics*, *125*(3), 376-393.

Madamanchi, N. R., & Runge, M. S. (2013). Redox signaling in cardiovascular health and disease. *Free Radical Biology and Medicine*, *61*, 473-501.

Mathai, C., Jourd'heuil, F. L., Pham, L. G. C., Gilliard, K., Balnis, J., Jen, A., Overmyer, K. A., Coon, J. J., Jaitovich, A., & Boivin, B. (2023). A role for cytoglobin in regulating intracellular hydrogen peroxide and redox signals in the vasculature. *bioRxiv*, 2023.2003. 2031.535146.

Meera, S., Sarangarajan, R., & Rajkumar, K. (2020). 8-Isoprostane: A salivary oxidative stress biomarker for oral submucous fibrosis and oral squamous cell carcinoma. *Journal of Oral and Maxillofacial Pathology*, *24*(2), 279-284.

Metsalu, T., & Vilo, J. (2015). ClustVis: a web tool for visualizing clustering of multivariate data using Principal Component Analysis and heatmap. *Nucleic acids research*, *43*(W1), W566-W570.

Milatovic, D., Montine, T. J., & Aschner, M. (2011). Measurement of isoprostanes as markers of oxidative stress. *In Vitro Neurotoxicology: Methods and Protocols*, 195-204.

Mills, P. R., Davies, R. J., & Devalia, J. L. (1999). Airway epithelial cells, cytokines, and pollutants. *American journal of respiratory and critical care medicine*, *160*(supplement_1), S38-S43.

Milne, G. L. (2017). Classifying oxidative stress by F2-Isoprostane levels in human disease: The re-imagining of a biomarker. *Redox biology*, *12*, 897.

Miyashita, L., Foley, G., Semple, S., Gibbons, J. M., Pade, C., McKnight, Á., & Grigg, J. (2023). Curbside particulate matter and susceptibility to SARS–CoV-2 infection. *Journal of Allergy and Clinical Immunology: Global*, *2*(4), 100141.

Molla, M. D., Akalu, Y., Geto, Z., Dagnew, B., Ayelign, B., & Shibabaw, T. (2020). Role of caspase-1 in the pathogenesis of inflammatory-associated chronic noncommunicable diseases. *Journal of inflammation research*, 749-764.

Mozos, I., & Luca, C. T. (2017). Crosstalk between oxidative and nitrosative stress and arterial stiffness. *Current vascular pharmacology*, *15*(5), 446-456.

Möller, M. N., Rios, N., Trujillo, M., Radi, R., Denicola, A., & Alvarez, B. (2019). Detection and quantification of nitric oxide–derived oxidants in biological systems. *Journal of Biological Chemistry*, *294*(40), 14776-14802.

Muhammad, Y., Kani, Y. A., Iliya, S., Muhammad, J. B., Binji, A., El-Fulaty Ahmad, A., Kabir, M. B., Umar Bindawa, K., & Ahmed, A. u. (2021). Deficiency of antioxidants and increased oxidative stress in COVID-19 patients: A cross-sectional comparative study in Jigawa, Northwestern Nigeria. *SAGE open medicine*, *9*, 2050312121991246.

Murgolo, N., Therien, A. G., Howell, B., Klein, D., Koeplinger, K., Lieberman, L. A., Adam, G. C., Flynn, J., McKenna, P., & Swaminathan, G. (2021). SARS-CoV-2 tropism, entry, replication, and propagation: Considerations for drug discovery and development. *Advances in Clinical Immunology, Medical Microbiology, COVID-19, and Big Data*, 753-775.

Nadkarni, R. R., Abed, S., & Draper, J. S. (2016). Organoids as a model system for studying human lung development and disease. *Biochemical and biophysical research communications*, *473*(3), 675-682.

NIH, COVID-19 Treatment Guidelines (2024). Retrieved 08.06.2024 from https://www.covid19treatmentguidelines.nih.gov/overview/clinical-spectrum/

Nova, N. (2021). Cross-species transmission of coronaviruses in humans and domestic mammals, what are the ecological mechanisms driving transmission, spillover, and disease emergence? *Frontiers in public health*, *9*, 717941.

Olagnier, D., Farahani, E., Thyrsted, J., Blay-Cadanet, J., Herengt, A., Idorn, M., Hait, A., Hernaez, B., Knudsen, A., & Iversen, M. B. (2020). SARS-CoV2-mediated suppression of NRF2-signaling reveals potent antiviral and anti-inflammatory activity of 4-octyl-itaconate and dimethyl fumarate. *Nature Communications*, *11*(1), 4938.

Orru, H., Ebi, K., & Forsberg, B. (2017). The interplay of climate change and air pollution on health. *Current environmental health reports*, *4*, 504-513.

Oztay, F., Kayalar, O., & Yildirim, M. (2019). Pulmonary oxidative stress and antioxidant defence system in the lung ageing and fibrotic and diabetic lungs. *Oxidative Stress in Lung Diseases: Volume 1*, 325-353.

Pansini, R., & Fornacca, D. (2021). Early spread of COVID-19 in the air-polluted regions of eight severely affected countries. *Atmosphere*, *12*(6), 795.

Patwa, A., & Shah, A. (2015). Anatomy and physiology of respiratory system relevant to anaesthesia. *Indian journal of anaesthesia*, *59*(9), 533-541.

Peng, L., Gao, L., Wu, X., Fan, Y., Liu, M., Chen, J., Song, J., Kong, J., Dong, Y., & Li, B. (2022). Lung organoids as model to study SARS-CoV-2 infection. *Cells*, *11*(17), 2758.

Pertea, M., Kim, D., Pertea, G. M., Leek, J. T., & Salzberg, S. L. (2016). Transcript-level expression analysis of RNA-seq experiments with HISAT, StringTie and Ballgown. *Nature protocols*, *11*(9), 1650-1667.

Polito, A. J., & Proud, D. (1998). Epithelial cells as regulators of airway inflammation. *Journal of allergy and clinical immunology*, *102*(5), 714-718.

Pu, S., Peng, S., Zhu, J., Liu, Z., Long, D., & Lim, T. (2022). Characteristics of PM2. 5 and its correlation with feed, manure and NH3 in a pig-fattening house. *Toxics*, *10*(3), 145.

Qiu, Y., Zhao, Y.-B., Wang, Q., Li, J.-Y., Zhou, Z.-J., Liao, C.-H., & Ge, X.-Y. (2020). Predicting the angiotensin converting enzyme 2 (ACE2) utilizing capability as the receptor of SARS-CoV-2. *Microbes and infection*, *22*(4-5), 221-225.

Qu, G., Li, X., Hu, L., & Jiang, G. (2020). An imperative need for research on the role of environmental factors in transmission of novel coronavirus (COVID-19). In: ACS Publications.

Quay, J. L., Reed, W., Samet, J., & Devlin, R. B. (1998). Air pollution particles induce IL-6 gene expression in human airway epithelial cells via NF-κ B activation. *American journal of respiratory cell and molecular biology*, *19*(1), 98-106.

Rahman, H. S., Aziz, M. S., Hussein, R. H., Othman, H. H., Omer, S. H. S., Khalid, E. S., Abdulrahman, N. A., Amin, K., & Abdullah, R. (2020). The transmission modes and sources of COVID-19: A systematic review. *International Journal of Surgery Open*, *26*, 125-136.

Rai, P. K. (2016). Particulate matter and its size fractionation. *Biomagnetic Monitoring of Particulate Matter*, *1*, 1-13.

Ramana, C. V. (2021). Lung Epithelial Regulation of BCL2 Related Protein A1 (BCL2A1) by Coronaviruses (SARS-CoV) and Type I Interferon Signaling. *bioRxiv*, 2021.2007. 2021.453244.

Ravindra, N. G., Alfajaro, M. M., Gasque, V., Huston, N. C., Wan, H., Szigeti-Buck, K., Yasumoto, Y., Greaney, A. M., Habet, V., & Chow, R. D. (2021). Single-cell longitudinal analysis of SARS-CoV-2 infection in human airway epithelium identifies target cells, alterations in gene expression, and cell state changes. *PLoS biology*, *19*(3), e3001143.

Rayner, R. E., Makena, P., Prasad, G. L., & Cormet-Boyaka, E. (2019). Optimization of normal human bronchial epithelial (NHBE) cell 3D cultures for in vitro lung model studies. *Scientific Reports*, *9*(1), 500.

Redza-Dutordoir, M., & Averill-Bates, D. A. (2016). Activation of apoptosis signalling pathways by reactive oxygen species. *Biochimica et Biophysica Acta (BBA)-Molecular Cell Research*, *1863*(12), 2977-2992.

Reimand, J., Isserlin, R., Voisin, V., Kucera, M., Tannus-Lopes, C., Rostamianfar, A., Wadi, L., Meyer, M., Wong, J., & Xu, C. (2019). Pathway enrichment analysis

and visualization of omics data using g: Profiler, GSEA, Cytoscape and EnrichmentMap. *Nature protocols*, *14*(2), 482-517.

Reshmi, R., & Abi, S. (2020). Covid-19 Pandemic-Insights and Challenges. *Journal ISSN*, *2766*, 2276.

Richter, M., Piwocka, O., Musielak, M., Piotrowski, I., Suchorska, W. M., & Trzeciak, T. (2021). From donor to the lab: a fascinating journey of primary cell lines. *Frontiers in Cell and Developmental Biology*, *9*, 711381.

Ritchie, H. R., Max. (2024). *Air Pollution*

. Retrieved 02.2024 from https://ourworldindata.org/air-pollution

Robinot, R., Hubert, M., de Melo, G. D., Lazarini, F., Bruel, T., Smith, N., Levallois, S., Larrous, F., Fernandes, J., & Gellenoncourt, S. (2021). SARS-CoV-2 infection induces the dedifferentiation of multiciliated cells and impairs mucociliary clearance. *Nature Communications*, *12*(1), 4354.

Rodrigues, T. S., Caetano, C. C., de Sá, K. S., Almeida, L., Becerra, A., Gonçalves, A. V., Lopes, L. d. S., Oliveira, S., Mascarenhas, D. P., & Batah, S. S. (2023). Casp4/11 contributes to Nlrp3 activation and covid-19 exacerbation. *The Journal of infectious diseases*, *227*(12), 1364-1375.

Rosas-Salazar, C., Kimura, K. S., Shilts, M. H., Strickland, B. A., Freeman, M. H., Wessinger, B. C., Gupta, V., Brown, H. M., Rajagopala, S. V., & Turner, J. H. (2021). SARS-CoV-2 infection and viral load are associated with the upper respiratory tract microbiome. *Journal of allergy and clinical immunology*, *147*(4), 1226-1233. e1222.

Sachs, N., Papaspyropoulos, A., Zomer-van Ommen, D. D., Heo, I., Böttinger, L., Klay, D., Weeber, F., Huelsz-Prince, G., Iakobachvili, N., & Amatngalim, G. D. (2019). Long-term expanding human airway organoids for disease modeling. *The EMBO journal*, *38*(4), e100300.

Sagawa, T., Tsujikawa, T., Honda, A., Miyasaka, N., Tanaka, M., Kida, T., Hasegawa, K., Okuda, T., Kawahito, Y., & Takano, H. (2021). Exposure to particulate matter upregulates ACE2 and TMPRSS2 expression in the murine lung. *Environmental Research*, *195*, 110722.

Saleh, J., Peyssonnaux, C., Singh, K. K., & Edeas, M. (2020). Mitochondria and microbiota dysfunction in COVID-19 pathogenesis. *Mitochondrion*, *54*, 1-7.

Sano, E., Suzuki, T., Hashimoto, R., Itoh, Y., Sakamoto, A., Sakai, Y., Saito, A., Okuzaki, D., Motooka, D., & Muramoto, Y. (2022). Cell response analysis in SARS-CoV-2 infected bronchial organoids. *Communications biology*, *5*(1), 516.

Schmidt, H. H., Stocker, R., Vollbracht, C., Paulsen, G., Riley, D., Daiber, A., & Cuadrado, A. (2015). Antioxidants in translational medicine. *Antioxidants & redox signaling*, *23*(14), 1130-1143.

Semiz, S. (2022). COVID19 biomarkers: What did we learn from systematic reviews? *Frontiers in cellular and infection microbiology*, *12*, 1038908.

Setti, L., Passarini, F., De Gennaro, G., Barbieri, P., Perrone, M. G., Borelli, M., Palmisani, J., Di Gilio, A., Torboli, V., & Fontana, F. (2020). SARS-Cov-2RNA found on particulate matter of Bergamo in Northern Italy: first evidence. *Environmental Research*, *188*, 109754.

Siednienko, J., Nowak, J., Moynagh, P. N., & Gorczyca, W. A. (2011). Nitric oxide affects IL-6 expression in human peripheral blood mononuclear cells involving cGMP-dependent modulation of NF-κB activity. *Cytokine*, *54*(3), 282-288.

Sigrist, C. J., Bridge, A., & Le Mercier, P. (2020). A potential role for integrins in host cell entry by SARS-CoV-2. *Antiviral research*, *177*, 104759.

Silva, M. J. A., Ribeiro, L. R., Lima, K. V. B., & Lima, L. N. G. C. (2022). Adaptive immunity to SARS-CoV-2 infection: A systematic review. *Frontiers in immunology*, *13*, 1001198.

Singh, K. K., Chaubey, G., Chen, J. Y., & Suravajhala, P. Decoding SARS-CoV-2 Hijacking of Host Mitochondria.

Soto, M. E., Guarner-Lans, V., Díaz-Díaz, E., Manzano-Pech, L., Palacios-Chavarría, A., Valdez-Vázquez, R. R., Aisa-Álvarez, A., Saucedo-Orozco, H., & Pérez-Torres, I. (2022). Hyperglycemia and loss of redox homeostasis in COVID-19 patients. *Cells*, *11*(6), 932.

Stanaway, J. D., Afshin, A., Gakidou, E., Lim, S. S., Abate, D., Abate, K. H., Abbafati, C., Abbasi, N., Abbastabar, H., & Abd-Allah, F. (2018). Global, regional, and national comparative risk assessment of 84 behavioural, environmental and occupational, and metabolic risks or clusters of risks for 195 countries and territories, 1990–2017: a systematic analysis for the Global Burden of Disease Study 2017. *The Lancet*, *392*(10159), 1923-1994.

Stark, R., Grzelak, M., & Hadfield, J. (2019). RNA sequencing: the teenage years. *Nature reviews genetics*, *20*(11), 631-656.

Stathopoulos, D., Loukides, S., & Syrigos, K. (2014). 8-Isoprostane in exhaled breath condensate of patients with non-small cell lung cancer: the effect of chemotherapy. *Anticancer Research*, *34*(9), 5143-5145.

Steensberg, A., Keller, C., Hillig, T., Frøsig, C., Wojtaszewski, J. F., Pedersen, B. K., Pilegaard, H., & Sander, M. (2007). Nitric oxide production is a proximal signaling event controlling exercise-induced mRNA expression in human skeletal muscle. *The FASEB Journal*, *21*(11), 2683-2694.

Stoermer, K. A., & Morrison, T. E. (2011). Complement and viral pathogenesis. *Virology*, *411*(2), 362-373.

Stölting, H., Baillon, L., Frise, R., Bonner, K., Hewitt, R. J., Molyneaux, P. L., Gore, M. L., Barclay, W. S., Saglani, S., & Lloyd, C. M. (2022). Distinct airway epithelial immune responses after infection with SARS-CoV-2 compared to H1N1. *Mucosal immunology*, *15*(5), 952-963.

Tang, H., Cheng, Z., Li, N., Mao, S., Ma, R., He, H., Niu, Z., Chen, X., & Xiang, H. (2020). The short-and long-term associations of particulate matter with inflammation and blood coagulation markers: a meta-analysis. *Environmental pollution*, *267*, 115630.

Tay, M. Z., Poh, C. M., Rénia, L., MacAry, P. A., & Ng, L. F. (2020). The trinity of COVID-19: immunity, inflammation and intervention. *Nature Reviews Immunology*, *20*(6), 363-374.

Thompson, A. M., Zanobetti, A., Silverman, F., Schwartz, J., Coull, B., Urch, B., Speck, M., Brook, J. R., Manno, M., & Gold, D. R. (2010). Baseline repeated measures from controlled human exposure studies: associations between ambient air pollution exposure and the systemic inflammatory biomarkers IL-6 and fibrinogen. *Environmental health perspectives*, *118*(1), 120-124.

Thomson, B. J. (2001). Viruses and apoptosis. *International journal of experimental pathology*, *82*(2), 65-76.

Thuy, L. T. T., Van Thuy, T. T., Matsumoto, Y., Hai, H., Ikura, Y., Yoshizato, K., & Kawada, N. (2016). Absence of cytoglobin promotes multiple organ abnormalities in aged mice. *Scientific Reports*, *6*(1), 24990.

Travaglio, M., Yu, Y., Popovic, R., Selley, L., Leal, N. S., & Martins, L. M. (2021). Links between air pollution and COVID-19 in England. *Environmental pollution*, *268*, 115859.

V'kovski, P., Kratzel, A., Steiner, S., Stalder, H., & Thiel, V. (2021). Coronavirus biology and replication: implications for SARS-CoV-2. *Nature Reviews Microbiology*, *19*(3), 155-170.

Van Eeden, S. F., & Sin, D. D. (2013). Oxidative stress in chronic obstructive pulmonary disease: a lung and systemic process. In (Vol. 20, pp. 27-29): Hindawi.

Vogler, M. (2012). BCL2A1: the underdog in the BCL2 family. *Cell Death & Differentiation*, *19*(1), 67-74.

Vollbracht, C., & Kraft, K. (2022). Oxidative stress and hyper-inflammation as major drivers of severe COVID-19 and long COVID: implications for the benefit of high-dose intravenous vitamin C. *Frontiers in pharmacology*, *13*, 899198.

Walls, A. C., Park, Y.-J., Tortorici, M. A., Wall, A., McGuire, A. T., & Veesler, D. (2020). Structure, function, and antigenicity of the SARS-CoV-2 spike glycoprotein. *Cell*, *181*(2), 281-292. e286.

Wang, B., Chen, H., Chan, Y. L., & Oliver, B. G. (2020). Is there an association between the level of ambient air pollution and COVID-19? *American Journal of Physiology-Lung Cellular and Molecular Physiology*, *319*(3), L416-L421.

Wang, F., Liu, J., & Zeng, H. (2020). Interactions of particulate matter and pulmonary surfactant: Implications for human health. *Advances in colloid and interface science*, *284*, 102244.

Wang, J., Mei, F., Bai, L., Zhou, S., Liu, D., Yao, L., Ahluwalia, A., Ghiladi, R. A., Su, L., & Shu, T. (2021). Serum nitrite and nitrate: A potential biomarker for post-covid-19 complications? *Free Radical Biology and Medicine*, *175*, 216-225.

Wang, T., Du, Z., Zhu, F., Cao, Z., An, Y., Gao, Y., & Jiang, B. (2020). Comorbidities and multi-organ injuries in the treatment of COVID-19. *The Lancet*, *395*(10228), e52.

Wang, X., Shen, C., Zhu, J., Shen, G., Li, Z., & Dong, J. (2019). Long noncoding RNAs in the regulation of oxidative stress. *Oxidative medicine and cellular longevity*, *2019*.

Wang, Z., Gerstein, M., & Snyder, M. (2009). RNA-Seq: a revolutionary tool for transcriptomics. *Nature reviews genetics*, *10*(1), 57-63.

Whitsett, J. A. (2018). Airway epithelial differentiation and mucociliary clearance. *Annals of the American thoracic society*, *15*(Supplement 3), S143-S148.

WHO. (2021). *Living guidance for clinical management of COVID-19: living guidance, 23 November 2021*.

WHO COVID-19 dashboard. Retrieved 08.06.2024 from https://data.who.int/dashboards/covid19/cases?n=c

Wieczfinska, J., Kleniewska, P., & Pawliczak, R. (2022). Oxidative stress-related mechanisms in SARS-CoV-2 infections. *Oxidative medicine and cellular longevity*, *2022*.

Wolff, D., Nee, S., Hickey, N. S., & Marschollek, M. (2021). Risk factors for Covid-19 severity and fatality: a structured literature review. *Infection*, *49*, 15-28.

Wolszczak-Biedrzycka, B., Dorf, J., Matowicka-Karna, J., Wojewódzka-Żeleźniakowicz, M., Żukowski, P., Zalewska, A., & Maciejczyk, M. (2024). Significance of nitrosative stress and glycoxidation products in the diagnosis of COVID-19. *Scientific Reports*, *14*(1), 9198.

Wu, M., Zhang, X., Lin, Y., & Zeng, Y. (2022). Roles of airway basal stem cells in lung homeostasis and regenerative medicine. *Respiratory Research*, *23*(1), 122.

Wu, X., Nethery, R. C., Sabath, M. B., Braun, D., & Dominici, F. (2020). Air pollution and COVID-19 mortality in the United States: Strengths and limitations of an ecological regression analysis. *Science advances*, *6*(45), eabd4049.

Xie, Y., Hou, W., Song, X., Yu, Y., Huang, J., Sun, X., Kang, R., & Tang, D. (2016). Ferroptosis: process and function. *Cell Death & Differentiation*, *23*(3), 369-379.

Xu, C., Inokuma, M. S., Denham, J., Golds, K., Kundu, P., Gold, J. D., & Carpenter, M. K. (2001). Feeder-free growth of undifferentiated human embryonic stem cells. *Nature biotechnology*, *19*(10), 971-974.

Xu, J.-B., Guan, W.-J., Zhang, Y.-L., Qiu, Z.-E., Chen, L., Hou, X.-C., Yue, J., Zhou, Y.-Y., Sheng, J., & Zhao, L. (2024). SARS-CoV-2 envelope protein impairs airway epithelial barrier function and exacerbates airway inflammation via increased intracellular Cl− concentration. *Signal transduction and targeted therapy*, *9*(1), 74.

Xu, X., Chen, P., Wang, J., Feng, J., Zhou, H., Li, X., Zhong, W., & Hao, P. (2020). Evolution of the novel coronavirus from the ongoing Wuhan outbreak and modeling of its spike protein for risk of human transmission. *Science China Life Sciences*, *63*, 457-460.

Yamada, T., & Takaoka, A. (2023). Innate immune recognition against SARS-CoV-2. *Inflammation and Regeneration*, *43*(1), 7.

Yan, B., Freiwald, T., Chauss, D., Wang, L., West, E., Bibby, J., Olson, M., Kordasti, S., Portilla, D., & Laurence, A. (2020). SARS-CoV2 drives JAK1/2-dependent local and systemic complement hyperactivation. *Research Square*.

Yan, H.-f., Zou, T., Tuo, Q.-z., Xu, S., Li, H., Belaidi, A. A., & Lei, P. (2021). Ferroptosis: mechanisms and links with diseases. *Signal transduction and targeted therapy*, *6*(1), 49.

Yao, Y., Pan, J., Wang, W., Liu, Z., Kan, H., Qiu, Y., Meng, X., & Wang, W. (2020). Association of particulate matter pollution and case fatality rate of COVID-19 in 49 Chinese cities. *Science of the Total Environment*, *741*, 140396.

Yin, X., Mead, B. E., Safaee, H., Langer, R., Karp, J. M., & Levy, O. (2016). Engineering stem cell organoids. *Cell stem cell*, *18*(1), 25-38.

Yu, J., Gerber, G. F., Chen, H., Yuan, X., Chaturvedi, S., Braunstein, E. M., & Brodsky, R. A. (2022). Complement dysregulation is associated with severe COVID-19 illness. *Haematologica*, *107*(5), 1095.

Yuksel, H., & Turkeli, A. (2017). Airway epithelial barrier dysfunction in the pathogenesis and prognosis of respiratory tract diseases in childhood and adulthood. *Tissue Barriers*, *5*(4), e1367458.

Zhang, Z., Zhu, Z., Chen, W., Cai, Z., Xu, B., Tan, Z., Wu, A., Ge, X., Guo, X., & Tan, Z. (2019). Cell membrane proteins with high N-glycosylation, high expression and multiple interaction partners are preferred by mammalian viruses as receptors. *Bioinformatics*, *35*(5), 723-728.

Zhao, Q., Meng, M., Kumar, R., Wu, Y., Huang, J., Deng, Y., Weng, Z., & Yang, L. (2020). Lymphopenia is associated with severe coronavirus disease 2019 (COVID-19) infections: A systemic review and meta-analysis. *International journal of infectious diseases*, *96*, 131-135.

Zhou, L., Zhu, L., Wu, X., Hu, S., Zhang, S., Ning, M., Yu, J., & Chen, M. (2023). Decreased TMIGD1 aggravates colitis and intestinal barrier dysfunction via the BANF1-NF-κB pathway in Crohn's disease. *BMC medicine*, *21*(1), 287.

Zhou, Y., Wang, M., Li, Y., Wang, P., Zhao, P., Yang, Z., Wang, S., Zhang, L., Li, Z., & Jia, K. (2021). SARS-CoV-2 Spike protein enhances ACE2 expression via facilitating Interferon effects in bronchial epithelium. *Immunology letters*, *237*, 33-41.

Zhu, Y., Xie, J., Huang, F., & Cao, L. (2020). Association between short-term exposure to air pollution and COVID-19 infection: Evidence from China. *Science of the Total Environment*, *727*, 138704.

Zhu, Z., Zhao, Z., Chen, X., Chu, Z., He, Y., Tan, Y., Zhou, J., & Tang, C. (2022). Effects of growth hormone/estrogen/androgen on COVID-19-type proinflammatory responses in normal human lung epithelial BEAS-2B cells. *BMC Molecular and Cell Biology*, *23*(1), 42.

Zsichla, L., & Müller, V. (2023). Risk factors of severe COVID-19: a review of host, viral and environmental factors. *Viruses*, *15*(1), 175.